

Aus dem
Lehrstuhl für Experimentelle Orthopädie und Arthroreforschung
Universität des Saarlandes
Zentrum für Experimentelle Orthopädie
Universitätsklinikum des Saarlandes
Leiter: Prof. Dr. med. Henning Madry

KUMULATIVE PROMOTION

**Innovative bildgebende Verfahren zur Darstellung experimenteller
Gelenkknorpeldefekte im translationalen Schafmodell**

**Dissertation zur Erlangung des Grades eines Doktors der Medizin
der Medizinischen Fakultät
der UNIVERSITÄT DES SAARLANDES
2015**

vorgelegt von: Lars Klaus Heinrich Goebel
geboren am: 04. Dezember 1985 in Saarlouis

Inhaltsverzeichnis

1	EINGESCHLOSSENE ORIGINALARBEITEN	3
2	ZUSAMMENFASSUNG.....	7
3	ABSTRACT	8
4	HAUPTTEIL	9
4.1	EINLEITUNG.....	9
4.2	DARSTELLUNG DER EINZELNEN PUBLIKATIONEN	13
4.3	DISKUSSION	19
4.4	AUSBlick.....	22
4.5	LITERATURVERZEICHNIS	23
5	ORIGINALARBEITEN	32
6	DANKSAGUNG	64
7	PUBLIKATIONEN.....	66
8	LEBENS LAUF	69

1 Eingeschlossene Originalarbeiten

In die vorliegende kumulative Dissertation sind folgende Veröffentlichungen (I-III) eingeschlossen, die in Fachzeitschriften im *peer reviewed* Verfahren publiziert wurden. Der Anteil und die Tätigkeit der Mitautoren an den einzelnen Publikationen werden folgend im Detail aufgelistet. Alle Mitautoren sind mit einer Veröffentlichung der Originalarbeiten im Rahmen dieser kumulativen Dissertation einverstanden.

- I. Orth P, **Goebel L**, Wolfram U, Ong MF, Gräber S, Kohn D, Cucchiarini M, Ignatius A, Pape D, Madry H. Effect of subchondral drilling on the microarchitecture of subchondral bone: analysis in a large animal model at 6 months. Am J Sports Med, 2012, 40(4):828-36.

Mitautoren:	Beitrag:
Orth, Patrick	Datenerhebung, Analyse und Interpretation der Daten, Ausarbeitung und Überarbeitung des Manuskripts
Goebel, Lars	Datenerhebung, Analyse und Interpretation der Daten, Überarbeitung des Manuskripts
Wolfram, Uwe	Technische Hilfe bei der Datenerhebung und Interpretation der Daten
Ong, Mei Fang	Hilfe bei der statistischen Analyse
Gräber, Stefan	Hilfe bei der statistischen Analyse
Kohn, Dieter	Kritische Durchsicht des Manuskripts
Cucchiarini, Magali	Analyse und Interpretation der Daten, Überarbeitung des Manuskripts
Ignatius, Anita	Kritische Durchsicht des Manuskripts
Pape, Dietrich	Tierversuche, Kritische Durchsicht des Manuskripts
Madry, Henning	Konzeption der Studie, Tierversuche, Analyse und Interpretation der Daten, Ausarbeitung und Überarbeitung des Manuskripts

- II. **Goebel L**, Orth P, Müller A, Zurakowski D, Bucker A, Cucchiarini M, Pape D, Madry H. Experimental scoring systems for macroscopic articular cartilage repair correlate with the MOCART score assessed by a high-field MRI at 9.4 Tesla - comparative evaluation of five macroscopic scoring systems in a large animal cartilage defect model. *Osteoarthritis Cartilage*, 2012, 20(9):1046-55.

Mitautoren:	Beitrag:
Goebel, Lars	Datenerhebung, Analyse und Interpretation der Daten, Ausarbeitung und Überarbeitung des Manuskripts
Orth, Patrick	Datenerhebung, Analyse und Interpretation der Daten, Überarbeitung des Manuskripts
Müller, Andreas	Technische Hilfe bei der Datenerhebung und Interpretation der Daten
Zurakowski, David	Hilfe bei der statistischen Analyse
Bücker, Arno	Kritische Durchsicht des Manuskripts
Cucchiarini, Magali	Analyse und Interpretation der Daten, Überarbeitung des Manuskripts
Pape, Dietrich	Tierversuche, Kritische Durchsicht des Manuskripts
Madry, Henning	Konzeption der Studie, Tierversuche, Analyse und Interpretation der Daten, Ausarbeitung und Überarbeitung des Manuskripts

- III. **Goebel L**, Zurakowski D, Müller A; Pape D, Cucchiarini M, Madry H. 2D and 3D MOCART scoring systems assessed by 9.4 Tesla high-field MRI correlate with elementary and complex histological scoring systems in a translational model of osteochondral repair. *Osteoarthritis Cartilage*, 2014, 22(10):1386-95.

Mitautoren:	Beitrag:
Goebel, Lars	Datenerhebung, Analyse und Interpretation der Daten, Ausarbeitung und Überarbeitung des Manuskripts
Zurakowski, David	Hilfe bei der statistischen Analyse
Müller, Andreas	Technische Hilfe bei der Datenerhebung und Interpretation der Daten
Pape, Dietrich	Tierversuche, Kritische Durchsicht des Manuskripts
Cucchiarini, Magali	Analyse und Interpretation der Daten, Überarbeitung des Manuskripts
Madry, Henning	Konzeption der Studie, Tierversuche, Analyse und Interpretation der Daten, Ausarbeitung und Überarbeitung des Manuskripts

2 Zusammenfassung

Fokale Knorpeldefekte entstehen häufig als Folge eines Traumas. Diese betreffen oft die gesamte osteochondrale Einheit, welche aus dem hyalinen Gelenkknorpel und dem darunterliegenden subchondralen Knochen besteht. In dieser Arbeit wurden zunächst die Veränderungen des subchondralen Knochens nach Pridie-Bohrung zur Behandlung vollschichtiger fokaler Gelenkknorpeldefekte mittels Microcomputertomographie untersucht. Die Ergebnisse zeigen, dass signifikante Veränderungen des subchondralen Knochens nach Pridie-Bohrung im translationalen Großtiermodell über einen klinisch relevanten Zeitraum persistieren. Die Entwicklung eines neuen makroskopischen Bewertungssystems der Knorpelreparatur und dessen Korrelation und Validierung an vier etablierten makroskopischen Bewertungssystemen sowie dem kernspintomographischen, für die *ex vivo* Analyse adaptierten, *2D Magnetic Resonance Observation of Cartilage Repair Tissue* (MOCART) - Bewertungssystem im 9,4 Tesla (T) Hochfeld-Magnetresonanztomographen (μ MRT) schlossen sich an. Darauf aufbauend erfolgte die Modifikation des 3D MOCART-Systems für *ex vivo* Untersuchungen im 9,4 T μ MRT und, gemeinsam mit dem adaptierten 2D MOCART-System, die Korrelation mit elementaren und komplexen histologischen Bewertungssystemen. Hier zeigte sich, dass die internen Korrelationen der makroskopischen, histologischen und MOCART-Systeme sehr hoch sind. Untersuchungsergebnisse im 9,4 T μ MRT korrelieren weiterhin mit wesentlichen Schlüsselparametern der makroskopischen und histologischen Defektreparatur. Somit ist das μ MRT hervorragend geeignet, um die Lücke zwischen Makroskopie und Histologie zur detaillierten Beurteilung der Reparatur fokaler Gelenkknorpeldefekte zu schließen. Zukünftige Studien müssen sich auf die *in vivo* Untersuchung von Gelenkknorpeldefekten im μ MRT und auf eine Implementierung dieser innovativen bildgebenden Verfahren in den klinischen Alltag fokussieren.

3 Abstract

Innovative imaging techniques for the evaluation of experimental cartilage repair in a translational sheep model

Focal articular cartilage defects are often of traumatic origin. Here, the entire osteochondral unit, containing the hyaline cartilage as well as the subarticular bone, is often affected. At first, alterations of the subchondral bone plate and the subarticular spongiosa after Pridie drilling to treat full-thickness focal cartilage defects were investigated using micro-computed tomography. The data suggest that significant subchondral bone changes after marrow stimulating techniques persist in translational large animal models for an extended period of time. Next, a new macroscopic scoring system to grade cartilage repair was developed, compared and validated with four pre-existing macroscopic scoring systems and the MRI based 2D Magnetic Resonance Observation of Cartilage Repair Tissue (MOCART) system, which was adapted for *ex vivo* analyses in a 9.4 Tesla (T) high-field magnetic resonance imaging scanner (μ MRI). Finally, the 3D MOCART system was modified for *ex vivo* studies and correlated together with the adapted 2D system at 9.4 T with elementary and complex histological scoring systems. Internal correlations of macroscopic, histological, and MOCART systems were very high. Moreover, at 9.4 T, μ MRI correlate with key parameters of macroscopic and histological articular cartilage defect repair. High-field MRI is well suited to close the gap between macroscopy and histology to allow for a detailed assessment of focal articular cartilage defect repair. Future studies have to focus on *in vivo* μ MRI imaging of articular cartilage repair as well as an implementation of these innovative imaging techniques in clinical routine.

4 Hauptteil

4.1 Einleitung

Verletzungen des hyalinen Gelenkknorpels heilen nicht und sind ein signifikantes Problem in der Orthopädie und Unfallchirurgie (Madry 2011). Sie werden anhand ihrer Tiefenausdehnung in voll- bzw. teilschichtige chondrale Defekte unterteilt (Orth 2013a). Osteochondrale Defekte resultieren, wenn die Zementlinie penetriert wird (Madry 2010; Orth 2013a). Der subchondrale Knochen, bestehend aus der subchondralen Knochenplatte und der subartikulären Spongiosa, bildet zusammen mit dem kalzifizierten Knorpel und dem hyalinen Gelenkknorpel die osteochondrale Einheit (Orth 2013a).

Markraumstimulierende Verfahren, wie die subchondrale Anbohrung nach Pridie (Pridie 1959), Mikrofrakturierung (Steadman 2002) oder die Abrasionsarthroplastik (Johnson 2001), sind zur Behandlung symptomatischer kleiner Knorpeldefekte indiziert. Die autologe Chondrozytentransplantation findet hingegen bei größeren Defekten, oder als Zweitlinientherapie, Anwendung (Brittberg 1994; Madry 2008; Ochs 2011).

Für experimentelle Fragestellungen stehen seit kurzem die Mikrocomputertomographie (μ CT) (Müller 1996; Barou 2002; Chen 2009; Chen 2011) und die Hochfeldmagnetresonanztomographie (μ MRT) (Kangarlu 2006; Krug 2009; Trattinig 2009; Moser 2010; Moser 2012) zur Verfügung. Beide Verfahren können auch für Fragestellungen der osteochondralen Defektreparatur angewendet werden. Die Stärke der μ CT liegt hierbei in der dreidimensionalen Darstellung von knöchernen Strukturen bis in den Submikrometerbereich. Allerdings ist deren Anwendbarkeit noch hauptsächlich auf die Untersuchung von kleinen Proben *ex vivo* beschränkt (Batiste 2004; Kangarlu 2006; Wang 2010), während erste Versuche bereits an Patienten durchgeführt wurden (van den Bergen 2009; Garnov 2013; Theysohn 2013).

Untersuchung des subchondralen Knochens mittels μ CT nach rekonstruktiv-chirurgischen Verfahren der Knorpelreparatur

Aktuelle klinische Untersuchungen zeigen, dass rekonstruktiv-chirurgische Verfahren der Knorpelreparatur auch signifikante Veränderungen im subchondralen Knochen induzieren (Saris 2009; Gomoll 2010; Fortier 2012; Eldracher 2014; Yan 2014). Beispielsweise wurden subchondrale Zysten, intraläsionale Osteophyten oder das generalisierte Voranschreiten der subchondralen Knochenplatte nach markraumeröffnenden Verfahren beschrieben (Orth 2012a; Orth 2013a; Eldracher 2014). Die Frage, ob derartige Veränderungen des subchondralen Knochens auch nach markraumeröffnenden Verfahren in einem translationalen Großtiermodell in einen klinisch relevanten Zeitraum auftreten, war der erste Schwerpunkt dieser Arbeit (Orth 2012b).

Vergleich der makroskopischen Reparatur fokaler Knorpeldefekte mit Untersuchungen im 9,4 Tesla μ MRT

Die makroskopische Beschreibung von Knorpeldefekten ist eine einfach anwendbare und schnelle Möglichkeit zur Beurteilung von Gelenkknorpeldefekten (O'Driscoll 1986; Noyes 1989; Smith 2005; Jung 2006). Im klinischen Kontext werden makroskopische Bewertungssysteme standardmäßig zur arthroskopischen Beschreibung von Gelenkknorpeldefekten angewendet (Smith 2005). Genauso ist auch die makroskopische Beurteilung von Knorpelchirurgie in der translationalen Forschung etabliert (O'Driscoll 1986; Jung 2006). Im Rahmen experimenteller Fragestellungen finden unter anderem μ MRT mit Feldstärken von 9,4 Tesla (T) Anwendung (Kangarlu 2006; Krug 2009; Trattinig 2009; van den Bergen 2009; Wang 2010; Moser 2012; Pachowsky 2014). Die Kernspintomographie ist hervorragend zur Beurteilung der Gelenkknorpelreparatur geeignet (Forney 2014). Da das Signal-zu-Rauschen-Verhältnis direkt mit der Feldstärke korreliert, können, insbesondere bei Anwendung entsprechender Spulensysteme, Auflösungen im niedrigen Mikrometerbereich erreicht werden, ein wesentlicher Faktor zur morphologischen Beschreibung der Gelenkknorpeldefektreparatur (Kangarlu

2006; Madry 2008; Krug 2009; Singh 2014). Hier ist die Anwendung meist auf die *ex vivo* Analyse von Explantaten bzw. die *in vivo* Untersuchung von kleinen Versuchstieren beschränkt. Interessanterweise stehen auch bereits erste μ MRT für die *in vivo* Untersuchung am Menschen zur Verfügung (O'Driscoll 1986; Noyes 1989; Barou 2002; Smith 2005; Krug 2009; Moser 2012; Orth 2012b; Garnov 2013; Singh 2014). Der zweite Schwerpunkt dieser Arbeit lag auf der Entwicklung eines neuen makroskopischen Bewertungssystems, welches valide und reproduzierbar zur Beurteilung der Gelenkknorpeldefektreparatur geeignet ist. Dieses neue makroskopische Bewertungssystem wurde dafür mit verschiedenen bereits etablierten makroskopischen Bewertungssystemen (Brittberg 1994; Saris 2009; Garnov 2013) und mit dem von Marlovits *et al.* entwickelten (klinischen) 2D *Magnetic Resonance Observation of Cartilage Repair Tissue* (MOCART)-System (Marlovits 2004; Marlovits 2006), aus Datensätzen die im 9,4 T μ MRT erzeugt wurden, verglichen (Goebel 2012).

Vergleich elementarer und komplexer histologischer Bewertungssysteme mit dem 2D und 3D MOCART-System im 9,4 T μ MRT

Die histologische Untersuchung des Reparaturgewebes im Rahmen translationaler Fragestellungen ist der Goldstandard, um Therapieeffekte beschreiben und vergleichen zu können (Orth 2012c). Sie erlaubt die Darstellung unterschiedlicher Zielstrukturen (Schmitz 2010). Verschiedene Studien bestätigen die hohe Intra- und Interbeobachterreliabilität der etablierten semiquantitativen Bewertungssysteme (Orth 2012c). Ein Nachteil histologischer Untersuchungen stellt die relativ lange Vorbereitungszeit von Präparaten aus knöchernen Proben dar. Mit ihrer Anfertigung ist zudem die irreversible Zerstörung der Proben verbunden. Weil parallele Schnittebenen des Probenmaterials angefertigt werden, sind histologische Untersuchungen in einer anderen Ebene des Raumes danach unmöglich. Um die Frage zu beantworten, inwieweit eine nicht destruktive Analyse Hinweise auf die Struktur des osteochondralen Reparaturgewebes geben kann, befasste sich der dritte Schwerpunkt dieser Arbeit mit dem Vergleich von Untersuchungen von osteochondralen Defekten im 9,4 T μ MRT mit histologischen Verfahren (Goebel

2014). Hierbei erfolgte ein Vergleich der 2D und 3D MOCART-Systeme (Marlovits 2004; Marlovits 2006; Welsch 2009; Welsch 2011) mit dem elementaren histologischen Bewertungssystem nach Wakitani (Wakitani 1994) und dem komplexeren System nach Sellers (Sellers 1997).

Beantwortete Fragestellungen

Im Rahmen der vorliegenden Arbeit lagen die Schwerpunkte auf der Untersuchung folgender Fragestellungen:

1. Führt die subchondrale Anbohrung fokaler Knorpeldefekte nach einem klinisch relevanten Zeitraum zu Veränderungen des subchondralen Knochens in einem translationalen Großtiermodell?
2. Kann anhand eines neu entwickelten makroskopischen Bewertungssystems, im Vergleich mit vier bereits etablierten makroskopischen Bewertungssystemen, die Gelenkknorpeldefektreparatur valide beschrieben werden und korrelieren diese mit Untersuchungen mit dem 2D MOCART-System im 9,4 T μ MRT?
3. Korrelieren die 2D und 3D MOCART-Bewertungssysteme im 9,4 T μ MRT mit elementaren und komplexen histologischen Bewertungssystemen und ermöglicht das 9,4 T μ MRT morphologische Aussagen über die histologische Defektreparatur?

4.2 Darstellung der einzelnen Publikationen

Der Einfluss der subchondralen Anbohrung nach Pridie auf die Mikroarchitektur des subchondralen Knochens - eine Untersuchung im Großtiermodell

Untersuchungen im Menschen, als auch im translationalen Tiermodell, beschreiben schlechtere Ergebnisse für Folgeeingriffe, beispielsweise einer autologen Chondrozytentransplantation als Zweittherapie (Minas 2009; Eldracher 2014), nach Anwendung markraumstimulierender Verfahren. Dabei ist der langfristige Effekt der Pridie-Bohrung auf den subchondralen Knochen bis dato noch unerforscht.

Um die Hypothese zu überprüfen, dass eine Pridie-Bohrung in einem klinisch relevanten Zeitraum zu Veränderungen der subchondralen Knochens führt, wurden in den gewichttragenden Anteil des medialen Femurkondylus des linken Kniegelenkes von 19 weiblichen, adulten Merinoschafen standardisierte, vollschichtige Gelenkknorpeldefekte (Größe 4 x 8 mm) erzeugt (Martini 2001; Orth 2012b; Orth 2013b; Pape 2013). Dazu erfolgte die Entfernung des hyalinen Gelenkknorpels bis zur Zementlinie, ohne diese zu penetrieren. Nach dem präoperativen radiologischen Ausschluss einer Arthrose wurden pro Defekt 6 standardisierte Bohrlöcher mit einem Durchmesser von 1,0 mm und einer Tiefe von 10 mm generiert. Postoperativ war den Tieren die Vollbelastung erlaubt. Sechs Monate nach dem Eingriff erfolgte die Entnahme der osteochondralen Proben aus den medialen Femurkondylen, um diese zunächst mittels μ CT morphologisch auf Zysten und intraläsionale Osteophyten zu untersuchen (Feldkamp 1989; Müller 1996; Hunziker 2007). Zwei unbehandelte mediale Femurkondylen eines nichtoperierten Versuchstiers dienten als Negativkontrolle (Osterhoff 2011). Daran schloss sich die Entwicklung einer standardisierten Methode an, um den subchondralen Knochen morphometrisch analysieren und verschiedene Knochenstrukturparameter bestimmen zu können. Der subchondrale Knochen unterhalb des Defekts wurde dann mit dem angrenzenden, intakten subchondralen Knochen verglichen.

Die Daten zeigten, dass der subchondrale Knochen im translationalen Schafmodell zuverlässig mittels μ CT in standardisierten *volumes of interest* beurteilt werden kann (Orth 2012b; Eldracher 2014). Die Analyse der Mikroarchitektur ergab, dass die subartikuläre Spongiosa keiner zonalen Gliederung unterliegt. Die subchondrale Bohrung führte in 63% der Fälle zur Ausbildung subchondraler Knochenzysten und in 23% der Fälle zur Bildung intraläsionaler Osteophyten. Im Vergleich mit dem Defekt angrenzenden subchondralen Knochen führte die Pridie-Bohrung zu signifikanten Veränderungen fast aller Mikroarchitekturparameter der subchondralen Knochenplatte und der subartikulären Spongiosa, vor allem zu einer Abnahme des Knochenvolumens, der Knochenvolumendichte, der Dicke der subchondralen Knochenplatte, der subartikulären Trabekel und der Knochendichte. Der Intertrabekelabstand war erhöht. Interessanterweise war auch der *trabecular pattern factor*, als inverser Parameter, erniedrigt, was *per se* einer erhöhten Konnektivität der subartikulären Spongiosa im Defekt entspricht.

Zusammenfassend zeigen die Ergebnisse, dass 6 Monate postoperativ signifikante strukturelle Veränderung der osteochondralen Einheit nachweisbar sind, was, übertragen in den klinischen Alltag, bedeutet, dass der subchondrale Knochen nach markraumeröffnenden Verfahren vulnerabel bleibt (Orth 2012b).

Experimentelle makroskopische Bewertungssysteme zur Beurteilung der Gelenkknorpelreparatur korrelieren mit dem MOCART Bewertungssystem in einem 9,4 T μ MRT - eine vergleichende Untersuchung von fünf makroskopischen Bewertungssystemen im Großtiermodell

Im Rahmen dieser Publikation (Goebel 2012) erfolgte zunächst die Entwicklung eines neuen Bewertungssystems zur makroskopischen Beurteilung der experimentellen Gelenkknorpelreparatur und die Korrelation und Validierung mit vier bereits etablierten makroskopischen Bewertungssystemen (O'Driscoll 1986; Noyes 1989; Smith 2005; Jung 2006; van den Borne 2007), sowie mit Untersuchungen im 9,4 T μ MRT (Batiste 2004; Krug 2009; Goebel 2012).

Die Untersuchungen erfolgten dazu an 38 vollschichtigen Gelenkknorpeldefekten aus medialen Femurkondylen, die verschiedene Reparaturstadien der Gelenkknorpeldefektreparatur darstellten. Ein Teil der osteochondralen Explantate ($n = 19$) wurde auch in einer Studie über den Einfluss der subchondralen Anbohrung auf die Mikroarchitektur des subchondralen Knochens (Orth 2012b) mittels μ CT analysiert.

Drei verschiedene Beobachter mit unterschiedlicher Erfahrung in der Knorpelforschung beurteilten mehrfach die makroskopische Knorpelreparatur zu verschiedenen Zeitpunkten ($n = 2$ bis 3). Das neu entwickelte makroskopische Bewertungssystem, das Protokoll A des (klinischen) ICRS-Systems (van den Borne 2007), das (klinische) Oswestry-Arthroscopie-System (van den Borne 2007), sowie die von Jung *et al.* (Jung 2006) und O'Driscoll *et al.* (O'Driscoll 1986) publizierten makroskopischen Bewertungssysteme für die Evaluation experimenteller Gelenkknorpelreparatur wurden angewendet und die einzelnen makroskopischen Parameter anschließend mit dem für die *ex vivo* Analyse adaptierten 2D MOCART-Bewertungssystem (Marlovits 2004; Marlovits 2006; Welsch 2009; Welsch 2011) als externem Referenzstandard, an Datensätzen aus Untersuchungen in einem 9,4 T μ MRT, korreliert (Goebel 2012).

Alle makroskopischen Bewertungssysteme zeigten eine hohe Intra- und Interbeobachter-Reliabilität und hohe interne Korrelationen. Der Intraklassenkorrelationskoeffizient (ICC) diente dabei als statistisches Verfahren zur Beschreibung einer Korrelation zwischen verschiedenen Beobachtern und Zeitpunkten (Shrout 1979). Das neu entwickelte makroskopische Bewertungssystem zeigte dabei für den Parameter "Gesamtpunktzahl" die höchste Intra- ($0,866 \leq \text{ICC} \leq 0,895$) und die höchste Interbeobachter-Reliabilität ($\text{ICC} = 0,905$). Die Anwendung von Cronbachs Alpha (Cronbach 1951) erfolgte zur Beurteilung der internen Konsistenz des neu entwickelten makroskopischen Bewertungssystems. Hier erbrachte ein mittleres Cronbachs Alpha von 0,782 den Nachweis einer guten Homogenität und Funktionsweise der einzelnen Parameter im neu entwickelten makroskopischen Bewertungssystem. Die "Gesamtpunktzahl" des 2D MOCART-Bewertungssystems korrelierte mit allen makroskopischen Bewertungssystemen ($P < 0,0001$). Das neu entwickelte makroskopische Bewertungssystem wies hierbei die höchste Korrelation mit dem μMRT -Parameter "Füllung des Defekts" (Spearman's rho = 0,765; $P < 0,0001$) auf.

Zusammenfassend wies diese Studie nach, dass "Gesamtpunktzahl" und "Füllung des Defekts", als zwei klinisch relevante Indikatoren der Knorpelreparatur, mit jedem der untersuchten makroskopischen Bewertungssysteme zuverlässig und direkt evaluiert werden können. Diese Ergebnisse unterstreichen den Wert makroskopischer Untersuchungen für die genaue Evaluation der Knorpelreparatur im präklinischen, translationalen Großtiermodell.

2D und 3D MOCART-Bewertungssysteme korrelieren mit elementaren und komplexen histologischen Bewertungssystemen - translationale Untersuchungen der osteochondralen Defektreparatur im 9,4 T μ MRT

Unter Anwendung des modifizierten 2D (Goebel 2012) und des neu adaptierten 3D MOCART-Systems (Welsch 2011; Goebel 2014) wurden die osteochondralen Einheiten von achtunddreißig Kondylen, die bereits für die Analyse der Korrelation des 2D MOCART-Bewertungssystems verwendet wurden (Goebel 2012), erneut untersucht. Zur Beurteilung der internen Korrelation beider Systeme erfolgte der Vergleich zwischen zwei Beobachtern und Zeitpunkten, sowie zwischen identischen Rekonstruktionen des 2D und 3D MOCART-Systems, als auch zwischen koronaren und sagittalen Rekonstruktionen innerhalb des 2D oder 3D MOCART-Systems. Nach Entkalkung der osteochondralen Explantate, Anfertigung koronarer Schnitte und Safranin-O- bzw. Hämatoxylin-Eosin-Färbung (Schmitz 2010; Orth 2012c) fand eine histologische Untersuchung der Gelenkknorpeldefekte durch Anwendung des elementarerer Wakitani- (Wakitani 1994) und des komplexeren Sellers-Systems (Sellers 1997) statt. Eine externe Korrelation der histologischen Untersuchungsergebnisse mit den sagittalen und koronaren Rekonstruktionen der 2D und 3D MOCART-Systeme des 9,4 T μ MRT erfolgte als letzter Schritt.

Der Nachweis hoher linearer Korrelationen zwischen den meisten Kategorien des 2D und 3D MOCART-Systems, sowie zwischen koronaren und sagittalen Rekonstruktionen innerhalb des 2D bzw. 3D MOCART-Systems, wurde erbracht, während die mittlere Gesamtpunktzahl des 3D MOCART-Systems für koronare und sagittale Rekonstruktionen durchschnittlich ca. 16 Punkte höher als im 2D MOCART-System lag. Durch eine Bland-Altman-Analyse (Bland 1986), die eine grafische Methode für den Vergleich zweier Messverfahren darstellt, und vor allem für den Vergleich neuer Messverfahren mit einem Goldstandard eingesetzt wird, konnte ein systemischer Fehler von 9-21 Punkten für koronare und 8-24 Punkten für sagittale Rekonstruktionen für den Vergleich des 3D mit dem 2D MOCART-System nachgewiesen werden. Dieser Fehler war für das gesamte Punktspektrum konstant.

„Defektfüllung“ und „Gesamtpunktzahl“ beider MOCART-Systeme korrelierten signifikant mit den entsprechenden Kategorien der Wakitani- und Sellers-Systeme (alle $P \leq 0,05$). Der Parameter „Subchondrale Knochenplatte“ korrelierte nur zwischen dem 3D MOCART- und dem Sellers-System ($P < 0,001$). Für das 3D MOCART-System waren die Korrelationen mit den histologischen Untersuchungen höher als mit dem 2D MOCART-System.

Diese Studie erbrachte den Nachweis einer hohen internen Korrelation zwischen den meisten Kategorien der 2D und 3D MOCART-Systeme. Untersucher müssen sich eines systemischen Fehlers bewusst sein, falls 2D und 3D MOCART-Daten verglichen werden sollen, da im 3D MOCART-System die Punktwerte im Schnitt höher liegen als im 2D MOCART-System. Histologische Kernparameter wie „Gesamtpunktzahl“ und „Defektfüllung“ konnten auch zuverlässig durch eine 9,4 T μ MRT-Untersuchung mittels 2D und 3D MOCART-System bestimmt werden. Der Parameter „Subchondrale Knochenplatte“ korrelierte nur für das 3D MOCART-System. Daher sollte dem 3D MOCART-System der Vorzug zur Analyse gegeben werden.

4.3 Diskussion

Der Schwerpunkt dieser Arbeit lag auf der Etablierung zweier hochauflösender bildgebender Verfahren zur Darstellung der osteochondralen Defektreparatur im translationalen Schafmodell. Durch Untersuchungen im μ CT erfolgte der Nachweis von Veränderungen der subchondralen Knochenplatte und der subartikulären Spongiosa in einem klinisch relevanten Zeitraum nach subchondraler Anbohrung. Ein neues makroskopisches Bewertungssystem wurde entwickelt und mit vier etablierten makroskopischen Bewertungssystemen korreliert. Daran schloss sich die Analyse der osteochondralen Einheiten aus den medialen Femurkorylen im 9,4 T μ MRT unter Anwendung des 2D MOCART-Systems an. Hier zeigten sich hohe Korrelationen zwischen den makroskopischen Bewertungssystemen sowie mit Schlüsselparametern des 2D MOCART-Systems. Nach erneuter Beurteilung der osteochondralen Defektreparatur durch die 2D und 3D MOCART-Bewertungssysteme erfolgte deren Vergleich mit einem elementaren und einem komplexen histologischen Bewertungssystem. Es fand der Nachweis hoher interner Korrelationen zwischen den 2D und 3D MOCART-Systemen statt, wobei ein systemischer Fehler bei dem Vergleich der beiden Systeme beachtet werden muss. Zusätzlich zeigten sich hohe Korrelationen mit Schlüsselparametern der histologischen Defektreparatur, sodass bereits durch die μ MRT-Untersuchung erste Aussagen über die zu erwartenden histologischen Untersuchungsergebnisse getroffen werden können.

Die Ergebnisse dieser Studien beschreiben erstens die Veränderungen des subchondralen Knochens und der subartikulären Spongiosa (Barou 2002; Chen 2009; Chen 2011; Orth 2012b; Orth 2013a; Chang 2014) nach Pridie-Bohrung zur Behandlung von vollschichtigen, fokalen Gelenkknorpeldefekten. Als Zweites erfolgte die Entwicklung eines neuen makroskopischen Bewertungssystems zur Beurteilung von fokalen Gelenkknorpeldefekten (Goebel 2012) und dessen Validierung an bereits etablierten makroskopischen Bewertungssystemen (O'Driscoll 1986; Smith 2005; Jung 2006; van den Borne 2007). Schließlich wurden die von Marlovits *et al.* (Marlovits 2004; Marlovits 2006) und Trattinig *et al.* (Trattinig 2009) entwickelten 2D und 3D MOCART-

Systeme für die *ex vivo* Analyse der osteochondralen Defektreparatur im 9,4 T μ MRT adaptiert (Goebel 2012; Goebel 2014; Roemer 2014). Es konnte ebenfalls nachgewiesen werden, dass Untersuchungen im 9,4 T μ MRT mit Kernparametern der makroskopischen (Goebel 2012) als auch der histologischen (Goebel 2014) Defektreparatur korrelieren. Somit schließt die μ MRT-Untersuchung die Lücke zwischen Makroskopie und Histologie und erlaubt die zerstörungsfreie Beurteilung der Gelenkknorpeldefektreparatur in verschiedenen dreidimensionalen Rekonstruktionen.

Markraumeröffnende Verfahren (Pridie 1959; Johnson 2001; Steadman 2002), wie sie zur Behandlung fokaler, vollschichtiger Knorpeldefekte angewendet werden, führen im translationalen Großtiermodell zu Veränderung der Mikroarchitektur des subchondralen Knochens (Feldkamp 1989; Chen 2009; Chen 2011; Fortier 2012; Orth 2012a; Zak 2014), die im μ CT nachweisbar sind und über mindestens 6 Monate *in vivo* bestehen (Orth 2012b). Orth *et al.* (Orth 2013a) beschreiben vier Kategorien von Veränderungen des subchondralen Knochens während der osteochondralen Defektreparatur: Das Voranschreiten der subchondralen Knochenplatte, die Bildung intraläsionaler Osteophyten, die Bildung subchondraler Knochenzysten sowie Veränderungen der knöchernen Mikroarchitekturparameter. Abhängig von der Art des markraumstimulierenden Verfahrens werden für die Mikrofrakturierung oder die Pridie-Bohrung unterschiedliche Reparaturmuster des subchondralen Knochens beschrieben (Chen 2009). Minas *et al.* (Minas 2009) berichtet über eine erhöhte Versagensrate der autologen Chondrozytentransplantation nach markraumstimulierenden Verfahren im Menschen während Dorotka *et al.* (Dorotka 2005) schlechtere histomorphometrische Ergebnisse der Gelenkknorpeldefektreparatur nachgewiesen hat. Allerdings werden auch nach einer autologen Chondrozytentransplantation Veränderungen des subchondralen Knochens, wie zum Beispiel das Voranschreiten der subchondralen Knochenplatte (Saris 2009), beschrieben (Orth 2013a).

Makroskopische Bewertungssysteme (O'Driscoll 1986; Noyes 1989; Smith 2005; Jung 2006; van den Borne 2007) stellen einfache und schnell anwendbare Möglichkeiten zur Beurteilung von Gelenkknorpeldefekten dar.

Obwohl im Rahmen von Arthroscopien regelhaft angewendet, sind wenige makroskopische Bewertungssysteme bis dato validiert worden (Smith 2005; van den Borne 2007). Daher ist ein neues makroskopisches Bewertungssystem entwickelt und mit etablierten makroskopischen Bewertungssystemen, sowie dem 2D MOCART-System im 9,4 T μ MRT, korreliert worden (Goebel 2012). Wenn eine Auflösung mit isometrischen Voxeln, wie hier von 120 x 120 x 120 μ m, gewählt wird, sind Rekonstruktionen in verschiedenen Ebenen ohne Informationsverlust möglich.

Die histologische Beurteilung von Gelenkknorpeldefekten ist in experimentellen Fragestellungen zur osteochondralen Reparatur Goldstandard (Wakitani 1994; Sellers 1997; Orth 2012c). Untersuchungen im 9,4 T μ MRT zeigten unter Anwendung der 2D und 3D MOCART-Systeme ebenfalls signifikante Korrelationen für „Defektfüllung“ und „Gesamtpunktzahl“ auf. Die „subchondrale Knochenplatte“ des Sellers-Systems korrelierte ebenfalls mit dem 3D MOCART-System (Goebel 2014).

4.4 Ausblick

Zukünftige Studien müssen den Effekt sowohl anderer markraumeröffnender Verfahren, wie der Mikrofrakturierung oder Abrasionsarthroplastik, als auch der autologen Chondrozytentransplantation auf den subchondralen Knochen untersuchen. Auch bleibt die Frage offen, welchen Effekt eine postoperative Entlastung der Defekte auf die Reparatur der subchondrale Knochenplatte bzw. subartikuläre Spongiosa hat. Ein weiteres Ziel liegt in der Anwendung neuer Untersuchungsmethoden im 9,4 T μ MRT, wie beispielsweise funktioneller als auch nicht-protonengebundener Bildgebung, und der Applikation von Kontrastmitteln, um Zielstrukturen besser darstellen zu können. Ferner müssen *in vivo* Untersuchungen im μ MRT die Anwendbarkeit der adaptierten 2D und 3D MOCART-Systeme bestätigen. Letztlich sollen die Ergebnisse in den klinischen Alltag eingebracht werden, mit dem Ziel bereits durch eine Magnetresonanztomografie eine Aussage über die histologischen Ergebnisse der Defektreparatur erhalten zu können.

4.5 Literaturverzeichnis

1. Barou O, Valentin D, Vico L, Tirode C, Barbier A, Alexandre C, Lafage-Proust MH (2002). High-resolution three-dimensional micro-computed tomography detects bone loss and changes in trabecular architecture early: comparison with DEXA and bone histomorphometry in a rat model of disuse osteoporosis. *Invest Radiol* 37:40-46.
2. Batiste DL, Kirkley A, Lavery S, Thain LM, Spouge AR, Gati JS, Foster PJ, Holdsworth DW (2004). High-resolution MRI and micro-CT in an ex vivo rabbit anterior cruciate ligament transection model of osteoarthritis. *Osteoarthritis Cartilage* 12:614-626.
3. Bland JM, Altman DG (1986). Statistical methods for assessing agreement between two methods of clinical measurement. *Lancet* 1:307-310.
4. Brittberg M, Lindahl A, Nilsson A, Ohlsson C, Isaksson O, Peterson L (1994). Treatment of deep cartilage defects in the knee with autologous chondrocyte transplantation. *N Engl J Med* 331:889-895.
5. Chang G, Xia D, Chen C, Madelin G, Abramson SB, Babb JS, Saha PK, Regatte RR (2014). 7T MRI detects deterioration in subchondral bone microarchitecture in subjects with mild knee osteoarthritis as compared with healthy controls. *J Magn Reson Imaging* 2014 Jun 30, doi: 10.1002/jmri.24683. Epub ahead of print.
6. Chen H, Chevrier A, Hoemann CD, Sun J, Ouyang W, Buschmann MD (2011). Characterization of subchondral bone repair for marrow-stimulated chondral defects and its relationship to articular cartilage resurfacing. *Am J Sports Med* 39:1731-1740.

7. Chen H, Sun J, Hoemann CD, Lascau-Coman V, Ouyang W, McKee MD, Shive MS, Buschmann MD (2009). Drilling and microfracture lead to different bone structure and necrosis during bone-marrow stimulation for cartilage repair. *J Orthop Res* 27:1432-1438.
8. Cronbach LJ (1951). Coefficient alpha and the internal structure of tests. *Psychometrika* 16:297-334.
9. Dorotka R, Bindreiter U, Macfelda K, Windberger U, Nehrer S (2005). Marrow stimulation and chondrocyte transplantation using a collagen matrix for cartilage repair. *Osteoarthritis Cartilage* 13:655-664.
10. Eldracher M, Orth P, Cucchiari M, Pape D, Madry H (2014). Small subchondral drill holes improve marrow stimulation of articular cartilage defects. *Am J Sports Med* 42:2741-2750.
11. Feldkamp LA, Goldstein SA, Parfitt AM, Jasion G, Kleerekoper M (1989). The direct examination of three-dimensional bone architecture in vitro by computed tomography. *J Bone Miner Res* 4:3-11.
12. Forney MC, Gupta A, Minas T, Winalski CS (2014). Magnetic Resonance Imaging of Cartilage Repair Procedures. *Magn Reson Imaging Clin N Am* 22:671-701.
13. Fortier LA, Cole BJ, McIlwraith CW (2012). Science and animal models of marrow stimulation for cartilage repair. *J Knee Surg* 25:3-8.
14. Garnov N, Grunder W, Thormer G, Trampel R, Turner R, Kahn T, Busse H (2013). In vivo MRI analysis of depth-dependent ultrastructure in human knee cartilage at 7 T. *NMR Biomed* 26:1412-1419.

15. Goebel L, Orth P, Müller A, Zurakowski D, Bucker A, Cucchiarini M, Pape D, Madry H (2012). Experimental scoring systems for macroscopic articular cartilage repair correlate with the MOCART score assessed by a high-field MRI at 9.4 T - comparative evaluation of five macroscopic scoring systems in a large animal cartilage defect model. *Osteoarthritis Cartilage* 20:1046-1055.
16. Goebel L, Zurakowski D, Müller A, Pape D, Cucchiarini M, Madry H (2014). 2D and 3D MOCART scoring systems assessed by 9.4 Tesla high-field MRI correlate with elementary and complex histological scoring systems in a translational model of osteochondral repair. *Osteoarthritis and Cartilage* 22:1386-95.
17. Gomoll AH, Madry H, Knutsen G, van Dijk N, Seil R, Brittberg M, Kon E (2010). The subchondral bone in articular cartilage repair: current problems in the surgical management. *Knee Surg Sports Traumatol Arthrosc* 18:434-447.
18. Hunziker EB (2007). Cartilage histomorphometry. *Methods Mol Med* 135:147-166.
19. Johnson LL (2001). Arthroscopic abrasion arthroplasty: a review. *Clin Orthop Relat Res* S306-317.
20. Jung M, Tuischer JS, Sergi C, Gotterbarm T, Pohl J, Richter W, Simank HG (2006). Local application of a collagen type I/hyaluronate matrix and growth and differentiation factor 5 influences the closure of osteochondral defects in a minipig model by enchondral ossification. *Growth Factors* 24:225-232.
21. Kangarlu A, Gahunia HK (2006). Magnetic resonance imaging characterization of osteochondral defect repair in a goat model at 8 T. *Osteoarthritis Cartilage* 14:52-62.

22. Krug R, Stehling C, Kelley DA, Majumdar S, Link TM (2009). Imaging of the musculoskeletal system in vivo using ultra-high field magnetic resonance at 7 T. *Invest Radiol* 44:613-618.
23. Madry H, Pape D (2008). Autologe Chondrozytentransplantation. *Der Orthopäde* 37:756-763.
24. Madry H, van Dijk CN, Mueller-Gerbl M (2010). The basic science of the subchondral bone. *Knee Surg Sports Traumatol Arthrosc* 18:419-433.
25. Madry H, Grün UW, Knutsen G (2011). Cartilage repair and joint preservation: medical and surgical treatment options. *Dtsch Arztebl Int* 108:669-677.
26. Marlovits S, Striessnig G, Resinger CT, Aldrian SM, Vecsei V, Imhof H, Trattnig S (2004). Definition of pertinent parameters for the evaluation of articular cartilage repair tissue with high-resolution magnetic resonance imaging. *Eur J Radiol* 52:310-319.
27. Marlovits S, Singer P, Zeller P, Mandl I, Haller J, Trattnig S (2006). Magnetic resonance observation of cartilage repair tissue (MOCART) for the evaluation of autologous chondrocyte transplantation: determination of interobserver variability and correlation to clinical outcome after 2 years. *Eur J Radiol* 57:16-23.
28. Martini L, Fini M, Giavaresi G, Giardino R (2001). Sheep model in orthopedic research: a literature review. *Comp Med* 51:292-299.
29. Minas T, Gomoll AH, Rosenberger R, Royce RO, Bryant T (2009). Increased failure rate of autologous chondrocyte implantation after previous treatment with marrow stimulation techniques. *Am J Sports Med* 37:902-908.

30. Moser E (2010). Ultra-high-field magnetic resonance: Why and when? *World J Radiol* 2:37-40.
31. Moser E, Stahlberg F, Ladd ME, Trattnig S (2012). 7-T MR - from research to clinical applications? *NMR Biomed* 25:695-716.
32. Müller R, Hahn M, Vogel M, Delling G, Ruegsegger P (1996). Morphometric analysis of noninvasively assessed bone biopsies: comparison of high-resolution computed tomography and histologic sections. *Bone* 18:215-220.
33. Noyes FR, Stabler CL (1989). A system for grading articular cartilage lesions at arthroscopy. *Am J Sports Med* 17:505-513.
34. O'Driscoll SW, Keeley FW, Salter RB (1986). The chondrogenic potential of free autogenous periosteal grafts for biological resurfacing of major full-thickness defects in joint surfaces under the influence of continuous passive motion. An experimental investigation in the rabbit. *J Bone Joint Surg Am* 68:1017-1035.
35. Ochs BG, Müller-Horvat C, Albrecht D, Schewe B, Weise K, Aicher WK, Rolaufts B (2011). Remodeling of articular cartilage and subchondral bone after bone grafting and matrix-associated autologous chondrocyte implantation for osteochondritis dissecans of the knee. *Am J Sports Med* 39:764-773.
36. Orth P, Cucchiarini M, Kaul G, Ong MF, Graber S, Kohn DM, Madry H (2012a). Temporal and spatial migration pattern of the subchondral bone plate in a rabbit osteochondral defect model. *Osteoarthritis Cartilage* 20:1161-1169.

37. Orth P, Goebel L, Wolfram U, Ong MF, Graber S, Kohn D, Cucchiari M, Ignatius A, Pape D, Madry H (2012b). Effect of Subchondral Drilling on the Microarchitecture of Subchondral Bone: Analysis in a Large Animal Model at 6 Months. *Am J Sports Med* 40:828-36.
38. Orth P, Zurakowski D, Wincheringer D, Madry H (2012c). Reliability, reproducibility and validation of five major histological scoring systems for experimental articular cartilage repair in the rabbit model. *Tissue Eng Part C Methods* 8:329-39.
39. Orth P, Cucchiari M, Kohn D, Madry H (2013a). Alterations of the subchondral bone in osteochondral repair-translational data and clinical evidence. *Eur Cell Mater* 25:299-316.
40. Orth P, Madry H (2013b). A low morbidity surgical approach to the sheep femoral trochlea. *BMC Musculoskelet Disord* 14:5.
41. Osterhoff G, Loffler S, Steinke H, Feja C, Josten C, Hepp P (2011). Comparative anatomical measurements of osseous structures in the ovine and human knee. *Knee* 18:98-103.
42. Pachowsky ML, Werner S, Marlovits S, Stelzeneder D, Renner N, Trattinig S, Welsch GH (2014). 3D-isotropic high-resolution morphological imaging and quantitative T2 mapping as biomarkers for gender related differences after matrix-associated autologous chondrocyte transplantation (MACT). *J Orthop Res* 32:1341-1348.
43. Pape D, Madry H (2013). The preclinical sheep model of high tibial osteotomy relating basic science to the clinics: standards, techniques and pitfalls. *Knee Surg Sports Traumatol Arthrosc* 21:228-236.
44. Pridie KH (1959). A Method of Resurfacing Osteoarthritic Knee Joints. *J Bone Joint Surg Br* 41-B:618-619.

45. Roemer FW, Guermazi A, Trattnig S, Apprich S, Marlovits S, Niu J, Hunter DJ, Welsch GH (2014). Whole joint MRI assessment of surgical cartilage repair of the knee: cartilage repair osteoarthritis knee score (CROAKS). *Osteoarthritis Cartilage* 22:779-799.
46. Saris DB, Vanlauwe J, Victor J, Almqvist KF, Verdonk R, Bellemans J, Luyten FP (2009). Treatment of symptomatic cartilage defects of the knee: characterized chondrocyte implantation results in better clinical outcome at 36 months in a randomized trial compared to microfracture. *Am J Sports Med* 37 Suppl 1:10S-19S.
47. Schmitz N, Lavery S, Kraus VB, Aigner T (2010). Basic methods in histopathology of joint tissues. *Osteoarthritis Cartilage* 18:S113-S116.
48. Sellers RS, Peluso D, Morris EA (1997). The effect of recombinant human bone morphogenetic protein-2 (rhBMP-2) on the healing of full-thickness defects of articular cartilage. *J Bone Joint Surg Am* 79:1452-1463.
49. Shrout PE, Fleiss JL (1979). Intraclass correlations: uses in assessing rater reliability. *Psychol Bull* 86:420-428.
50. Singh A, Haris M, Cai K, Kogan F, Hariharan H, Reddy R (2014). High resolution T1rho mapping of in vivo human knee cartilage at 7T. *PLoS One* 9:e97486.
51. Smith GD, Taylor J, Almqvist KF, Erggelet C, Knutsen G, Garcia Portabella M, Smith T, Richardson JB (2005). Arthroscopic assessment of cartilage repair: a validation study of 2 scoring systems. *Arthroscopy* 21:1462-1467.
52. Steadman JR, Rodkey WG, Briggs KK (2002). Microfracture to treat full-thickness chondral defects: surgical technique, rehabilitation, and outcomes. *J Knee Surg* 15:170-176.

53. Theysohn JM, Kraff O, Maderwald S, Kokulinsky PC, Ladd ME, Barkhausen J, Ladd SC (2013). MRI of the ankle joint in healthy non-athletes and in marathon runners: image quality issues at 7.0 T compared to 1.5 T. *Skeletal Radiol* 42:261-267.
54. Trattnig S, Domayer S, Welsch GW, Mosher T, Eckstein F (2009). MR imaging of cartilage and its repair in the knee-a review. *Eur Radiol* 19:1582-1594.
55. van den Bergen B, van den Berg CA, Klomp DW, Lagendijk JJ (2009). SAR and power implications of different RF shimming strategies in the pelvis for 7T MRI. *J Magn Reson Imaging* 30:194-202.
56. van den Borne MP, Raijmakers NJ, Vanlauwe J, Victor J, de Jong SN, Bellemans J, Saris DB (2007). International Cartilage Repair Society (ICRS) and Oswestry macroscopic cartilage evaluation scores validated for use in Autologous Chondrocyte Implantation (ACI) and microfracture. *Osteoarthritis Cartilage* 15:1397-1402.
57. Wakitani S, Goto T, Pineda SJ, Young RG, Mansour JM, Caplan AI, Goldberg VM (1994). Mesenchymal cell-based repair of large, full-thickness defects of articular cartilage. *J Bone Joint Surg Am* 76:579-592.
58. Wang M, Radjenovic A, Stapleton TW, Venkatesh R, Williams S, Ingham E, Fisher J, Jin Z (2010). A novel and non-destructive method to examine meniscus architecture using 9.4 Tesla MRI. *Osteoarthritis Cartilage* 18:1417-1420.
59. Welsch GH, Zak L, Mamisch TC, Resinger C, Marlovits S, Trattnig S (2009). Three-dimensional magnetic resonance observation of cartilage repair tissue (MOCART) score assessed with an isotropic three-dimensional true fast imaging with steady-state precession sequence at 3.0 Tesla. *Invest Radiol* 44:603-612.

60. Welsch GH, Zak L, Mamisch TC, Paul D, Lauer L, Mauerer A, Marlovits S, Trattnig S (2011). Advanced morphological 3D magnetic resonance observation of cartilage repair tissue (MOCART) scoring using a new isotropic 3D proton-density, turbo spin echo sequence with variable flip angle distribution (PD-SPACE) compared to an isotropic 3D steady-state free precession sequence (True-FISP) and standard 2D sequences. *J Magn Reson Imaging* 33:180-188.
61. Yan JY, Tian FM, Wang WY, Cheng Y, Song HP, Zhang YZ, Zhang L (2014). Parathyroid hormone (1-34) prevents cartilage degradation and preserves subchondral bone micro-architecture in guinea pigs with spontaneous osteoarthritis. *Osteoarthritis Cartilage* 22:1869-77.
62. Zak L, Krusche-Mandl I, Aldrian S, Trattnig S, Marlovits S (2014). Clinical and MRI evaluation of medium- to long-term results after autologous osteochondral transplantation (OCT) in the knee joint. *Knee Surg Sports Traumatol Arthrosc* 22:1288-1297.

5 Originalarbeiten

- I. Orth P, **Goebel L**, Wolfram U, Ong MF, Gräber S, Kohn D, Cucchiarini M, Ignatius A, Pape D, Madry H. Effect of subchondral drilling on the microarchitecture of subchondral bone: analysis in a large animal model at 6 months. Am J Sports Med, 2012, 40(4):828-36.

Reprinted from American Journal of Sports Medicine, Copyright © 2012, American Orthopaedic Society for Sports Medicine, doi: 10.1177/0363546511430376.

Effect of Subchondral Drilling on the Microarchitecture of Subchondral Bone

Analysis in a Large Animal Model at 6 Months

Patrick Orth,^{*,†} MD, Lars Goebel,^{*} Uwe Wolfram,[‡] PhD, Mei Fang Ong,[§] PhD, Stefan Gräber,[§] PhD, Dieter Kohn,[†] MD, Magali Cucchiari,^{*} PhD, Anita Ignatius,[‡] DVM, Dietrich Pape,^{||} MD, and Henning Madry,^{*,†||} MD
Investigation performed at Center of Experimental Orthopaedics, Saarland University, Homburg, Germany

Background: Marrow stimulation techniques such as subchondral drilling are clinically important treatment options for symptomatic small cartilage defects. Little is known about whether they induce deleterious changes in the subchondral bone.

Hypothesis: Subchondral drilling induces substantial alterations of the microarchitecture of the subchondral bone that persist for a clinically relevant postoperative period in a preclinical large animal model.

Study Design: Controlled laboratory study.

Methods: Standardized full-thickness chondral defects in the medial femoral condyles of 19 sheep were treated by subchondral drilling. Six months postoperatively, the formation of cysts and intralesional osteophytes was evaluated. A standardized methodology was developed to segment the ovine subchondral unit into reproducible volumes of interest (VOIs). Indices of bone structure were determined by micro-computed tomography (micro-CT).

Results: Analysis of the microarchitecture revealed the absence of zonal stratification in the ovine subarticular spongiosa, permitting an unimpeded and simultaneous analysis of the entire subchondral trabecular network. Subchondral drilling led to the formation of subchondral bone cysts (63%) and intralesional osteophytes (26%). Compared with the adjacent unaffected subchondral bone, drilling induced significant alterations in nearly all parameters for the microarchitecture of the subchondral bone plate and the subarticular spongiosa, most importantly in bone volume, bone surface/volume ratio, trabecular thickness, separation, pattern factor, and bone mineral density (BMD) (all $P \leq .01$).

Conclusion: The data show that the ovine subchondral bone can be reliably evaluated using micro-CT with standardized VOIs. We report that subchondral drilling deteriorates the microarchitecture both of the subchondral bone plate and subarticular spongiosa and decreases BMD. These results suggest that the entire osteochondral unit is altered after drilling for an extended postoperative period.

Clinical Relevance: The subchondral bone remains fragile after subchondral drilling for longer durations than previously expected. Further evaluations of structural subchondral bone parameters of patients undergoing marrow stimulation are warranted.

Keywords: marrow stimulation technique; subchondral drilling; micro-CT; subchondral bone; sheep

The subchondral bone, formed by the subchondral bone plate and the subarticular spongiosa,⁹ plays a key role in supporting the articular cartilage.²⁴ It transmits load and fulfills important metabolic functions within the osteochondral unit.²⁴ The subchondral bone plate is perforated when marrow stimulation techniques are applied to treat articular cartilage defects,^{36,43} allowing precursor cells from the bone marrow to migrate into the lesion.⁴¹ Subsequently, the remodeling of the subchondral bone proceeds along with the induction of chondrogenesis and fibrocartilaginous repair.⁴¹

Marrow stimulation techniques, such as subchondral drilling³⁶ or microfracture,⁴³ are important first-line treatment options for symptomatic small chondral defects^{13,29,38} and exhibit good clinical results.^{20,42} However, recent clinical evidence suggests that they may induce alterations in the subchondral bone plate such as intralesional osteophytes, which persist and may play a role in the degeneration of the repair tissue.^{7,28,47} Moreover, autologous chondrocyte implantation (ACI) for articular cartilage defects previously treated with marrow stimulation techniques has a 3-fold higher failure rate than for untreated defects,²⁸ suggesting an involvement of the subchondral bone in the inferior outcome of such essential second-line treatments.¹³

Although conventional computed tomography (CT) and magnetic resonance imaging (MRI) provide valuable

information about cartilage repair and the subchondral bone,^{30,47} these techniques give restricted information about the microstructure of the subchondral bone, which might be of prognostic value for patients undergoing subchondral drilling. High-resolution micro-CT is a powerful tool for the imaging of bone,¹⁰ allowing for an objective measurement of the 3-dimensional microarchitecture on a microscopic scale.³⁷ Micro-CT correlates not only with conventional 2-dimensional histomorphometry but also determines structural changes in bone in an even more precise fashion.³¹ Despite its importance, few clinical investigations have focused on the influence of marrow stimulation on the microarchitecture of the subchondral bone,^{7,28,29,47} and only recently, its effects in small animal models for up to 3 months postoperatively were reported.^{5,6} In particular, the effects of subchondral drilling on the subchondral microarchitecture after 6 months in a preclinical large animal model have not, to our best knowledge, been evaluated.

We hypothesized that subchondral drilling induces substantial and relevant alterations of the microarchitecture of the subchondral bone that persist for an extended postoperative period. To reflect the clinical situation¹ as closely as possible, a sheep model of a full-thickness chondral defect in the medial femoral condyle was chosen.

MATERIALS AND METHODS

Study Design

Chondral defects in the weightbearing area of the medial femoral condyles of sheep were treated by subchondral drilling. Analyses were performed after 6 months to allow for a clinically relevant assessment. The subchondral bone beneath the normal articular cartilage adjacent to the defects served as an intraindividual control group.

Animals

Twenty-three healthy, skeletally mature, Merino ewes aged between 2 and 4 years (mean body weight [BW], 70 ± 20 kg) received water ad libitum, were fed a standard diet, and were monitored at all times by a veterinary surgeon. All animal experiments were conducted in accordance with the national legislation on protection of animals and the National Institutes of Health (NIH) Guidelines for the Care and Use of Laboratory Animals (NIH Publication 85-23, Rev 1985) and were approved by the local governmental animal care committee. Osteoarthritis was excluded by

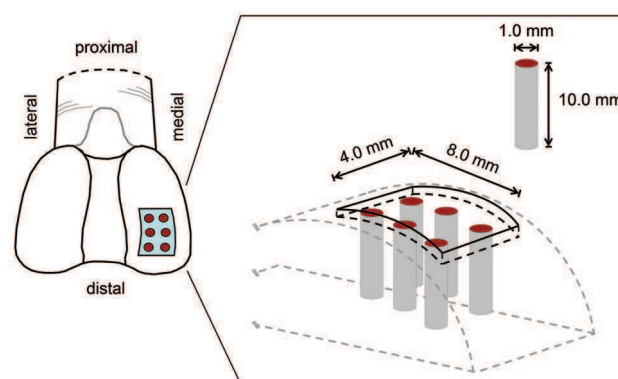


Figure 1. Schematic illustration of the surgical procedure on ovine femoral condyles. A rectangular 4 × 8-mm full-thickness chondral defect was created in the weightbearing zone of each of the 19 medial femoral condyles. In a 1-step marrow stimulation procedure, 6 subchondral drill holes were introduced within each defect to a depth of 10.0 mm using a 1.0-mm K-wire.

preoperative radiological examination. One animal (without operative treatment) served to determine a possible zonal stratification within the subarticular spongiosa of normal ovine subchondral bone.

Anesthesia, Surgery, and Postoperative Treatment

Following a 12-hour fast, animals were sedated with 2% Rompun (Bayer, Leverkusen, Germany) at 0.05 mg/kg BW and endotracheally intubated after intravenous administration of 20 mL of 2% propofol (AstraZeneca, Wedel, Germany) and carprofen (1.4 mg/kg BW; Pfizer, Berlin, Germany). Anesthesia was maintained by inhalation of 1.5% isoflurane (Baxter, Unterschleißheim, Germany) and intravenous administration of propofol (6–12 mg/kg BW/h).

The left stifle joints were entered through a medial parapatellar approach. The patella was dislocated laterally and the knee flexed to 90°. One small full-thickness chondral defect was created within the weightbearing zone of the medial condyle of the distal femur using a custom-made, rectangular 4 × 8-mm punch (Figure 1). The defect was outlined down to the cement line. The entire calcified cartilage layer was meticulously and completely removed using a rectangular curette. Six subchondral drill holes were introduced within each defect with a 1.0-mm Kirschner wire (K-wire) to a depth of 10 mm in a standardized fashion (Figure 1). No connection between the drill holes or collapse of the subchondral bone plate was observed. After thorough rinsing, the joint was closed in layers.

*Address correspondence to Henning Madry, MD, Center of Experimental Orthopaedics, Saarland University, Kirrberger Strasse, Building 37, D-66421 Homburg, Germany (e-mail:henning.madry@uks.eu).

[†]Center of Experimental Orthopaedics, Saarland University, Homburg, Germany.

[‡]Department of Orthopaedic Surgery, Saarland University Medical Center, Homburg, Germany.

[§]Institute of Orthopaedic Research and Biomechanics, Center for Musculoskeletal Research, University of Ulm, Ulm, Germany.

^{||}Institute of Medical Biometry, Epidemiology and Medical Informatics, Saarland University Medical Center, Homburg, Germany.

[¶]Olympic Medical Center, Centre Hospitalier de Luxembourg, Clinique d'Eich, Luxembourg, Luxembourg.

One or more of the authors has declared the following potential conflict of interest or source of funding: This work has been supported by the Deutsche Arbeitsgemeinschaft für Arthroskopie (AGA Forschungsförderung Nr. 29 to Dietrich Pape and Henning Madry). Drs Madry and Orth also received funding for subchondral bone research by the Gesellschaft für Orthopädisch-Traumatologische Sportmedizin.

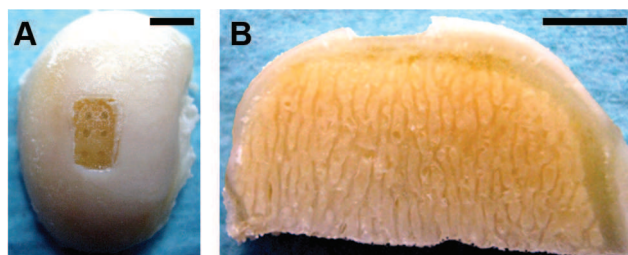


Figure 2. Macroscopic images of an ovine medial femoral condyle that underwent creation of standardized full-thickness cartilage defects (4×8 mm), treated by 6 subchondral drill holes per defect: (A) top view, (B) frontal plane with the trabecular subchondral network identifiable. Scale bar: 4.0 mm.

Postoperatively, 3 mL of 0.25% fentanyl/levomethadone (MSD, Unterschleißheim, Germany) and amoxicillin clavulanate (30 mg/kg BW; Pfizer) were administered. Carprofen (1.8 mg/kg BW) was administered subcutaneously for 2 weeks postoperatively. The animals were allowed immediate full weightbearing.

Because of wound infections, 3 animals were sacrificed between 1 and 6 weeks postoperatively and excluded. Six months after surgery, animals ($n = 20$) were sacrificed. The stifle joints were examined macroscopically, and the mean condylar width was determined (18.6 ± 1.4 mm). Macroscopic filling of the defects was graded by 3 independent investigators (0 points, repair tissue in level with adjacent cartilage; 1 point, $>50\%$ of defect depth or hypertrophy; 2 points, $\leq 50\%$ of defect depth; 3 points, 0% of defect depth; 4 points, subchondral bone damage). Medial femoral condyles were dissected in a standardized manner (Figure 2): The anterior parts of the defects (4×4 mm) were placed in 4% formalin for 24 hours and stored in 70% ethanol until further micro-CT analysis, while the posterior parts were subjected to analyses unrelated to this study.

Micro-CT Imaging

The specimens from medial femoral condyles of the 19 operated sheep and of 1 untreated sheep were scanned in a microfocused x-ray CT scanner (Skyscan 1172, Skyscan, Kontich, Belgium). The device possesses a moveable 10-MP camera and an x-ray tube ($<5\text{-}\mu\text{m}$ spot size; Hamamatsu, Hamamatsu City, Japan), allowing for a maximal nominal resolution below $0.8\text{ }\mu\text{m}$.

For the acquisition of 16-bit x-ray shadow transmission images (1000–1100 per specimen), the tube voltage was set at 70 kV, and the current was 140 μA . All specimens were scanned within 70% ethanol at a spatial resolution of $15\text{ }\mu\text{m}$. Projections were obtained at 0.4° intervals with 1770-millisecond exposure time and a combined 0.5-mm aluminum/copper filter interposed. Ring artifact correction, frame averaging, and random movement were engaged (4, 3, and 15, respectively, no units). Images were reconstructed by a modified Feldkamp cone-beam algorithm¹⁰ (NRecon, Skyscan). Frontal sections were used for further evaluation.

Thresholding levels of gray values, which mimic bone as closely as possible (range, 89–255), were set for segmentation of binary images. To express gray values as mineral content (bone mineral density [BMD]), calcium hydroxyapatite (CaHA) phantom rods immersed in 70% ethanol with known BMD values (250 and 750 mg CaHA/ cm^3) were employed for calibration.

Subchondral Bone Cysts and Intralesional Osteophytes

To distinguish between drill holes and cyst formation (DataViewer, Skyscan), the minimum diameter of cysts was 3.0 mm (triple diameter of drill holes). Cysts were rated on a scale of 1 to 4 based on their horizontal diameter, applying a modified scoring system¹⁵ (1, horizontal cyst diameter <4.0 mm; 2, <5.0 mm; 3, <6.0 mm; 4, >6.0 mm) (Appendix 1, available in the online version of this article at <http://ajs.sagepub.com/supplemental/>). Within a depth of 10.0 mm (corresponding to the depth of the drill holes), the maximal vertical cyst diameter was also determined (Appendix 1, available online).

Intralesional osteophytes were defined as newly formed bone apical to the cement line, projected into the cartilage layer. No minimum level was defined for the size of osteophytes (Figure 3). Osteophyte location was either central (between drill holes) or peripheral (between drill hole and adjacent subchondral bone plate) (Appendix 1, available online).

Standardized Definition of Volumes of Interest

To evaluate the microarchitecture of normal subchondral bone plate and to determine possible zonal stratification within the subarticular spongiosa of untreated condyles ($n = 2$), volumes of interest (VOIs) were defined as follows: For the subchondral bone plate, its borders were traced using analysis software (CTAnalyzer, Skyscan). Anatomic landmarks such as the cement line (apical) and the subarticular spongiosa (basal) were respected (Figure 4). Three VOIs with identical thickness were then positioned in parallel and on top of each other within the subarticular spongiosa, named zone 1 (apical), zone 2 (middle), and zone 3 (basal) (Figure 4).

A standard for the definition and location of 6 comparable VOIs was developed to allow for a reproducible micro-CT evaluation of ovine subchondral bone (Figure 5): based on the size of the original defects and allowing a safety margin to the cutting planes of the specimens, standardized dimensions of 3.5 mm in width (frontal plane) and length (sagittal plane) were set for all VOIs. The VOI “subchondral bone plate–defect” (SBP-defect) involves exclusively the subchondral bone plate within the defect. “Subarticular spongiosa–defect” (SAS-defect) was located strictly basally to the SBP-defect within trabecular bone. The total depth (apical-basal orientation) of these 2 VOIs did not exceed 10 mm, corresponding to the depth of the drill holes. The VOIs “subchondral bone plate–lateral” (SBP-lateral) and “subchondral bone plate–medial” (SBP-medial) were placed within the subchondral bone plate neighboring the

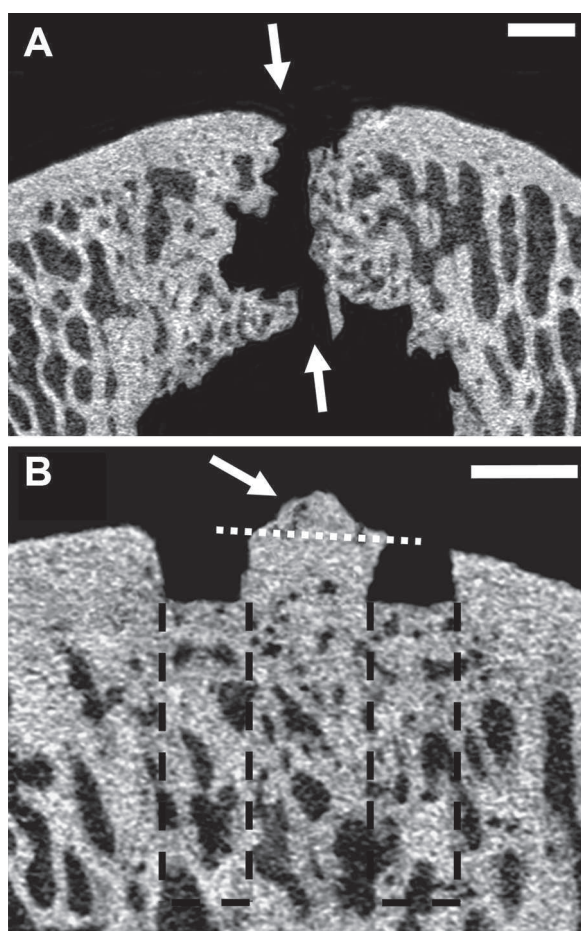


Figure 3. Representative micro-CT images of subchondral bone cysts (A) and intralesional osteophytes (B; arrowhead) in the frontal plane. (A) Cysts always originated from the drilling canal (arrowheads: proximal and distal canal openings). The funnel-shaped loss of subchondral bone tissue (apical opening of the drill hole) shows no callus formation and represents an area of bone resorption. (B) Openings of the former drill holes (black dashed lines) can still be identified. Intralesional osteophytes protruded into the cartilage defects originating from the former cement line (white dotted line). Scale bar: 1.0 mm.

SBP-defect lateral or medial. Beneath SBP-lateral and SBP-medial, “subarticular spongiosa–lateral” (SAS-lateral) and “subarticular spongiosa–medial” (SAS-medial) adjoined. Cysts were excluded, and overlapping of individual VOIs was avoided (Figure 5). A total of 122 standardized VOIs (19 operated condyles with 6 VOIs each; 2 untreated condyles with 4 VOIs each) were defined independently by 2 investigators (L.G. for 11 animals and P.O. for 8 animals) (Appendix 2, available online).

First, differences in subchondral microarchitecture between unaffected bone neighboring the defects laterally (SBP-lateral, SAS-lateral) and medially (SBP-medial, SAS-medial) were evaluated. Second, to test the standardized VOI definition in ovine subchondral bone for reproducibility, micro-CT indices of untreated regions (SBP-lateral, SBP-

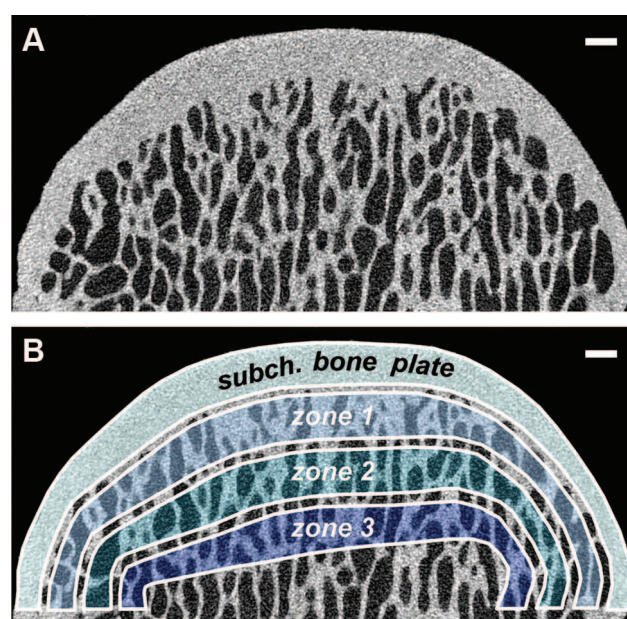


Figure 4. To analyze the microarchitecture of the subchondral bone plate and to detect a possible zonal stratification within untreated subarticular spongiosa, the volumes of interest “subchondral bone plate,” “zone 1,” “zone 2,” and “zone 3” were defined. No major structural differences were observed between zones 1 to 3. Scale bar: 1.0 mm.

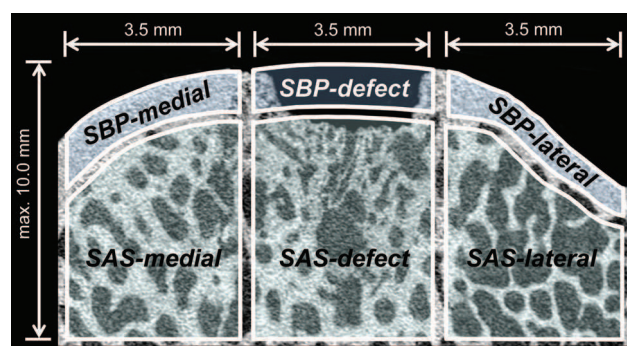


Figure 5. Standardized regions of interest for the evaluation of subchondral bone changes following subchondral drilling. Six standardized volumes of interest were defined on micro-CT images. SBP, subchondral bone plate; SAS, subarticular spongiosa; SBP-defect/SAS-defect, subchondral bone within the drilled defect area; SBP-lateral/SAS-lateral, situated lateral to the defects; SBP-medial/SAS-medial: situated medial to the defects. At the level of the subchondral bone plate, all micro-CT parameters varied significantly between defects and adjacent bone plate. In agreement, for the subarticular spongiosa, most parameters confirmed alterations resulting from drilling (Table 2).

medial, SAS-lateral, and SAS-medial) were compared between the 2 independent investigators. Third, to assess the effect of subchondral drilling on the subchondral bone, micro-CT results of defect areas (SBP-defect and SAS-defect)

TABLE 1
Descriptive Presentation of Micro-Computed Tomography Parameters of Volumes of Interest (VOIs)
Within Normal, Untreated Ovine Condyles^a

Parameter	VOI, mean \pm standard deviation			
	Subchondral Bone Plate	Zone 1	Zone 2	Zone 3
BMD, mg/cm ³	809.34 \pm 156.50	785.98 \pm 140.73	784.83 \pm 135.04	782.52 \pm 128.79
BV/TV, %	92.22 \pm 0.50	44.07 \pm 0.11	40.54 \pm 1.14	37.71 \pm 1.72
BS/BV, mm ⁻¹	9.69 \pm 1.77	19.85 \pm 1.27	21.01 \pm 0.47	21.68 \pm 0.20
BS/TV, mm ⁻¹	8.94 \pm 1.68	8.75 \pm 0.54	8.52 \pm 0.43	8.18 \pm 0.45
Ct.Th, mm	0.19 \pm 0.03	NA	NA	NA
Tb.Th, mm	NA	0.15 \pm 0.01	0.15 \pm 0.01	0.14 \pm 0.01
Tb.Sp, mm	NA	0.31 \pm 0.01	0.29 \pm 0.01	0.29 \pm 0.01
Tb.Pf, mm ⁻¹	NA	-11.17 \pm 5.43	-8.16 \pm 5.95	-6.50 \pm 5.20
Tb.N, mm ⁻¹	NA	2.96 \pm 0.28	2.77 \pm 0.29	2.61 \pm 0.27
SMI, -/-	NA	-1.57 \pm 1.02	-0.85 \pm 1.23	-0.50 \pm 1.08
DA, -/-	NA	0.94 \pm 0.08	0.88 \pm 0.01	0.83 \pm 0.02
FD, -/-	NA	2.34 \pm 0.05	2.31 \pm 0.05	2.29 \pm 0.05

^aZones 1 to 3 of subarticular spongiosa represent VOIs of the same thickness than the cortical subchondral bone plate. Bone mineral density and bone volume were higher in cortical than in trabecular subchondral bone. No apparent differences in micro-computed tomography indices were detected between zones 1, 2, and 3, indicating the absence of zonal stratification within the subarticular spongiosa. Values are given as mean \pm standard deviation. BMD, bone mineral density; BV/TV, bone volume fraction; BS/BV, bone surface/volume ratio; BS/TV, bone surface density; Ct.Th, cortical thickness; Tb.Th, trabecular thickness; Tb.Sp, trabecular separation; Tb.Pf, trabecular pattern factor; Tb.N, trabecular number; SMI, structure model index; DA, degree of anisotropy; FD, fractal dimension; NA, not applicable (parameters for trabecular subarticular spongiosa not suitable for cortical subchondral bone plate and vice versa).

were compared with adjacent, unaffected bone (SBP-lateral/medial: SBP-adjacent; SAS-lateral/medial: SAS-adjacent).

significant. All calculations were made with SPSS (Version 17.0, SPSS Inc, Chicago, Illinois).

Micro-CT Structure Indices

The following 3-dimensional structural parameters were determined in all standardized VOIs using the software provided by the manufacturer (CTAnalyzer, Skyscan): BMD, bone volume fraction (BV/TV), bone surface/volume ratio (BS/BV), and bone surface density (BS/TV). Cortical thickness (Ct.Th) was evaluated only within the subchondral bone plate, while trabecular thickness (Tb.Th), trabecular separation (Tb.Sp), trabecular pattern factor (Tb.Pf), trabecular number (Tb.N), structure model index (SMI), degree of anisotropy (DA), and fractal dimension (FD) were assessed in the subarticular spongiosa. All parameters were computed in a direct 3-dimensional fashion without any model assumptions required for 2-dimensional analysis.

Statistical Analysis

Comparison of micro-CT indices between 2 independent investigators (Appendix 2, available online) was performed using the Mann-Whitney *U* test. Results of the micro-CT evaluation of normal ovine condyles (*n* = 2) are presented in a descriptive fashion (Table 1). Comparison of micro-CT indices (1) within VOIs comprising adjacent (lateral vs medial) subchondral bone (Table 2) and (2) between defects and unaffected subchondral bone (Table 2) was evaluated using the Wilcoxon test. Correlation between macroscopic fill grade and BMD and BV/TV was tested applying Pearson correlation coefficients (*r*). A value of *P* < .05 was considered

RESULTS

Macroscopic Examination of the Stifle Joints

Six months postoperatively, no joint effusion, macroscopic inflammation, periarticular osteophytes, or adhesions were observed. The defects could always be identified. The color of the repair tissue varied between translucent and white. In most defects, filling was insufficient; sometimes the defect extended into the adjacent cartilage. No collapse of the subchondral bone plate was observed.

Subchondral Bone Cysts and Intralesional Osteophytes

Subchondral cysts or intralesional osteophytes were present in 74% of all treated condyles. Five of the 19 joints (26%) exhibited neither cysts nor osteophytes.

Bone cysts always originated from the canal of the K-wire. A total of 16 single subchondral bone cysts were detected in 12 condyles (63% of all specimens; *n* = 19). Two cysts were present in 4 of the condyles (Figure 3A). Most of the cysts were less than 4.0 mm in diameter. Only one cyst had a horizontal diameter of larger than 6.0 mm (Appendix 1, available online). In the case when 2 subchondral cysts were present in one condyle, they were mostly small. There was no difference between mean vertical and horizontal cyst diameters (4.3 and 4.2 mm, respectively; *P* > .05) (Appendix 1, available online).

TABLE 2
Comparison of Micro-Computed Tomography Parameters Between Volumes of Interest (VOIs)
Neighboring the Defect Sites Laterally or Medially and VOIs Comprising the Subchondral
Bone Beneath Drilled Cartilage Defects and Adjacent, Unaffected Subchondral Bone^a

Parameter	VOI, mean \pm standard deviation											
	SBP-Lateral	SBP-Medial	<i>P</i>	SBP-Adjacent	SBP-Defect	<i>P</i>	SAS-Lateral	SAS-Medial	<i>P</i>	SAS-Adjacent	SAS-Defect	<i>P</i>
BMD, mg/cm ³	919.87 \pm 26.62	925.32 \pm 33.64	.58	922.59 \pm 30.05	861.24 \pm 41.07	<.001	890.25 \pm 39.89	897.90 \pm 40.83	.56	894.08 \pm 40.00	843.36 \pm 36.52	<.001
BV/TV, %	97.20 \pm 1.58	95.80 \pm 4.08	.21	96.50 \pm 3.13	45.15 \pm 27.13	<.001	58.26 \pm 9.49	53.90 \pm 12.25	.10	56.08 \pm 11.03	44.83 \pm 11.49	.01
BS/BV, mm ⁻¹	6.68 \pm 1.56	9.20 \pm 3.96	.01	7.94 \pm 3.23	18.91 \pm 11.68	<.001	14.34 \pm 2.76	13.55 \pm 2.25	.47	13.94 \pm 2.51	17.42 \pm 3.90	.001
BS/TV, mm ⁻¹	6.47 \pm 1.39	8.67 \pm 3.20	.01	7.57 \pm 2.68	6.08 \pm 1.86	.03	8.19 \pm 1.34	7.13 \pm 1.22	.01	7.66 \pm 1.37	7.51 \pm 1.36	.89
Ct.Th, mm	0.31 \pm 0.07	0.28 \pm 0.06	.17	0.29 \pm 0.07	0.22 \pm 0.06	<.001	NA	NA		NA	NA	
Tb.Th, mm	NA	NA		NA	NA		0.21 \pm 0.03	0.22 \pm 0.04	.18	0.22 \pm 0.04	0.18 \pm 0.03	<.001
Tb.Sp, mm	NA	NA		NA	NA		0.25 \pm 0.05	0.33 \pm 0.12	.01	0.29 \pm 0.10	0.48 \pm 0.21	.001
Tb.Pf, mm ⁻¹	NA	NA		NA	NA		-9.46 \pm 7.90	-8.97 \pm 7.97	.57	-9.21 \pm 7.83	-12.73 \pm 6.91	.01
Tb.N, mm ⁻¹	NA	NA		NA	NA		2.81 \pm 0.57	2.46 \pm 0.65	.06	2.64 \pm 0.63	2.46 \pm 0.56	.26
SMI, -/-	NA	NA		NA	NA		-1.87 \pm 1.97	-1.89 \pm 2.53	.89	-1.88 \pm 2.24	-1.96 \pm 1.65	.95
DA, -/-	NA	NA		NA	NA		0.29 \pm 0.13	0.37 \pm 0.13	.04	0.33 \pm 0.14	0.27 \pm 0.10	.08
FD, -/-	NA	NA		NA	NA		2.27 \pm 0.08	2.24 \pm 0.09	.12	2.26 \pm 0.09	2.34 \pm 0.08	<.001

^aWithin the subchondral bone plate (SBP) and the subarticular spongiosa (SAS), most indices did not exhibit significant differences between lateral (SBP-L, SAS-L) and medial (SBP-M, SAS-M); bone mineral density values did not vary significantly. The subchondral bone plate and subarticular spongiosa treated by subchondral drilling exhibited significantly different indices compared to the untreated subchondral bone. Results were considered significantly different for $P < .05$. BMD, bone mineral density; BV/TV, bone volume fraction; BS/BV, bone surface/volume ratio; BS/TV, bone surface density; Ct.Th, cortical thickness; Tb.Th, trabecular thickness; Tb.Sp, trabecular separation; Tb.Pf, trabecular pattern factor; Tb.N, trabecular number; SMI, structure model index; DA, degree of anisotropy; FD, fractal dimension; NA, not applicable (parameters for trabecular subarticular spongiosa not suitable for cortical subchondral bone plate and vice versa).

Intralesional osteophytes emerged either in the central ($n = 4$) or peripheral part ($n = 2$) of the subchondral bone plate, never above the drill holes. A total of 6 intralesional osteophytes were detected within 5 defects (26% of all specimens) (Figure 3B). In one defect, osteophytes appeared both in a central and peripheral location (Appendix 1, available online).

Zonal Stratification Within the Subarticular Spongiosa in Normal Condyles

Among the 3 zones defined (Figure 4), only the Tb.Pf and SMI decreased from apical (zone 1) to basal (zone 3) (Table 1). No other evidence for structural alterations within the subarticular spongiosa from apical to basal was detected. In particular, BMD values remained constant within the entire subarticular spongiosa.

Analysis of the Subchondral Bone Adjacent to the Defects

At the level of the subchondral bone plate, most structure indices remained constant between VOIs neighboring the defects lateral or medial (Figure 5), except for BS/BV and BS/TV values, which were elevated ($P = .01$) in the medial subchondral bone plate (Table 2). Within the adjacent subarticular spongiosa, the majority of structure indices, including BMD, also did not differ between medial and lateral. The BS/TV was only 1.1-fold higher, and Tb.Sp as well as the DA was 1.3-fold lower when comparing lateral with medial subarticular spongiosa (all $P < .05$) (Table 2). Most importantly, BMD remained constant between lateral and medial cortical (920 ± 27 vs 925 ± 35 mg CaHA/cm³) and trabecular ($890 \pm$

40 vs 898 ± 41 mg CaHA/cm³) subchondral bone, as indicated by the small standard deviations (Table 2).

Reproducibility of the Definition of VOIs

Independent VOI definition by 2 investigators yielded similar results for micro-CT parameters in unaffected subchondral bone (Appendix 2, available online). Except for BMD values (909 ± 31 vs 948 ± 23 mg CaHA/cm³) in the medial subchondral bone plate ($P = .01$), no significant differences were found for structure indices between both investigators (all other $P > .05$), indicating a good reproducibility of the described method.

Influence of Drilling on Subchondral Bone Structure Indices

When the subchondral bone was perforated by subchondral drilling, micro-CT analysis revealed highly significant differences in most parameters of microarchitecture compared with the adjacent regions (Table 2 and Figure 6). Within the subchondral bone plate, BMD, BV/TV, and Ct.Th decreased up to 2.1-fold after subchondral drilling compared with the subchondral bone plate of the adjacent regions (all $P < .001$). In contrast, BS/BV increased 2.4-fold after drilling ($P < .001$).

In good agreement with these data, BMD and BV/TV were decreased within the subarticular spongiosa within the regions of drilling (Figure 6), while BS/BV was increased (Table 2). Notably, Tb.Sp was 1.7-fold elevated, consistently with the lower Tb.Th in the regions subjected to drilling. Surprisingly, Tb.Pf, an inverse index of connectivity, was 1.4-fold decreased ($P = .01$), indicating an

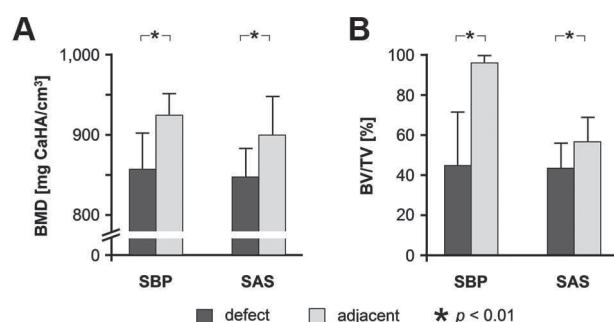


Figure 6. Influence of subchondral drilling on bone mineral density and bone volume of the subchondral unit. The subchondral bone plate (SBP-defect) and subarticular spongiosa (SAS-defect) subjected to Pridie drilling exhibited a significant decrease in bone mineral density (A) and bone volume fraction (B) when compared with the untreated subchondral bone plate (SBP-adjacent) and untreated subarticular spongiosa (SAS-adjacent), respectively. Values are given as mean \pm standard deviation.

increased connectivity within trabecular subchondral bone after Pridie drilling.

Pearson correlation coefficients between the macroscopic fill grade of the cartilage lesions and BMD or BV/TV were low for the subchondral bone plate (both $r = .40$) and the subarticular spongiosa ($r = .23$ and $r = -.03$, respectively).

DISCUSSION

In the present study, the effect of subchondral drilling on the microarchitecture of the subchondral bone beneath a full-thickness cartilage defect was evaluated in a preclinical large animal model after 6 months *in vivo*. A standardized methodology for micro-CT analysis of ovine subchondral bone was developed and its reproducibility confirmed. A possible structural zonal stratification of the microarchitecture of normal subarticular spongiosa was ruled out. The data show that drilling induces the formation of intralesional osteophytes and subchondral bone cysts. Most importantly, the data reveal that 6 months postoperatively, bone volume and mineral density of the subchondral bone below a cartilage defect are still significantly decreased, indicating a reduced degree of mineralization at this time point. Consequently, the original microarchitecture of the subchondral bone is not re-established 6 months after subchondral drilling in this *in vivo* model.

Many of the experimental studies on the effect of marrow stimulation techniques^{13,29} were performed in the rabbit model and have focused on the articular cartilage.^{25,27} Only a few investigations of the subchondral bone after marrow stimulation were performed in a large animal model.^{8,48} Chen et al⁶ studied bone compaction around lapine subchondral defects created by marrow stimulation using micro-CT and found incomplete reconstitution of normal bone structure and continued remodeling after 3 months.⁵ To evaluate effects of subchondral drilling at

a later time in a preclinical model, the present study was performed after 6 months in sheep. Concerning the joint surface, this model resembles the human knee joint¹¹ more closely than that of a small animal.

As high-resolution CT correlates significantly with conventional histomorphometry^{2,31} and allows for a noninvasive depiction of osseous microarchitecture³⁷ using standardized parameters,³⁵ no additional histological evaluation was performed here. Because bone strength is not only determined by bone mass but also by its 3-dimensional structure and degree of mineralization,⁴⁴ micro-CT indices may provide further insights into failure mechanisms of subchondral bone.^{14,33}

In the present study, arthrotomy and subchondral drilling of chondral defects did not induce thickening of the subchondral bone plate. Bone cysts (63%) formed more frequently than intralesional osteophytes (26%). The development of these osteophytes after drilling shares similarities with the formation of fracture callus⁴⁵ and occurs more frequently in humans than in sheep, reported in 54% to 70% after microfracture⁷ or ACI.⁴⁷ Subchondral cysts are thought to be caused by an influx of synovial fluid into the subarticular bone,⁴⁶ which may have been facilitated by the surgical perforation of the subchondral bone plate. In sheep, cyst formation occurred in 50% of untreated osteochondral defects.⁴⁰ In patients, their incidence is reduced.²⁹ Vasiliadis et al⁴⁷ identified cysts in 39% of human knees after ACI. Possible explanations include species differences, the nature of the synovial fluid, the thickness of the subchondral bone plate, the presence of microcracks,⁴ or differences in weightbearing (immediately postoperative for the animals in contrast to the limited weightbearing for several weeks in patients).³

The result of a micro-CT analysis depends on the location of VOIs. In particular, a pre-existing microarchitectural pattern in cortical or trabecular subchondral bone may bias the obtained findings and therefore must be identified. For example, Macneil and Boyd²³ compared 9-mm sections of the distal radius using micro-CT and found regional differences that are relevant for clinical BMD measurements. Marchand et al²⁵ described a standardized micro-CT analysis to evaluate a narrow rim (1 mm) of lapine subchondral bone at day 1 after drilling. In the present study, care was taken to analyze in detail the microarchitecture directly beneath the subchondral bone plate and to a depth sufficient to display drilling-induced and clinically relevant structural alterations. Here, zones 1 to 3 comprise approximately the triple thickness of the subchondral bone plate and correspond to the depth of the drill holes. Within these regions, most indices, including BMD, remained constant, suggesting that there is no layered or columnar stratification pattern within ovine subarticular spongiosa.

A standard was established to reproducibly define VOIs comprising either defects or adjacent (lateral/medial) cortical and trabecular subchondral bone. In unaffected bone (SBP-adjacent, SAS-adjacent), micro-CT parameters are expected to remain constant between different specimens: Because of breeding and domestication, genetic and biological diversity of sheep is decreased, resulting in a lower biological variability that renders variances in subchondral microarchitecture

unlikely.²¹ Here, micro-CT indices of untreated subchondral bone were similar for 2 independent investigators, suggesting that VOI definition in ovine subchondral bone is reproducible and comparable with previous results.²⁵

Different choices of negative controls were available to design the present study, the most important of which being either to compare microstructural parameters from the subchondral bone of the defect site with the adjacent regions within the same animal or to omit the marrow stimulation procedure after defect creation. The latter would have required either additional animals receiving defects in an identical location that would have been left untreated or additional defects in a different location of the femoral condyle of the same animals. Importantly, subchondral drilling results in the formation of a repair tissue filling the defect, while untreated chondral defects remain empty.^{16,19} These discrepancies in cartilage repair would have added another variable (ie, the repair tissue) that potentially might have complicated the validation of the findings. Such a setting would have led to comparing the Pridie drilling group (repair tissue layer) with an untreated control group (no repair tissue). As negative controls should not produce a change from the normal state,¹⁸ we chose to obtain baseline data by selecting an intraindividual approach in which the defect site was compared with the adjacent bone of the same condyle after ruling out possible zonal differences therein, allowing for a high degree of resemblance.

Subchondral drilling resulted in significant changes in the microarchitecture of the subchondral bone such as reduced mineralization, bone volume, and Ct.Th as well as increased BS/BV of the subchondral bone plate. Simultaneously, trabeculae of the subarticular spongiosa were significantly thinner and more complex, while voids were enlarged. Interestingly, connectivity of the subarticular spongiosa was increased, indicated by the decreased Tb.Pf. This finding might reflect an attempt to stabilize the perforated subarticular spongiosa despite decreased Tb.Th and increased separation.

The obtained BMD values of untreated bone are supported by recent data for ovine femora (730-1050 mg CaHA/cm³)²⁶ or vertebrae (1020-1330 mg CaHA/cm³).⁴⁹ The BS/TV values were consistent with conventional histomorphometry of ovine spongiosa (24%-58%).^{40,48} Values for BS/TV (49%) and Tb.Th (0.23 mm) of the human distal radius²² are also comparable with the present data for sheep. Therefore, the results of this animal study may be of value to shed light on the clinical problem of subchondral bone changes in patients.

Taken together, the data suggest that subchondral drilling in patients does not solely induce changes in the microarchitecture of the subchondral bone such as intralesional osteophytes but also weakens the entire osteochondral unit. Interestingly, this impairment of subchondral bone integrity did not correlate with the macroscopic filling of the cartilage lesion. Therefore, (arthroscopic) visualization of cartilage defects in patients might be insufficient to comprehensively evaluate osteochondral repair. While a direct translation into the clinical situation is limited, these data support the concept that the subchondral bone remains fragile after drilling for longer periods than previously expected. In

accordance, Gill et al¹² reported resorption of subchondral bone 6 weeks after microfracture for full-thickness cartilage defects but found subchondral bone reconstitution by 12 weeks in primates. In goats, immediate full weightbearing of untreated osteochondral defects led to inferior subchondral bone repair after 1 year.¹⁷ From a clinical standpoint, these findings suggest that the postoperative phase of restricted weightbearing may be necessary not only to support articular cartilage repair but also to protect the remodeling of the subchondral bone. Here, immediate weightbearing and full range of motion may have exerted harsh biomechanical and biological conditions to the lesions, unlike in a clinical setting. Thus, although restricted weightbearing may be difficult to achieve in animals, future studies will have to assess the effect of different rehabilitation protocols,³ together with the influence of defect depth and size, on subchondral bone restoration: In patients, a defect size of maximal 400 mm² is recommended for marrow stimulation techniques.^{13,28} As the defects created in the present study were comparably small (32 mm²; ovine medial condylar width: 19 mm^{34,39}) compared with the human medial condylar width of 27 mm,^{32,34} subchondral bone changes in larger defects still have to be evaluated.

CONCLUSION

In conclusion, micro-CT allows us to reliably evaluate the microarchitecture of the subchondral bone in a preclinical large animal model. A standardized methodology capable of defining relevant VOIs and depicting subchondral bone alterations after subchondral drilling was developed. Micro-CT analysis revealed the absence of zonal stratification in the ovine subarticular spongiosa, permitting an unimpeded and simultaneous analysis of the entire subchondral trabecular network. Pridie drilling frequently leads to the formation of subchondral bone cysts and intralesional osteophytes in sheep. Most importantly, drilling weakens the entire microarchitecture of the cortical and trabecular subchondral bone. These substantial and relevant alterations of the subchondral bone persist for an extended postoperative period. Further investigations on microarchitectural alterations of the subchondral bone in patients undergoing marrow stimulation are warranted.

REFERENCES

1. Aroen A, Loken S, Heir S, et al. Articular cartilage lesions in 993 consecutive knee arthroscopies. *Am J Sports Med.* 2004;32(1):211-215.
2. Barou O, Valentin D, Vico L, et al. High-resolution three-dimensional micro-computed tomography detects bone loss and changes in trabecular architecture early: comparison with DEXA and bone histomorphometry in a rat model of disuse osteoporosis. *Invest Radiol.* 2002;37(1):40-46.
3. Brandt KD. Response of joint structures to inactivity and to reloading after immobilization. *Arthritis Rheum.* 2003;49(2):267-271.
4. Burr DB, Radin EL. Microfractures and microcracks in subchondral bone: are they relevant to osteoarthritis? *Rheum Dis Clin North Am.* 2003;29(4):675-685.
5. Chen H, Chevrier A, Hoemann CD, Sun J, Ouyang W, Buschmann MD. Characterization of subchondral bone repair for marrow-stimulated chondral defects and its relationship to articular cartilage resurfacing. *Am J Sports Med.* 2011;39(8):1731-1740.

6. Chen H, Sun J, Hoemann CD, et al. Drilling and microfracture lead to different bone structure and necrosis during bone-marrow stimulation for cartilage repair. *J Orthop Res*. 2009;27(11):1432-1438.
7. Cole BJ, Farr J, Winalski CS, et al. Outcomes after a single-stage procedure for cell-based cartilage repair: a prospective clinical safety trial with 2-year follow-up. *Am J Sports Med*. 2011;39(6):1170-1179.
8. Dorotka R, Bindreiter U, Macfelda K, Windberger U, Nehrer S. Marrow stimulation and chondrocyte transplantation using a collagen matrix for cartilage repair. *Osteoarthritis Cartilage*. 2005;13(8):655-664.
9. Duncan H, Jundt J, Riddle JM, Pitchford W, Christopherson T. The tibial subchondral plate: a scanning electron microscopic study. *J Bone Joint Surg Am*. 1987;69(8):1212-1220.
10. Feldkamp LA, Goldstein SA, Parfitt AM, Jesion G, Kleerekoper M. The direct examination of three-dimensional bone architecture in vitro by computed tomography. *J Bone Miner Res*. 1989;4(1):3-11.
11. Frisbie DD, Cross MW, McIlwraith CW. A comparative study of articular cartilage thickness in the stifle of animal species used in human pre-clinical studies compared to articular cartilage thickness in the human knee. *Vet Comp Orthop Traumatol*. 2006;19(3):142-146.
12. Gill TJ, McCulloch PC, Glasson SS, Blanchet T, Morris EA. Chondral defect repair after the microfracture procedure: a nonhuman primate model. *Am J Sports Med*. 2005;33(5):680-685.
13. Gomoll AH, Farr J, Gilllogly SD, Kercher J, Minas T. Surgical management of articular cartilage defects of the knee. *J Bone Joint Surg Am*. 2010;92(14):2470-2490.
14. Goulet RW, Goldstein SA, Ciarelli MJ, Kuhn JL, Brown MB, Feldkamp LA. The relationship between the structural and orthogonal compressive properties of trabecular bone. *J Biomech*. 1994;27(4):375-389.
15. Hoemann CD, Hurtig M, Rossomacha E, et al. Chitosan-glycerol phosphate/blood implants improve hyaline cartilage repair in ovine microfracture defects. *J Bone Joint Surg Am*. 2005;87(12):2671-2686.
16. Hunziker EB, Rosenberg LC. Repair of partial-thickness defects in articular cartilage: cell recruitment from the synovial membrane. *J Bone Joint Surg Am*. 1996;78(5):721-733.
17. Jackson DW, Lalor PA, Aberman HM, Simon TM. Spontaneous repair of full-thickness defects of articular cartilage in a goat model: a preliminary study. *J Bone Joint Surg Am*. 2001;83:53-64.
18. Johnson PD, Besselsen DG. Practical aspects of experimental design in animal research. *ILAR J*. 2002;43(4):202-206.
19. Jubel A, Andermahr J, Schiffer G, et al. Transplantation of de novo scaffold-free cartilage implants into sheep knee chondral defects. *Am J Sports Med*. 2008;36(8):1555-1564.
20. Knutsen G, Drogset JO, Engebretsen L, et al. A randomized trial comparing autologous chondrocyte implantation with microfracture: findings at five years. *J Bone Joint Surg Am*. 2007;89(10):2105-2112.
21. Little CB, Smith MM, Cake MA, Read RA, Murphy MJ, Barry FP. The OARSI histopathology initiative: recommendations for histological assessments of osteoarthritis in sheep and goats. *Osteoarthritis Cartilage*. 2010;18 Suppl 3:S80-S92.
22. Lochmuller EM, Kristin J, Matsuura M, et al. Measurement of trabecular bone microstructure does not improve prediction of mechanical failure loads at the distal radius compared with bone mass alone. *Calcif Tissue Int*. 2008;83(4):293-299.
23. Macneil JA, Boyd SK. Bone strength at the distal radius can be estimated from high-resolution peripheral quantitative computed tomography and the finite element method. *Bone*. 2008;42(6):1203-1213.
24. Madry H, van Dijk CN, Mueller-Gerbl M. The basic science of the subchondral bone. *Knee Surg Sports Traumatol Arthrosc*. 2010;18(4):419-433.
25. Marchand C, Chen H, Buschmann MD, Hoemann CD. Standardized three-dimensional volumes of interest with adapted surfaces for more precise subchondral bone analyses by micro-computed tomography. *Tissue Eng Part C Methods*. 2011;17(4):475-484.
26. Meller R, Neddermann A, Willbold E, et al. The relation between tunnel widening and bone mineral density after anterior cruciate ligament reconstruction: an experimental study in sheep. *Arthroscopy*. 2010;26(4):481-487.
27. Menche DS, Frenkel SR, Blair B, et al. A comparison of abrasion burr arthroplasty and subchondral drilling in the treatment of full-thickness cartilage lesions in the rabbit. *Arthroscopy*. 1996;12(3):280-286.
28. Minas T, Gomoll AH, Rosenberger R, Royce RO, Bryant T. Increased failure rate of autologous chondrocyte implantation after previous treatment with marrow stimulation techniques. *Am J Sports Med*. 2009;37(5):902-908.
29. Mithoefer K, McAdams T, Williams RJ, Kreuz PC, Mandelbaum BR. Clinical efficacy of the microfracture technique for articular cartilage repair in the knee: an evidence-based systematic analysis. *Am J Sports Med*. 2009;37(10):2053-2063.
30. Muller-Gerbl M. The subchondral bone plate. *Adv Anat Embryol Cell Biol*. 1998;141:III-XI, 1-134.
31. Muller R, Hahn M, Vogel M, Delling G, Rueggsegger P. Morphometric analysis of noninvasively assessed bone biopsies: comparison of high-resolution computed tomography and histologic sections. *Bone*. 1996;18(3):215-220.
32. Murshed KA, Çiçekcibaşı AE, Karabacakoglu A, Seker M, Ziyhan T. Distal femur morphometry: a gender and bilateral comparative study using magnetic resonance imaging. *Surg Radiol Anat*. 2005;27(2):108-112.
33. Nazarian A, Stauber M, Zurakowski D, Snyder BD, Muller R. The interaction of microstructure and volume fraction in predicting failure in cancellous bone. *Bone*. 2006;39(6):1196-1202.
34. Osterhoff G, Löffler S, Steinke H, Feja C, Josten C, Hepp P. Comparative anatomical measurements of osseous structures in the ovine and human knee. *Knee*. 2011;18(2):98-103.
35. Parfitt AM, Drezner MK, Glorieux FH, et al. Bone histomorphometry: standardization of nomenclature, symbols, and units. Report of the ASBMR Histomorphometry Nomenclature Committee. *J Bone Miner Res*. 1987;2(6):595-610.
36. Pridie KH. A method of resurfacing knee joints: proceedings of the British Orthopaedic Association. *J Bone Joint Surg Br*. 1959;41:618.
37. Rueggsegger P, Koller B, Muller R. A microtomographic system for the nondestructive evaluation of bone architecture. *Calcif Tissue Int*. 1996;58(1):24-29.
38. Safran MR, Seiber K. The evidence for surgical repair of articular cartilage in the knee. *J Am Acad Orthop Surg*. 2010;18(5):259-266.
39. Schinhan M, Gruber M, Vavken P, et al. Critical-size defect induces unicompartmental osteoarthritis in a stable ovine knee [published online ahead of print August 4, 2011]. *J Orthop Res*. doi:10.1002/jor.21521.
40. Schlichting K, Schell H, Kleemann RU, et al. Influence of scaffold stiffness on subchondral bone and subsequent cartilage regeneration in an ovine model of osteochondral defect healing. *Am J Sports Med*. 2008;36(12):2379-2391.
41. Shapiro F, Koide S, Glimcher MJ. Cell origin and differentiation in the repair of full-thickness defects of articular cartilage. *J Bone Joint Surg Am*. 1993;75(4):532-553.
42. Steadman JR, Briggs KK, Rodrigo JJ, Kocher MS, Gill TJ, Rodkey WG. Outcomes of microfracture for traumatic chondral defects of the knee: average 11-year follow-up. *Arthroscopy*. 2003;19(5):477-484.
43. Steadman JR, Rodkey WG, Rodrigo JJ. Microfracture: surgical technique and rehabilitation to treat chondral defects. *Clin Orthop Relat Res*. 2001;391 (Suppl):S362-S369.
44. Turner CH. Biomechanics of bone: determinants of skeletal fragility and bone quality. *Osteoporos Int*. 2002;13(2):97-104.
45. van der Kraan PM, van den Berg WB. Osteophytes: relevance and biology. *Osteoarthritis Cartilage*. 2007;15(3):237-244.
46. van Dijk CN, Reilingh ML, Zengerink M, van Bergen CJ. Osteochondral defects in the ankle: why painful? *Knee Surg Sports Traumatol Arthrosc*. 2010;18(5):570-580.
47. Vasiladis HS, Danielson B, Ljungberg M, McKeon B, Lindahl A, Peterson L. Autologous chondrocyte implantation in cartilage lesions of the knee: long-term evaluation with magnetic resonance imaging and delayed gadolinium-enhanced magnetic resonance imaging technique. *Am J Sports Med*. 2010;38(5):943-949.
48. von Rechenberg B, Akens MK, Nadler D, et al. Changes in subchondral bone in cartilage resurfacing: an experimental study in sheep using different types of osteochondral grafts. *Osteoarthritis Cartilage*. 2003;11(4):265-277.
49. Wu ZX, Liu D, Wan SY, Cui G, Zhang Y, Lei W. Sustained-release rhBMP-2 increased bone mass and bone strength in an ovine model of postmenopausal osteoporosis. *J Orthop Sci*. 2011;16(1):99-104.

- II. **Goebel L**, Orth P, Müller A, Zurakowski D, Bücken A, Cucchiaroni M, Pape D, Madry H. Experimental scoring systems for macroscopic articular cartilage repair correlate with the MOCART score assessed by a high-field MRI at 9.4 Tesla - comparative evaluation of five macroscopic scoring systems in a large animal cartilage defect model. *Osteoarthritis Cartilage*, 2012, 20(9):1046-55.

Reprinted from Osteoarthritis and Cartilage, Copyright © 2012, with permission from Elsevier, doi: 10.1016/j.joca.2012.05.010.

Osteoarthritis and Cartilage



Experimental scoring systems for macroscopic articular cartilage repair correlate with the MOCART score assessed by a high-field MRI at 9.4 T – comparative evaluation of five macroscopic scoring systems in a large animal cartilage defect model

L. Goebel †, P. Orth †‡, A. Müller §, D. Zurakowski || ¶, A. Bückner §, M. Cucchiariini †, D. Pape #, H. Madry †‡*

† Center of Experimental Orthopaedics, Saarland University Medical Center, Kirrberger Straße, Building 37, D-66421 Homburg/Saar, Germany

‡ Department of Orthopaedic Surgery, Saarland University Medical Center, Kirrberger Straße, Building 37, D-66421 Homburg/Saar, Germany

§ Department of Diagnostic and Interventional Radiology, Saarland University Medical Center, Kirrberger Straße, Building 57, D-66421 Homburg/Saar, Germany

|| Department of Anesthesia, Children's Hospital Boston, Harvard Medical School, Boston, MA 02115, USA

¶ Department of Surgery, Children's Hospital Boston, Harvard Medical School, Boston, MA 02115, USA

Department of Orthopaedic Surgery, Centre Hospitalier, Clinique d'Eich, 76, Rue d'Eich, 1460 Luxembourg, Luxembourg, Germany

ARTICLE INFO

Article history:

Received 12 January 2012

Accepted 30 May 2012

Keywords:

Cartilage repair

Scoring system

MRI

Validation

Animal model

Sheep

SUMMARY

Objective: To develop a new macroscopic scoring system which allows for an overall judgment of experimental articular cartilage repair and compare it with four existing scoring systems and high-field magnetic resonance imaging (MRI).

Methods: A new macroscopic scoring system was developed to assess the repair of cartilage defects. Cartilage repair was graded by three observers with different experience in cartilage research at 2–3 time points and compared with the protocol A of the international cartilage repair society (ICRS) cartilage repair assessment score, the Oswestry arthroscopy score, and macroscopic grading systems designed by Jung and O'Driscoll. Parameters were correlated with the two-dimensional (2D) magnetic resonance observation of cartilage repair tissue (MOCART) score based on a 9.4 T MRI as an external reference standard.

Results: All macroscopic scores exhibited high intra- and interobserver reliability and high internal correlation. The newly developed macroscopic scoring system had the highest intraobserver [$0.866 \leq \text{intraclass correlation (ICC)} \leq 0.895$] and the highest interobserver reliability ($\text{ICC} = 0.905$) for “total points”. Here, Cronbach's alpha indicated good homogeneity and functioning of the items ($\text{mean} = 0.782$). “Total points” of the 2D MOCART score correlated with all macroscopic scores (all $P < 0.0001$). The newly developed macroscopic scoring system yielded the highest correlation for the MRI parameter “defect fill” ($\rho = 0.765$; all $P < 0.0001$).

Conclusions: “Total points” and “defect fill”, two clinically relevant indicators of cartilage repair, can be reliably and directly assessed by macroscopic evaluation, using either system. These data support the use of macroscopic assessment to precisely judge cartilage repair in preclinical large animal models.

© 2012 Osteoarthritis Research Society International. Published by Elsevier Ltd. All rights reserved.

Introduction

The macroscopic evaluation of the repair tissue in articular cartilage defects in animal models allows for a first overall judgment of its quality^{1,2}. Here, important parameters of cartilage repair such as “defect fill” and “surface” can be directly assessed, long before the results of the histological, molecular biological, gene expressions, or biochemical analyses^{3–5} are available.

Quantitative macroscopic scoring systems need to accurately reflect the different parameters of cartilage repair and allow for an objective comparison between treatment groups and therapeutic

* Address correspondence and reprint requests to: Henning Madry, Kirrberger Strasse, Building 37–38, D-66421 Homburg/Saar, Germany. Tel: 49-6841-1624515; Fax: 49-6841-1624988.

E-mail addresses: l.goebel@gmx.de (L. Goebel), patrick.orth@uks.eu (P. Orth), andreas.mueller@uniklinikum-saarland.de (A. Müller), david.zurakowski@childrens.harvard.edu (D. Zurakowski), Arno.Buecker@uniklinikum-saarland.de (A. Bückner), mmcucchiariini@hotmail.com (M. Cucchiariini), dietrichpape@yahoo.de (D. Pape), henning.madry@uks.eu (H. Madry).

approaches^{6–12}. Yet, only few scores to reliably and precisely describe the macroscopic appearance of the repair tissue were developed so far^{13–17}. The system proposed by O'Driscoll and colleagues (O'Driscoll score)¹⁵ is a classical descriptive score for experimental articular cartilage repair, while other systems such as the international cartilage repair society (ICRS) score^{16,17} and the Oswestry arthroscopy score (Oswestry score)¹³ have been designed for clinical grading of cartilage repair. To date, however, only these two clinical macroscopic scores have been validated^{13,18}. The reproducibility and reliability of macroscopic scoring systems for experimental cartilage repair have not, to our best knowledge, been assessed.

Magnetic resonance imaging (MRI) is another non-invasive tool to assess articular cartilage repair^{19,20}. Due to the small size of specimen and the necessity to correctly select the different individual parameters, MRI requires complex optimization. Lee *et al.*²¹ already tested the accordance between the magnetic resonance observation of cartilage repair tissue (MOCART) score^{22,23} and arthroscopic findings following autologous chondrocyte transplantation²⁴ in a clinical setting²¹. A good correlation for degree of defect repair, filling and surface quality, and mild-to-moderate reliability for integration and adhesions were reported²¹. However, whether macroscopic repair of experimentally created articular cartilage defects correlates with the MOCART score assessed by a high-field MRI remains unknown.

The first aim of this study was to develop a new macroscopic scoring system based on an extended selection of parameters and items that may allow for a more detailed and comprehensive macroscopic analysis of experimental cartilage repair. We compared the intra- and interobserver reliability, and internal correlation of this novel score with other systems such as the protocol A of the ICRS score^{16,17}, the Oswestry score¹³, the O'Driscoll score¹⁵, and a macroscopic score utilized by Jung *et al.* (Jung score)¹⁴. Finally, we tested the hypothesis that the data from different macroscopic scoring systems significantly correlate with the respective parameters obtained using a 9.4 T high-field MRI, applying the MOCART score^{22–25} as an external reference standard.

Materials and methods

Study design

A newly developed macroscopic scoring system (Table I, Fig. 1) was established based on photographs of 38 standardized chondral defects (size 4 × 6 mm, *n* = 19 animals) from an experimental investigation on the effect of marrow stimulation on articular cartilage defects²⁶. Within a time period of 8 months, 1,520 blinded macroscopic observations of cartilage defects were made by three observers with different experience in cartilage repair at 2–3 time points. A minimum interval of 8 weeks was kept between observations. The data of this assessment were next compared with the ICRS^{16,17}, Oswestry¹³, Jung¹⁴, and O'Driscoll¹⁵ scores. The explanted osteochondral units containing the defects were then scanned in a 9.4 T MRI (Fig. 2). The two-dimensional (2D) MOCART score for cartilage defects was applied^{22–25}. Finally, the data of the macroscopic evaluation were correlated with the results of the MRI examination.

Animal experiments

In 22 healthy, skeletally mature female Merino sheep (age between 2 years and 4 years; average weight 70 ± 20 kg), standardized full-thickness chondral defects were created in the weight-bearing area of the medial femoral condyle in each stifle joint. Three sheep were excluded due to infection. Animal experiments were in

Table I

Newly developed semiquantitative macroscopic scoring system for the macroscopic description of articular cartilage repair

Newly developed macroscopic scoring system		
Parameter	Item	Points
Color of the repair tissue	Hyaline or white	0
	Predominantly white (>50%)	1
	Predominantly translucent (>50%)	2
	Translucent	3
	No repair tissue	4
Presence of blood vessels in the repair tissue	No	0
	Less than 25% of the repair tissue	1
	25–50% of the repair tissue	2
	50–75% of the repair tissue	3
	More than 75% of the repair tissue	4
Surface of the repair tissue	Smooth, homogeneous	0
	Smooth, heterogeneous	1
	Fibrillated	2
	Incomplete new repair tissue	3
Filling of the defect	No repair tissue	4
	In level with adjacent cartilage	0
	>50% repair of defect depth or hypertrophy	1
	<50% repair of defect depth	2
	0% repair of defect depth	3
Degeneration of adjacent articular cartilage	Subchondral bone damage	4
	Normal	0
	Cracks and/or fibrillations in integration zone	1
	Diffuse osteoarthritic changes	2
	Extension of the defect into the adjacent cartilage	3
	Subchondral bone damage	4
Total points		20

The reverse scale consists of five major parameters and 25 items. A total number of 20 points is achieved for the worst possible result.

accordance with the German legislation on protection of animals and the NIH Guidelines for the Care and Use of Laboratory Animals [NIH Publication 85–23, Rev. 1985] and were approved by the local governmental animal care committee. Animals were fed a standard diet, received water *ad libitum*, and were monitored at all times. After a 12-h fast, sheep were sedated with 0.05 mg/kg body weight 2% rompun (Bayer, Leverkusen, Germany) and received a general anesthesia with intravenous application of 20 ml of 2% propofol (Astra-Zeneca, Wedel, Germany) and 1.4 mg/kg body weight carprofen (Pfizer, Berlin, Germany). Animals were then intubated. Anesthesia was maintained by inhalation of 1.5% isoflurane (Baxter, Unterschleißheim, Germany) and intravenous application of propofol (6–12 mg/kg body weight/h). Preoperative radiographs had excluded osteoarthritis.

A medial parapatellar approach was chosen to enter the stifle joint. A standardized, rectangular 4 × 6 mm full-thickness chondral defect was created in the medial femoral condyle using a custom-made precision surgical instrument. Articular cartilage, including the calcified cartilage, was meticulously removed down to the cement line. No bleeding from the subchondral bone was observed. Six subchondral drill holes (diameter: 1.0 mm) were then introduced into each defect using a Kirschner wire to a depth of 10 mm in a standardized manner²⁶. Postoperatively, animals received 3 ml of 0.25% fentanyl/levomethadone (MSD, Unterschleißheim, Germany), 30 mg/kg body weight amoxicillin clavulanate (Pfizer) and 1.8 mg/kg body weight carprofen. Animals were allowed full weight-bearing immediately after surgery. After 6 months, sheep were sacrificed in general anesthesia. The stifle joints were explanted and high-resolution digital photographs of the defects were taken using a Canon PowerShot A480 camera (Canon, Tokyo, Japan) with 10 mega pixels and a specific macroscopic lens under standardized conditions including illumination with a 40 W

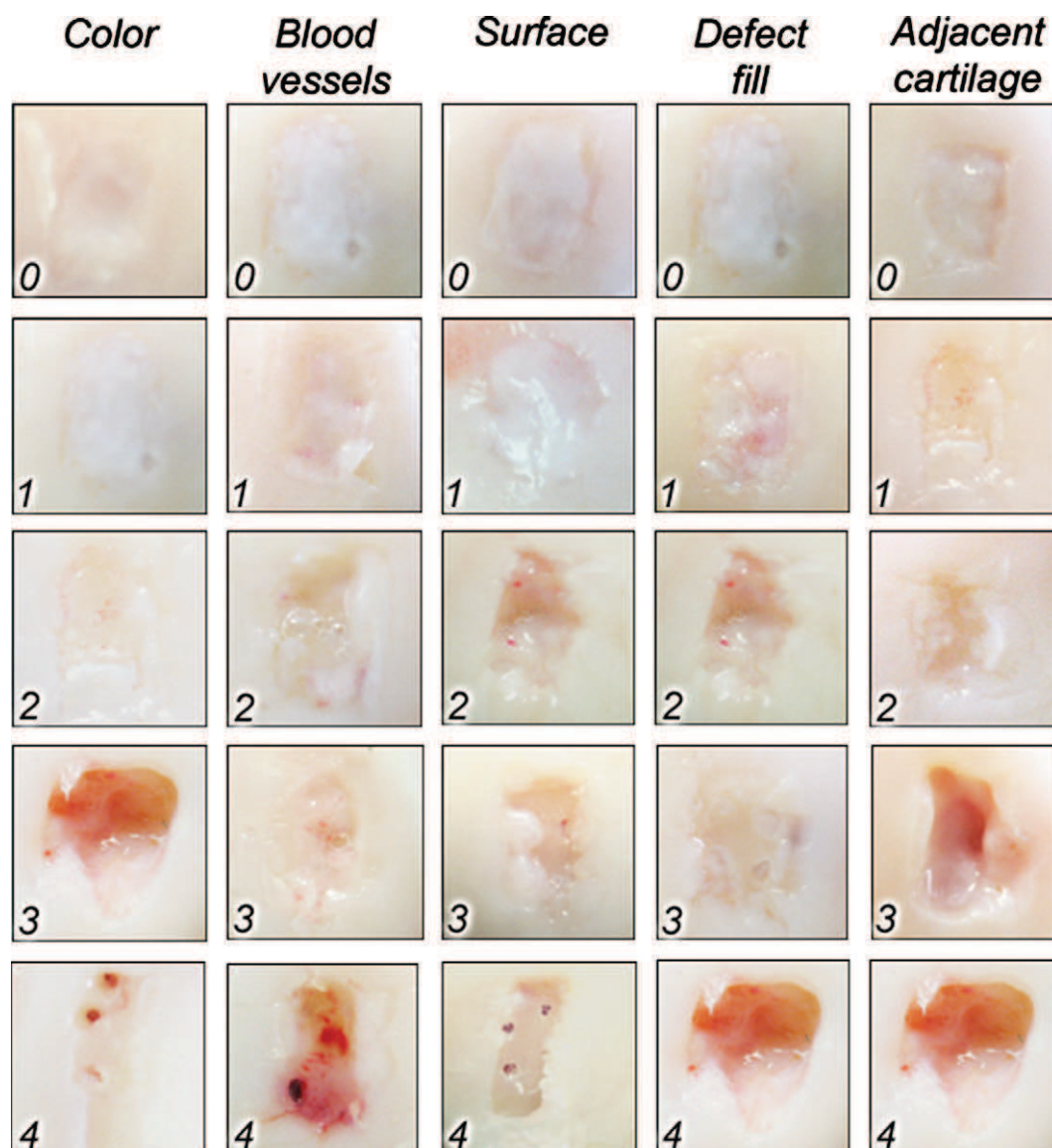


Fig. 1. Representative examples of articular cartilage defects corresponding to each item of each parameter of the newly developed macroscopic scoring system. Selected pictures display the mean score values of the three observers and 2–3 time points. Digits indicate the number of points it would receive in the scoring system.

incandescent reflector light bulb (Osram, Munich, Germany) placed at the constant distance of 50 cm to the cartilage specimens with an approximate illuminance of 2160 lx. The 38 medial condyles were then explanted and the anterior two-third of the condyles were fixated in 4% formalin for 48 h, then transferred to 70% ethanol and prepared for MRI investigation.

Description of the newly developed macroscopic score

The inverse scoring system ranges from 0 points (excellent repair cartilage) to 20 points (cartilage defect without any repair tissue and extension into the adjacent cartilage; Table I, Fig. 1). Five major evaluation parameters with a total of 25 items were defined as follows:

1. “Color of the repair tissue”: any identifiable repair tissue is evaluated.
2. “Presence of blood vessels in the repair tissue”: indicated by the appearance of red color or blood vessels in the repair tissue^{27–29}.

3. “Surface of the repair tissue”: ranging from no repair within the defect to a smooth, homogeneous surface^{3,30}.
4. “Filling of the defect”: a subchondral bone damage receives worst grading, filling in level with the adjacent cartilage receives best grading^{3,30}.
5. “Degeneration of adjacent articular cartilage”: degree of osteoarthritic changes in the adjacent articular cartilage^{3,31}.

Macroscopic evaluation

From each defect, one or two photographs were chosen by observer A for best image quality and printed on high quality photo paper (Ultra Premium Photo Paper, Kodak, Rochester, NY) in the size 13.0 cm × 18.0 cm displaying the defect site at a 12-fold magnification (ca. 5.0 × 7.0 cm). The photographs of the 38 articular cartilage defects were independently scored twice by three observers (A, B and C) using the four different grading systems and the newly developed macroscopic scoring system, additionally applied a third time by two observers (A and C). Between each

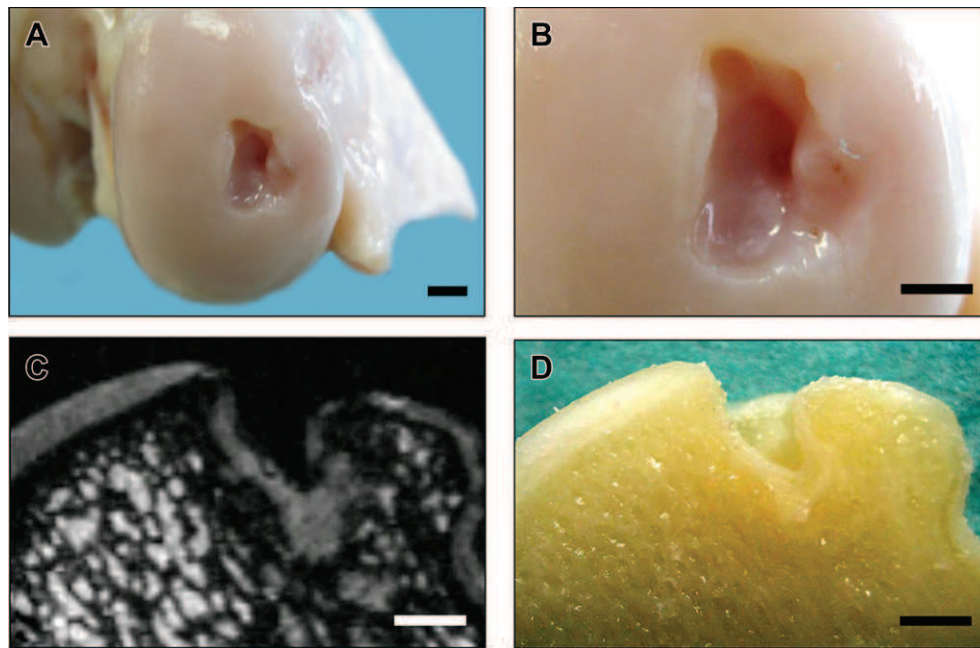


Fig. 2. Example of macroscopic and MRI assessment of a representative cartilage defect specimen illustrating (a) the macroscopic picture of the exposed stifle joint after sacrifice, (b) standardized photographs of the articular cartilage defects, (c) the coronal plane reconstruction of the articular cartilage defect examined in a 9.4 T high-field MRI setting, and (d) the macroscopic aspect of a section through the articular cartilage defect in the congruent plane. Bar: 4 mm.

evaluation, a minimum time interval of 8 weeks was kept to prevent any bias by recognition. Mean value, standard deviation, internal correlation, intra- and interobserver reliability were assessed for the newly developed macroscopic scoring system as well as for the ICRS^{16,17}, Oswestry¹³, Jung¹⁴, and O'Driscoll¹⁵ scores. The ICRS and Oswestry scores were developed for arthroscopic assessment of cartilage repair in patients; the O'Driscoll and Jung scores for a rabbit and minipig model of cartilage defects.

The ICRS score^{16,17} was applied unchanged. "Stiffness on probing" of the Oswestry score¹³ was excluded. In the original publication of the Jung score¹⁴, "contracture" and "adhesions" were rated with 1 point for the existence of either pathology. Assuming this to be an error, it has been rectified. As the original O'Driscoll score¹⁵ only compares single parameters between treatment groups, we allocated point values to each item (maximum number: 8 points for worst result): "Contractures", "adhesions", "erosions" or a 'rough' "regenerated tissue" was rated 1 point. The parameter "restoration of the patellar groove" was replaced by "restoration of the joint contour" with 1 point for 'partial' and 2 points for 'no restoration'.

Each scoring system was applied by three observers with different levels of experience in cartilage repair: observer A was a medical student with no experience in grading of articular cartilage defects, observer B was a registrar for orthopaedic surgery, observer C was a consultant for orthopaedic surgery. Prior to evaluation, observer A had received a 1 h training unit on arthroscopic images of human articular cartilage defects.

Evaluation by 9.4 T high-field MRI

The explanted medial condyles were examined in a 9.4 T high-field MRI scanner developed for imaging of small animals (Biospec Avance III 9.4/20, Bruker Biospin, Ettlingen, Germany) with a gradient strength of 675 mT/m (BGA 12S gradient system), using a circular polarized volume coil (inner diameter: 40 mm) adapted for imaging experiments of rat brain, in receive/transmit configuration. A three-dimensional (3D) spoiled gradient echo (GE) sequence was chosen to perform isovolumetric scans of the osteochondral

samples. Minimum voxel size was $120 \times 120 \times 120 \mu\text{m}$, and optimized imaging parameters were evaluated as: repetition time (TR): 10 ms, time echo (TE): 3 ms, flip angle (FA): 10° , number of excitations (NEX): 10 and bandwidth (BW): 98684.2 kHz. To minimize acquisition time and warming of the samples and the employed coil system, readout direction was placed in alignment with the longest dimension of the scanned objects, adapting the matrix size to completely cover the samples (typically consisting of a set of $256 \times 128 \times 128$ voxels). Consecutive to the scans, reconstructions in three orthogonal planes were performed in identical spatial resolution (Paravision 5.1, JIVE tool, Bruker Biospin) and analyzed with ImageJ version 1.45 (NIH, Bethesda, MD, USA). The condyles were evaluated using a modification of the 2D MOCART score described by Marlovits *et al.*^{22,23} (Table II), a clinical scoring system for cartilage repair^{12,21–23}. According to a previously published point scale for the 2D MOCART score by Trattnig *et al.*²⁵, images of the coronal and sagittal plane of the samples were evaluated in parallel by observer A. In a standardized procedure, only the anterior 3.5 mm of the defects were analyzed to avoid any influence caused by sample preparation. Results were correlated to the different macroscopic scoring systems (Fig. 2).

Statistical evaluation

Results are expressed as mean value \pm standard deviation. To determine a possible relationship between macroscopic data and MRI findings, mean values of each macroscopic scoring system were correlated with each other and with the 2D MOCART score for the identical parameters "surface" and "defect fill", as well as "total points" values using Spearman's rho. The average differences in mean "total points" values of the different macroscopic scoring systems are the sum of the differences in point values between the observations divided by the number of observations. Wilcoxon rank-sum test was applied to determine a statistical significance. Intraclass correlation (ICC) was used to assess intra- and interobserver reliability with 95% confidence intervals (CIs) to describe the precision of the estimated ICC reliabilities³². A z-test was used to

Table II

Modification of the clinical 2D MOCART score developed by Marlovits *et al.*^{22,23} for the evaluation of *ex vivo* osteochondral samples

2D MOCART score		
Parameter	Item	Points
Defect fill	Subchondral bone exposed	0
	Incomplete < 50%	5
	Incomplete > 50%	10
	Complete	20
	Hypertrophy	15
Cartilage interface	Complete	15
	Demarcating border visible	10
	Defect visible < 50%	5
	Defect visible > 50%	0
	Surface intact	10
Surface	Surface damaged < 50% of depth	5
	Surface damaged > 50% of depth	0
Adhesions	Yes	5
	No	0
Structure	Homogeneous	5
	Inhomogeneous or cleft formation	0
Signal intensity	Normal	30
	Nearly normal	10
	Abnormal	0
Subchondral lamina	Intact	5
	Not intact	0
Subchondral bone	Intact	5
	Granulation tissue, cyst, sclerosis	0
Effusion	No effusion	5
	Effusion	0
Total points		100

Point allocation was used consistently as described by Trattnig *et al.*²⁵. The parameter “signal intensity” was adopted from the 3D MOCART score⁴⁴ where only one sequence is applied. Note that the parameters “adhesions” and “effusion” were determined by clinical examination. MRI parameters “structure”, “signal intensity”, “subchondral lamina”, “effusion”, and “subchondral bone” of the repair tissue were not correlated with macroscopy; “edema” of bone marrow was excluded^{22–25}.

compare the “total points” interobserver ICC between the newly developed macroscopic scoring system and each of the other four scores with $z = (ICC_1 - ICC_2) / \text{SQRT} (SE_1^2 + SE_2^2)$; SE: standard error, SQRT: square root. Internal consistency of the newly developed macroscopic scoring system was assessed by Cronbach’s alpha to measure the psychometric functioning of the items as a set. Calculations were performed with SPSS version 19.0 (SPSS Inc/IBM, Chicago, IL, USA). All *P* values are two-tailed and a *P* value < 0.05 was considered to be statistically significant.

Results

Internal correlation between the five macroscopic scores

Mean values and standard deviations were calculated for the different observers and time points (Table III). To determine internal correlation of the five macroscopic scores, results of eight examinations and three investigators were averaged and Spearman’s rho was calculated for “total points” and identical parameters of each score (Table IV). All scores showed a good correlation, with rho values > 0.8 or < −0.8 for “total points” (all *P* < 0.0001) and rho values > 0.5 or < −0.5 for individual parameters (all *P* ≤ 0.0014). The highest correlation was found between Oswestry and Jung scores for “total points” (rho = 0.956). The Oswestry score had the lowest correlation with the O’Driscoll score for the parameter “defect fill” (rho = −0.504).

Intra- and interobserver reliability of the five macroscopic scores

When different time points were assessed by one single observer, average differences in “total points” values were of 0.74 ± 0.29 (range 0.13–1.92) for the newly developed macroscopic scoring

system, 1.38 ± 0.34 (0.21–2.81) for the ICRS score, 0.71 ± 0.20 (0.24–1.40) for the O’Driscoll score, 0.31 ± 0.28 (0.11–0.68) for the Oswestry score and 0.24 ± 0.23 (0.18–0.32) for the Jung score. Accordingly, average differences in “total points” values between the three observers (A, B, C) were very low with 0.74 ± 0.09 (range 0.41–1.11) for the newly developed macroscopic scoring system, 0.75 ± 0.34 (0.37–1.12) for the ICRS score, 0.17 ± 0.21 (0.08–0.26) for the O’Driscoll score, 0.28 ± 0.57 (0.20–0.42) for the Oswestry score, and 0.30 ± 0.19 (0.18–0.45) for the Jung score. Statistical evaluation revealed no significant differences for mean intra- and interobserver differences for the five scoring systems tested (all *P* ≥ 0.200).

The intraobserver reliability for “total points” of the newly developed macroscopic scoring system was the highest among all scores evaluated ($0.866 \leq \text{ICC} \leq 0.895$; Table V). All scores were characterized by moderate-to-strong ICC values (all *P* < 0.0001 for the five scores and the three observers), except for “surface” of the O’Driscoll, Oswestry and Jung scores.

Interobserver reliability for observers with different levels of experience in cartilage research was next determined (Table VI). The newly developed macroscopic scoring system reached the highest interobserver reliability upon ICC analysis of “total points” (ICC = 0.905; *P* < 0.0001). All other systems showed also significant correlations (all *P* ≤ 0.0008), with ICCs between 0.590 (“surface” in Oswestry score) and 0.933 (“defect fill” in Oswestry score) for all scores and parameters tested.

Internal consistency of the parameters of the newly developed macroscopic scoring system

Cronbach’s alpha was calculated for the newly developed macroscopic scoring system to test for internal consistency of the single parameters. Cronbach’s alpha was reasonable good with 0.734 for observer A, 0.837 for observer B, and 0.774 for observer C, i.e., a mean value of 0.782. This indicates good homogeneity and functioning of the items in the newly developed macroscopic scoring system.

Evaluation of cartilage defects by 9.4 T high-field MRI using the 2D MOCART score

Next, all of the 38 cartilage defects were scanned with a high-field MRI at 9.4 T as an external reference standard to allow for an independent correlation of the different macroscopic scores. The 2D MOCART score (Table II) was then applied to grade articular cartilage repair. The resulting mean point values were 4.81 ± 2.80 for “defect fill”, 0.94 ± 2.64 for “cartilage interface”, 0.44 ± 1.37 for “surface”, 5.00 ± 0.00 for “adhesions”, 0.19 ± 0.87 for “structure”, 8.88 ± 4.87 for “signal intensity”, 0.25 ± 1.10 for “subchondral lamina”, 0.38 ± 1.33 for “subchondral bone”, and 4.88 ± 0.79 for “effusion”. “Total points” values for individual defects ranged from 10 to 70 points (with 0 points reflective of poor repair, and 100 points reflective of excellent repair), confirming a broad spectrum of the different repair grades. The mean “total points” value was 25.75 ± 9.37 points.

Correlation between macroscopic and MRI evaluation of the articular cartilage defects

Individual parameters of the 2D MOCART score were next correlated with the matching individual parameters of the different macroscopic scores, i.e., “defect fill” and “surface” (Table IV). “Defect fill” exhibited the highest correlation with the matching parameter of the newly developed macroscopic scoring system (rho = −0.765; *P* < 0.0001). It also correlated with this parameter in

Table III
Results of the five scoring systems evaluated for all observers and different time points

	Parameter	A – I	A – II	A – III	A – mean	B – I	B – II	B – mean	C – I	C – II	C – III	C – mean	All – mean
New score	Color of repair tissue	1.66 (1.05)	1.39 (1.17)	1.39 (1.13)	1.48 (1.11)	1.92 (1.30)	1.95 (1.35)	1.93 (1.32)	1.71 (0.84)	1.66 (0.78)	1.82 (0.93)	1.73 (0.84)	1.69 (1.09)
	Coverage with blood vessels	0.87 (1.23)	0.92 (1.26)	0.92 (1.42)	0.90 (1.30)	1.00 (1.14)	0.53 (0.83)	0.76 (1.02)	0.84 (1.20)	0.79 (1.34)	1.18 (1.43)	0.94 (1.33)	0.88 (1.24)
	Surface of the repair tissue	2.58 (1.03)	2.50 (1.11)	2.68 (1.19)	2.59 (1.10)	3.61 (0.97)	3.50 (0.86)	3.55 (0.91)	2.50 (1.06)	3.05 (0.9)	3.61 (1.00)	3.07 (1.08)	3.00 (1.11)
	Filling of the defect	1.55 (1.05)	2.05 (1.11)	2.00 (1.12)	1.87 (1.12)	1.79 (0.91)	1.53 (0.76)	1.66 (0.84)	1.55 (0.89)	1.71 (0.90)	1.97 (0.88)	1.75 (0.90)	1.77 (0.97)
	Degeneration of adjacent cartilage	1.53 (1.22)	1.47 (1.03)	1.05 (1.01)	1.35 (1.10)	1.37 (0.85)	1.42 (0.72)	1.39 (0.78)	1.34 (1.24)	1.66 (1.10)	1.29 (0.69)	1.43 (1.04)	1.39 (1.01)
	Total points	8.18 (3.92)	8.34 (3.48)	8.05 (3.88)	8.19 (3.74)	9.68 (4.07)	8.92 (3.6)	9.30 (3.84)	7.95 (3.83)	8.87 (3.76)	9.87 (3.91)	8.89 (3.88)	8.73 (3.83)
ICRS score	Degree of defect repair	n. d.	1.45 (1.11)	1.58 (1.18)	1.51 (1.14)	1.63 (1.08)	1.87 (1.12)	1.75 (1.10)	n. d.	1.45 (1.06)	1.45 (1.03)	1.45 (1.04)	1.57 (1.09)
	Integration to border zone	n. d.	0.29 (0.65)	0.08 (0.36)	0.18 (0.53)	0.74 (0.64)	1.26 (1.00)	1.00 (0.88)	n. d.	0.00 (0.00)	3.00 (0.00)	1.50 (1.51)	0.89 (1.18)
	Macroscopic appearance	n. d.	1.05 (0.77)	1.34 (1.10)	1.20 (0.95)	0.71 (0.73)	1.08 (0.94)	0.89 (0.86)	n. d.	1.16 (0.80)	0.97 (0.72)	1.07 (0.81)	1.05 (0.88)
	Total points	n. d.	2.79 (1.93)	3.00 (2.24)	2.89 (2.08)	3.08 (2.26)	4.21 (2.79)	3.64 (2.59)	n. d.	2.61 (1.84)	5.42 (1.65)	4.01 (2.24)	3.52 (2.35)
O'Driscoll score	Contractures	n. d.	0.00 (0.00)	0.00 (0.00)	0.00 (0.00)	0.00 (0.00)	0.00 (0.00)	0.00 (0.00)	n. d.	0.00 (0.00)	0.00 (0.00)	0.00 (0.00)	0.00 (0.00)
	Adhesions	n. d.	0.00 (0.00)	0.00 (0.00)	0.00 (0.00)	0.00 (0.00)	0.00 (0.00)	0.00 (0.00)	n. d.	0.00 (0.00)	0.00 (0.00)	0.00 (0.00)	0.00 (0.00)
	Erosions	n. d.	1.00 (0.00)	0.21 (0.41)	0.61 (0.49)	1.00 (0.00)	0.55 (0.50)	0.78 (0.42)	n. d.	0.08 (0.27)	0.26 (0.45)	0.17 (0.38)	0.52 (0.50)
	Regenerated tissue	n. d.	0.95 (0.23)	0.84 (0.37)	0.89 (0.31)	0.92 (0.27)	0.87 (0.34)	0.89 (0.31)	n. d.	0.87 (0.34)	0.97 (0.16)	0.92 (0.27)	0.90 (0.30)
	Restoration of the patellar groove	n. d.	1.71 (0.57)	1.21 (0.58)	1.46 (0.62)	1.11 (0.45)	1.11 (0.45)	1.11 (0.45)	n. d.	1.63 (0.59)	1.58 (0.60)	1.61 (0.59)	1.39 (0.59)
	Total points	n. d.	3.66 (0.75)	2.26 (1.06)	2.96 (1.15)	3.03 (0.64)	2.53 (0.95)	2.78 (0.84)	n. d.	2.58 (0.86)	2.82 (0.87)	2.70 (0.86)	2.81 (0.96)
Oswestry score	Graft level with surrounding cartilage	n. d.	0.16 (0.55)	0.11 (0.45)	0.13 (0.50)	0.16 (0.55)	0.21 (0.62)	0.18 (0.58)	n. d.	0.11 (0.45)	0.16 (0.55)	0.13 (0.50)	0.15 (0.53)
	Integration with surrounding cartilage	n. d.	0.08 (0.27)	0.00 (0.00)	0.04 (0.14)	0.18 (0.39)	0.47 (0.60)	0.33 (0.53)	n. d.	0.00 (0.00)	0.00 (0.00)	0.00 (0.00)	0.12 (0.35)
	Appearance of surface	n. d.	0.37 (0.67)	0.32 (0.62)	0.34 (0.64)	0.16 (0.44)	0.58 (0.64)	0.37 (0.59)	n. d.	0.05 (0.23)	0.13 (0.34)	0.09 (0.29)	0.27 (0.54)
	Color of graft	n. d.	0.58 (0.76)	0.89 (0.69)	0.74 (0.74)	0.61 (0.72)	0.53 (0.69)	0.57 (0.70)	n. d.	0.82 (0.69)	0.79 (0.41)	0.80 (0.70)	0.70 (0.68)
	Total points	n. d.	1.18 (1.57)	1.32 (1.25)	1.25 (1.42)	1.11 (1.66)	1.79 (2.08)	1.45 (1.90)	n. d.	0.97 (1.10)	1.08 (1.00)	1.03 (1.05)	1.24 (1.50)
Jung score	Contractures	n. d.	1.00 (0.00)	1.00 (0.00)	1.00 (0.00)	1.00 (0.00)	1.00 (0.00)	1.00 (0.00)	n. d.	1.00 (0.00)	1.00 (0.00)	1.00 (0.00)	1.00 (0.00)
	Adhesions	n. d.	1.00 (0.00)	1.00 (0.00)	1.00 (0.00)	1.00 (0.00)	1.00 (0.00)	1.00 (0.00)	n. d.	1.00 (0.00)	1.00 (0.00)	1.00 (0.00)	1.00 (0.00)
	Macroscopic synovialitis	n. d.	0.97 (0.16)	0.97 (0.16)	0.97 (0.16)	0.97 (0.16)	0.97 (0.16)	0.97 (0.16)	n. d.	0.97 (0.16)	0.97 (0.16)	0.97 (0.16)	0.97 (0.16)
	Defect filling	n. d.	0.61 (0.64)	0.71 (0.61)	0.66 (0.62)	0.84 (0.55)	0.92 (0.54)	0.88 (0.54)	n. d.	0.61 (0.64)	0.76 (0.54)	0.68 (0.59)	0.74 (0.59)
	Defect surface	n. d.	0.11 (0.31)	0.26 (0.45)	0.18 (0.39)	0.16 (0.37)	0.18 (0.39)	0.17 (0.38)	n. d.	0.03 (0.16)	0.08 (0.27)	0.05 (0.22)	0.14 (0.34)
	Defect integration	n. d.	0.11 (0.31)	0.00 (0.00)	0.05 (0.22)	0.08 (0.27)	0.16 (0.37)	0.12 (0.33)	n. d.	0.00 (0.00)	0.00 (0.00)	0.00 (0.00)	0.06 (0.23)
	Defect color	n. d.	0.74 (0.79)	0.79 (0.70)	0.76 (0.75)	0.45 (0.50)	0.45 (0.69)	0.45 (0.60)	n. d.	0.68 (0.70)	0.79 (0.41)	0.74 (0.57)	0.65 (0.66)
	Total points	n. d.	4.53 (1.45)	4.74 (1.39)	4.63 (1.41)	4.50 (1.35)	4.68 (1.61)	4.9 (1.48)	n. d.	4.29 (1.37)	4.61 (1.00)	4.45 (1.20)	4.56 (1.37)

Data are expressed as: mean value (standard deviation). A, B, and C indicate the different observers; I–III the different time points. A – mean, B – mean, and C – mean indicate mean point values for all observations by observer A, B, or C, respectively; All – mean indicates mean point values for all observations, and all observers together. n. d.: not determined. New score: newly developed macroscopic scoring system.

Table IV

Internal correlation of the five evaluated macroscopic scoring systems and the external correlation with MOCART score

		Internal correlation								External correlation	
		Oswestry score		O'Driscoll score		Jung score		ICRS score		MOCART score	
		rho	P	rho	P	rho	P	rho	P	rho	P
New score	Defect fill	−0.516	0.0011	0.850	<0.0001	−0.928	<0.0001	−0.950	<0.0001	−0.765	<0.0001
	Surface	−0.882	<0.0001	0.658	<0.0001	−0.723	<0.0001	−0.944	<0.0001	−0.053	0.750
	Total points	−0.917	<0.0001	0.829	<0.0001	−0.920	<0.0001	−0.834	<0.0001	−0.632	<0.0001
ICRS score	Defect fill	0.516	0.0011	−0.858	<0.0001	0.925	<0.0001			0.760	<0.0001
	Surface	0.904	<0.0001	−0.644	<0.0001	0.736	<0.0001			0.042	0.801
	Total points	0.925	<0.0001	−0.807	<0.0001	0.915	<0.0001			0.687	<0.0001
Jung score	Defect fill	0.545	0.0005	−0.845	<0.0001					0.703	<0.0001
	Surface	0.733	<0.0001	−0.700	<0.0001					0.191	0.249
	Total points	0.956	<0.0001	−0.815	<0.0001					0.668	<0.0001
O'Driscoll score	Defect fill	−0.504	0.0014							−0.702	<0.0001
	Surface	−0.700	<0.0001							−0.289	0.079
	Total points	−0.800	<0.0001							−0.610	<0.0001
Oswestry score	Defect fill									0.543	0.0005
	Surface									0.103	0.537
	Total points									0.693	<0.0001

Identical parameters included in the five different macroscopic scores and “total points” values were directly correlated; mean value of all examinations was used. External correlation with 2D MOCART score was assessed by 9.4 T high-field MRI as external reference standard. Spearman's rho and *P* values were determined. Significant rho values are in bold. New score: newly developed macroscopic scoring system.

all other scores, albeit to a lesser degree (all $P \leq 0.0005$). “Surface” of the 2D MOCART score did not correlate significantly with an identical macroscopic parameter in none of the five systems ($0.079 \leq P \leq 0.801$; Table IV).

When “total points” of the MOCART score were correlated with “total points” of all macroscopic scoring systems, the highest correlation was observed for the Oswestry score ($\rho = 0.693$), while all others also showed a moderate correlation (all $P \leq 0.0001$, Table IV).

Discussion

The data of the present study show that all of the five macroscopic scores exhibited high intra- and interobserver reliability and high internal correlation. The newly developed macroscopic scoring

system had the highest intraobserver and the highest interobserver reliability among all five scores for “total points”. The reproducibility among observers with different levels of experience in articular cartilage research remained constant for all five scores. The newly developed macroscopic scoring system contains 25 items, the highest number of all scores tested. When the individual parameters of the different macroscopic scores were correlated with the corresponding parameters of the 2D MOCART score based on a 9.4 T MRI evaluation as an external reference standard, the parameter “defect fill” exhibited the highest correlation with the corresponding parameter of the newly developed macroscopic scoring system. “Total points” of all five macroscopic scores reflected well the data from the “total points” of the 2D MOCART score. This suggests that

Table V

Intraobserver reliability of the five macroscopic scoring systems

	Observer A	Observer B	Observer C
	ICC (95% CI)	ICC (95% CI)	ICC (95% CI)
New score			
Defect fill	0.864 (0.781–0.922)	0.907 (0.847–0.947)	0.832 (0.733–0.902)
Surface	0.701 (0.548–0.815)	0.751 (0.570–0.862)	0.702 (0.544–0.818)
Total points	0.878 (0.801–0.929)	0.866 (0.757–0.928)	0.895 (0.830–0.940)
ICRS score			
Defect fill	0.973 (0.949–0.986)	0.700 (0.492–0.831)	0.827 (0.691–0.906)
Surface	0.732 (0.541–0.850)	0.680 (0.463–0.820)	0.715 (0.515–0.841)
Total points	0.851 (0.732–0.920)	0.802 (0.651–0.892)	0.886 (0.792–0.939)
O'Driscoll score			
Defect fill	0.606 (0.359–0.774)	0.868 (0.761–0.928)	0.700 (0.490–0.831)
Surface	0.485 (0.200–0.694)	0.733 (0.543–0.852)	0.327 (0.014–0.583)
Total points	0.595 (0.344–0.767)	0.721 (0.525–0.845)	0.730 (0.537–0.850)
Oswestry score			
Defect fill	0.791 (0.633–0.886)	0.846 (0.724–0.917)	0.791 (0.634–0.886)
Surface	0.875 (0.772–0.933)	0.585 (0.330–0.760)	0.236 (0.002–0.514)
Total points	0.758 (0.581–0.867)	0.770 (0.600–0.874)	0.785 (0.624–0.882)
Jung score			
Defect fill	0.876 (0.775–0.934)	0.782 (0.618–0.880)	0.728 (0.535–0.849)
Surface	0.538 (0.268–0.730)	0.539 (0.269–0.731)	0.493 (0.210–0.700)
Total points	0.783 (0.620–0.881)	0.757 (0.580–0.866)	0.736 (0.548–0.855)

ICC for assessing intraobserver reliability. All ICC are statistically significant at a *P* level < 0.0001, except “surface” for O'Driscoll (observer A: $P = 0.0009$; observer C: $P = 0.0212$), Oswestry (observer C: $P = 0.0738$, not significant) and Jung (observer A: $P = 0.0002$; observer B: $P = 0.0002$ and observer C: $P = 0.0004$) scores. Significant ICC values are in bold. New score: newly developed macroscopic scoring system.

Table VI

Interobserver reliability of the five macroscopic scoring systems

	ICC	95% CI	P
New score			
Defect fill	0.852	0.763–0.915	<0.0001
Surface	0.727	0.582–0.839	<0.0001
Total points	0.905	0.845–0.947	<0.0001
ICRS score			
Defect fill	0.843	0.750–0.909	<0.0001
Surface	0.774	0.651–0.866	<0.0001
Total points	0.833	0.734–0.903	<0.0001
O'Driscoll score			
Defect fill	0.687	0.534–0.809	<0.0001
Surface	0.801	0.689–0.883	<0.0001
Total points	0.824	0.722–0.897	<0.0001
Oswestry score			
Defect fill	0.933	0.888–0.962	<0.0001
Surface	0.590	0.414–0.743	0.0008
Total points	0.778	0.656–0.869	<0.0001
Jung score			
Defect fill	0.816	0.711–0.893	<0.0001
Surface	0.625	0.455–0.767	<0.0001
Total points	0.838	0.742–0.905	<0.0001

ICC for assessing interobserver reliability of three observers. Interobserver reliability for all scoring systems is statistically significant compared to a correlation of zero, with highest “total points” reliability for the newly developed macroscopic scoring system. However, no significant differences were detected in “total points” interobserver reliability between the new score compared to “total points” ICC for ICRS ($z = 1.24$, $P = 0.2169$), O'Driscoll ($z = 0.78$, $P = 0.4379$), Oswestry ($z = 1.90$, $P = 0.0574$), and Jung “total points” ($z = 1.18$, $P = 0.2365$). Significant ICC values are in bold. New score: newly developed macroscopic scoring system.

“defect fill” and “total points”, two clinically relevant indicators of the quality of articular cartilage repair, can be reliably assessed at a very early time point by macroscopic evaluation. These data support the use of macroscopic assessment for a precise first-line judgment of articular cartilage repair in preclinical large animal models.

Macroscopic evaluations are important tools in articular cartilage research. For example, the Osteoarthritis Research Society International (OARSI) strongly recommended such assessments in its histopathology initiative^{33,34} to grade osteoarthritis in different animal models. Similarly, macroscopic evaluation is also routinely performed in animal models of focal articular cartilage defects (i.e., for rabbits^{9,15,35}, dogs^{7,36}, goats³⁷, sheep^{10,38}, or horses³⁹).

A scoring system must be practicable to apply and reproducible within and between different observers and time points. An elementary score with less parameters should, in theory, result in a higher intra- and interobserver reliability, whereas a more complex scoring system may allow discriminating between minor differences. High intra- and interobserver reliability and internal correlation of all scoring systems tested suggest that they are effective tools to macroscopically characterize articular cartilage repair. The newly developed macroscopic scoring system contains 25 items, the highest number of all scores evaluated. Internal consistency of the single parameters of this new score was high, as indicated by a mean Cronbach's alpha of 0.782, demonstrating good homogeneity and functioning of the individual items. They are organized in five individual parameters that may allow for a more detailed and comprehensive macroscopic first-line analysis of cartilage repair. This score yielded the highest intra- and interobserver reliability, allowing for an in-depth description of macroscopic details. It may therefore serve to precisely evaluate macroscopic cartilage repair. For example, five different characteristics can be chosen that reflect the surface of the repair tissue, similarly to the ICRS score^{38,40}, allowing for a more detailed description in contrast to i.e., the Jung score¹⁴ that uses only two items (“rough” and “smooth”).

All of the evaluated scores contain different individual parameters. “Integration” is evaluated in the Jung, Oswestry, ICRS and MOCART score, “color” only in the Oswestry, Jung and the newly developed macroscopic scoring system, “contractures” are assessed by Jung and O'Driscoll, “adhesions” by the MOCART, Jung and O'Driscoll scores, “erosions” by O'Driscoll score and “macroscopic synovialitis” by the Jung score. Therefore, only the parameters “defect fill” and “surface” were compared as they are common among all scores. Interestingly, they correlate significantly among all macroscopic grading systems. “Defect fill” also correlates with MRI, its radiological counterpart. This indicates the value of both, macroscopy and MRI, as independent tools to evaluate articular cartilage repair.

Osteoarthritis³¹ is a clinically paramount potential long-term consequence of a focal cartilage defect⁴¹. The parameter “degeneration of adjacent articular cartilage” was therefore included in the newly developed macroscopic scoring system, aiming to reflect the major histopathological features of the different grades of osteoarthritis^{33,34,42}. It may be of particular value for the assessment of the long-term effects of different experimental cartilage repair procedures on the development of osteoarthritis. Osteoarthritic changes were not acknowledged in all other previously published macroscopic scoring systems.

“Blood vessels” were incorporated in the newly developed macroscopic scoring system because they were present in 58% of all defects. Angiogenesis occurs during endochondral ossification²⁷, inflammation²⁸, and osteoarthritis²⁹, and may reflect degeneration of the osteochondral unit.

The present study holds some limitations: due to a lower level of magnification compared with microscopic³⁷ or arthroscopic^{13,16–18}

assessments, macroscopic scoring may not distinguish between minor and major disruptions of the repair tissue¹³. However, macroscopic scoring allows for an overall judgment of the entire repair tissue, a critical point that is achievable in microscopic scoring only by evaluating numerous serial sections^{3,30}. Likewise, different grades of demarcating borders^{2,13,16,17,43}, as seen for example by arthroscopic magnification of (the often larger) articular cartilage defects in patients, are difficult to assess macroscopically. Therefore, and because such distinguishable margins were seen in all of the cartilage defects evaluated here, a detailed assessment of the demarcating border was excluded in the newly developed macroscopic scoring system. Macroscopic evaluation of blood vessels depends on the identification of red color in a semi-translucent tissue, making a reliable evaluation of deep vessels difficult. Finally, and since all scoring methods should be used purpose-specific, the ICRS^{16,17}, Oswestry¹³ and MOCART scores^{22,23,44} were not used according to their intended clinical use, while the O'Driscoll¹⁵ and Jung¹⁴ scores were developed for different animal models.

MRI is an important non-destructive method to examine cartilage pathologies^{12,19,45–47} and the clinical benchmark to non-invasively evaluate cartilage repair^{11,12,48}. Usually, standard MRI scanners for clinical routine explorations reach field strengths of 1.5–3 T, the major parameter for maximal spatial resolution, also allowing for an *in vivo* examination of large animals⁴⁹. High-field MRI scanners provide even higher spatial resolutions, while still receiving a good signal-to-noise ratio within a relatively short scanning time. Thus, high-field MRI may be regarded as a bridge between macroscopic and histologic evaluations⁵⁰, as it reaches the very small voxel sizes of 120 µm in three orthogonal planes. In addition, multiplanar reconstruction of the MRI data allows for observations of the repair tissue in different planes, a critical feature that is difficult to achieve using histological sections.

In conclusion, a new scoring system for macroscopic cartilage defect grading was developed and compared to four existing scores and high-field MRI at 9.4 T. This newly developed macroscopic scoring system was characterized by the highest intra- and interobserver reliability for “total points”, with a good homogeneity and functioning of the individual items. All other macroscopic scores exhibited comparable intra- and interobserver reliabilities. Importantly, the newly developed macroscopic scoring system correlated best with the MRI parameter “defect fill”. The other macroscopic scoring systems also correlated mild-to-moderate with the MOCART parameters “total points” and “defect fill”. Complex grading systems, such as the newly developed macroscopic scoring system or the ICRS score, are well suited to describe the complex pattern of cartilage repair, while elementary grading systems, such as the Oswestry score, are also capable of discerning macroscopic aspects of repair. The significant correlation of macroscopic cartilage repair with the corresponding MRI parameters therefore supports the continuing use of macroscopic assessment to precisely judge articular cartilage repair in preclinical large animal models.

Author contributions

Conception and design of the study: Henning Madry. Acquisition of the data: Lars Goebel, Patrick Orth, Andreas Müller, David Zurakowski, Dietrich Pape, Henning Madry. Analysis and interpretation: Lars Goebel, Patrick Orth, Andreas Müller, David Zurakowski, Arno Bücker, Magali Cucchiari, Dietrich Pape, Henning Madry. All authors participated in drafting and critically revising of the article, and final approval.

Role of funding source

Supported in part by the *Gesellschaft für Arthroskopie und Gelenkchirurgie (AGA)*. This study sponsor was not involved in the study design, data collection or analysis or in the writing of the manuscript. Furthermore, it did not affect the decision to submit the manuscript for publication.

Competing interests

All authors declare no competing interests.

References

- van Susante JL, Buma P, Schuman L, Homminga GN, van den Berg WB, Veth RP. Resurfacing potential of heterologous chondrocytes suspended in fibrin glue in large full-thickness defects of femoral articular cartilage: an experimental study in the goat. *Biomaterials* 1999;20:1167–75.
- Ahsan T, Sah RL. Biomechanics of integrative cartilage repair. *Osteoarthritis Cartilage* 1999;7:29–40.
- Orth P, Zurakowski D, Winchinger D, Madry H. Reliability, reproducibility and validation of five major histological scoring systems for experimental articular cartilage repair in the rabbit model. *Tissue Eng Part C Methods* 2012;18:329–39.
- Hoemann CD. Molecular and biochemical assays of cartilage components. *Methods Mol Med* 2004;101:127–56.
- Changoor A, Nelea M, Methot S, Tran-Khanh N, Chevrier A, Restrepo A, et al. Structural characteristics of the collagen network in human normal, degraded and repair articular cartilages observed in polarized light and scanning electron microscopies. *Osteoarthritis Cartilage* 2011;19:1458–68.
- Buckwalter JA. Articular cartilage injuries. *Clin Orthop Relat Res* 2002;402:21–37.
- Lee CR, Grodzinsky AJ, Hsu HP, Spector M. Effects of a cultured autologous chondrocyte-seeded type II collagen scaffold on the healing of a chondral defect in a canine model. *J Orthop Res* 2003;21:272–81.
- Hunziker EB. Articular cartilage repair: are the intrinsic biological constraints undermining this process insuperable? *Osteoarthritis Cartilage* 1999;7:15–28.
- Kandel RA, Chen H, Clark J, Renlund R. Transplantation of cartilaginous tissue generated in vitro into articular joint defects. *Artif Cells Blood Substit Immobil Biotechnol* 1995;23:565–77.
- Pilliar RM, Kandel RA, Grynblas MD, Zalzal P, Hurtig M. Osteochondral defect repair using a novel tissue engineering approach: sheep model study. *Technol Health Care* 2007;15:47–56.
- Vanlauwe J, Saris DB, Victor J, Almqvist KF, Bellemans J, Luyten FP, et al. Five-year outcome of characterized chondrocyte implantation versus microfracture for symptomatic cartilage defects of the knee: early treatment matters. *Am J Sports Med* 2011;39:2566–74.
- Saris DB, Vanlauwe J, Victor J, Almqvist KF, Verdonk R, Bellemans J, et al. Treatment of symptomatic cartilage defects of the knee: characterized chondrocyte implantation results in better clinical outcome at 36 months in a randomized trial compared to microfracture. *Am J Sports Med* 2009;37(Suppl 1):10S–9S.
- Smith GD, Taylor J, Almqvist KF, Erggelet C, Knutsen G, Garcia Portabella M, et al. Arthroscopic assessment of cartilage repair: a validation study of 2 scoring systems. *Arthroscopy* 2005;21:1462–7.
- Jung M, Tuischer JS, Sergi C, Gotterbarm T, Pohl J, Richter W, et al. Local application of a collagen type I/hyaluronate matrix and growth and differentiation factor 5 influences the closure of osteochondral defects in a minipig model by enchondral ossification. *Growth Factors* 2006;24:225–32.
- O'Driscoll SW, Keeley FW, Salter RB. The chondrogenic potential of free autogenous periosteal grafts for biological resurfacing of major full-thickness defects in joint surfaces under the influence of continuous passive motion. An experimental investigation in the rabbit. *J Bone Joint Surg Am* 1986;68:1017–35.
- Brittberg M, Winalski CS. Evaluation of cartilage injuries and repair. *J Bone Joint Surg Am* 2003;85-A(Suppl 2):58–69.
- Peterson L, Minas T, Brittberg M, Nilsson A, Sjogren-Jansson E, Lindahl A. Two- to 9-year outcome after autologous chondrocyte transplantation of the knee. *Clin Orthop Relat Res* 2000;374:212–34.
- van den Borne MP, Raijmakers NJ, Vanlauwe J, Victor J, de Jong SN, Bellemans J, et al. International Cartilage Repair Society (ICRS) and Oswestry macroscopic cartilage evaluation scores validated for use in Autologous Chondrocyte Implantation (ACI) and microfracture. *Osteoarthritis Cartilage* 2007;15:1397–402.
- Recht M, Bobic V, Burstein D, Disler D, Gold G, Gray M, et al. Magnetic resonance imaging of articular cartilage. *Clin Orthop Relat Res* 2001;391 Suppl:S379–96.
- Roemer FW, Crema MD, Trattnig S, Guermazi A. Advances in imaging of osteoarthritis and cartilage. *Radiology* 2011;260:332–54.
- Lee KT, Choi YS, Lee YK, Cha SD, Koo HM. Comparison of MRI and arthroscopy in modified MOCART scoring system after autologous chondrocyte implantation for osteochondral lesion of the talus. *Orthopedics* 2011;34:e356–62.
- Marlovits S, Singer P, Zeller P, Mandl I, Haller J, Trattnig S. Magnetic resonance observation of cartilage repair tissue (MOCART) for the evaluation of autologous chondrocyte transplantation: determination of interobserver variability and correlation to clinical outcome after 2 years. *Eur J Radiol* 2006;57:16–23.
- Marlovits S, Striessnig G, Resinger CT, Aldrian SM, Vecsei V, Imhof H, et al. Definition of pertinent parameters for the evaluation of articular cartilage repair tissue with high-resolution magnetic resonance imaging. *Eur J Radiol* 2004;52:310–9.
- Brittberg M. Cell carriers as the next generation of cell therapy for cartilage repair: a review of the matrix-induced autologous chondrocyte implantation procedure. *Am J Sports Med* 2010;38:1259–71.
- Trattnig S, Ba-Ssalamah A, Pinker K, Plank C, Vecsei V, Marlovits S. Matrix-based autologous chondrocyte implantation for cartilage repair: noninvasive monitoring by high-resolution magnetic resonance imaging. *Magn Reson Imaging* 2005;23:779–87.
- Orth P, Goebel L, Wolfram U, Ong MF, Graber S, Kohn D, et al. Effect of subchondral drilling on the microarchitecture of subchondral bone: analysis in a large animal model at 6 months. *Am J Sports Med* 2012;40:828–36.
- Gerber HP, Vu TH, Ryan AM, Kowalski J, Werb Z, Ferrara N. VEGF couples hypertrophic cartilage remodeling, ossification and angiogenesis during endochondral bone formation. *Nat Med* 1999;5:623–8.
- Murata M, Yudoh K, Masuko K. The potential role of vascular endothelial growth factor (VEGF) in cartilage: how the angiogenic factor could be involved in the pathogenesis of osteoarthritis? *Osteoarthritis Cartilage* 2008;16:279–86.
- Pesesse L, Sanchez C, Henrotin Y. Osteochondral plate angiogenesis: a new treatment target in osteoarthritis. *Joint Bone Spine* 2011;78:144–9.
- Sellers RS, Peluso D, Morris EA. The effect of recombinant human bone morphogenetic protein-2 (rhBMP-2) on the

- healing of full-thickness defects of articular cartilage. *J Bone Joint Surg Am* 1997;79:1452–63.
31. Goldring MB, Goldring SR. Articular cartilage and subchondral bone in the pathogenesis of osteoarthritis. *Ann N Y Acad Sci* 2010;1192:230–7.
 32. Shrout PE, Fleiss JL. Intraclass correlations: uses in assessing rater reliability. *Psychol Bull* 1979;86:420–8.
 33. Aigner T, Cook JL, Gerwin N, Glasson SS, Lavery S, Little CB, et al. Histopathology atlas of animal model systems – overview of guiding principles. *Osteoarthritis Cartilage* 2010;18:S2–6.
 34. Pritzker KPH, Aigner T. Terminology of osteoarthritis cartilage and bone histopathology – a proposal for a consensus. *Osteoarthritis Cartilage* 2010;18:S7–9.
 35. Madry H, Kaul G, Cucchiari M, Stein U, Zurakowski D, Remberger K, et al. Enhanced repair of articular cartilage defects in vivo by transplanted chondrocytes overexpressing insulin-like growth factor I (IGF-I). *Gene Ther* 2005;12:1171–9.
 36. Cook SD, Patron LP, Salkeld SL, Rueger DC. Repair of articular cartilage defects with osteogenic protein-1 (BMP-7) in dogs. *J Bone Joint Surg Am* 2003;85-A(Suppl 3):116–23.
 37. Niederauer GG, Slivka MA, Leatherbury NC, Korvick DL, Harroff HH, Ehler WC, et al. Evaluation of multiphase implants for repair of focal osteochondral defects in goats. *Biomaterials* 2000;21:2561–74.
 38. Munirah S, Samsudin OC, Chen HC, Salmah SH, Aminuddin BS, Ruszymah BH. Articular cartilage restoration in load-bearing osteochondral defects by implantation of autologous chondrocyte-fibrin constructs: an experimental study in sheep. *J Bone Joint Surg Br* 2007;89:1099–109.
 39. Fortier LA, Potter HG, Rickey EJ, Schnabel LV, Foo LF, Chong LR, et al. Concentrated bone marrow aspirate improves full-thickness cartilage repair compared with microfracture in the equine model. *J Bone Joint Surg Am* 2010;92:1927–37.
 40. Kreuz PC, Steinwachs MR, Erggelet C, Krause SJ, Konrad G, Uhl M, et al. Results after microfracture of full-thickness chondral defects in different compartments in the knee. *Osteoarthritis Cartilage* 2006;14:1119–25.
 41. Schinhan M, Gruber M, Vavken P, Dorotka R, Samouh L, Chiari C, et al. Critical-size defect induces unicompartmental osteoarthritis in a stable ovine knee. *J Orthop Res* 2012;30:214–20.
 42. Little CB, Smith MM, Cake MA, Read RA, Murphy MJ, Barry FP. The OARSI histopathology initiative – recommendations for histological assessments of osteoarthritis in sheep and goats. *Osteoarthritis Cartilage* 2010;18:S80–92.
 43. Kaul G, Cucchiari M, Remberger K, Kohn D, Madry H. Failed cartilage repair for early osteoarthritis defects: a biochemical, histological and immunohistochemical analysis of the repair tissue after treatment with marrow-stimulation techniques. *Knee Surg Sports Traumatol Arthrosc* 2012 Jan 06, <http://dx.doi.org/10.1007/s00167-011-1853-x>. Epub ahead of print.
 44. Welsch GH, Zak L, Mamisch TC, Resinger C, Marlovits S, Trattnig S. Three-dimensional magnetic resonance observation of cartilage repair tissue (MOCART) score assessed with an isotropic three-dimensional true fast imaging with steady-state precession sequence at 3.0 Tesla. *Invest Radiol* 2009;44:603–12.
 45. Le Graverand MP, Buck RJ, Wyman BT, Vignon E, Mazzuca SA, Brandt KD, et al. Change in regional cartilage morphology and joint space width in osteoarthritis participants versus healthy controls: a multicentre study using 3.0 Tesla MRI and Lyon-Schuss radiography. *Ann Rheum Dis* 2010;69:155–62.
 46. Hunter DJ, Buck R, Vignon E, Eckstein F, Brandt K, Mazzuca SA, et al. Relation of regional articular cartilage morphometry and meniscal position by MRI to joint space width in knee radiographs. *Osteoarthritis Cartilage* 2009;17:1170–6.
 47. Conaghan PG, Felson D, Gold G, Lohmander S, Totterman S, Altman R. MRI and non-cartilaginous structures in knee osteoarthritis. *Osteoarthritis Cartilage* 2006;14(Suppl A):A87–94.
 48. Trattnig S, Winalski CS, Marlovits S, Jurvelin JS, Welsch GH, Potter HG. Magnetic resonance imaging of cartilage repair. *Cartilage* 2011;2:5–26.
 49. Jones CW, Willers C, Keogh A, Smolinski D, Fick D, Yates PJ, et al. Matrix-induced autologous chondrocyte implantation in sheep: objective assessments including confocal arthroscopy. *J Orthop Res* 2008;26:292–303.
 50. Foster JE, Maciewicz RA, Taberner J, Dieppe PA, Freemont AJ, Keen MC, et al. Structural periodicity in human articular cartilage: comparison between magnetic resonance imaging and histological findings. *Osteoarthritis Cartilage* 1999;7:480–5.

- III. **Goebel L**, Zurakowski D, Müller A, Pape D, Cucchiarini M, Madry H. 2D and 3D MOCART scoring systems assessed by 9.4 Tesla high-field MRI correlate with elementary and complex histological scoring systems in a translational model of osteochondral repair. *Osteoarthritis Cartilage*, 2014, 22(10):1386-95.

Reprinted from Osteoarthritis and Cartilage, Copyright © 2014, with permission from Elsevier, doi: 10.1016/j.joca.2014.05.027.

Osteoarthritis and Cartilage



2D and 3D MOCART scoring systems assessed by 9.4 T high-field MRI correlate with elementary and complex histological scoring systems in a translational model of osteochondral repair



L. Goebel ^{†‡}, D. Zurakowski [§], A. Müller ^{||}, D. Pape [¶], M. Cucchiariini [†], H. Madry ^{†‡*}

[†] Center of Experimental Orthopaedics, Saarland University Medical Center, Kirrberger Straße, Building 37, 66421 Homburg/Saar, Germany

[‡] Department of Orthopaedic Surgery, Saarland University Medical Center, Kirrberger Straße, Building 37, 66421 Homburg/Saar, Germany

[§] Departments of Anesthesia and Surgery, Children's Hospital Boston, Harvard Medical School, Boston, MA 02115, USA

^{||} Department of Diagnostic and Interventional Radiology, Saarland University Medical Center, Kirrberger Straße, Building 57, 66421 Homburg/Saar, Germany

[¶] Department of Orthopaedic Surgery, Centre Hospitalier, Clinique d'Eich, 76, Rue d'Eich, L-1460 Luxembourg, Luxembourg

ARTICLE INFO

Article history:

Received 1 February 2014

Accepted 30 May 2014

Keywords:

Osteochondral unit

Cartilage repair

Histological analysis

MRI

Correlation

Sheep

SUMMARY

Objective: To compare the 2D and 3D MOCART system obtained with 9.4 T high-field magnetic resonance imaging (MRI) for the *ex vivo* analysis of osteochondral repair in a translational model and to correlate the data with semiquantitative histological analysis.

Methods: Osteochondral samples representing all levels of repair (sheep medial femoral condyles; $n = 38$) were scanned in a 9.4 T high-field MRI. The 2D and adapted 3D MOCART systems were used for grading after point allocation to each category. Each score was correlated with corresponding reconstructions between both MOCART systems. Data were next correlated with corresponding categories of an elementary (Wakitani) and a complex (Sellers) histological scoring system as gold standards.

Results: Correlations between most 2D and 3D MOCART score categories were high, while mean total point values of 3D MOCART scores tended to be 15.8–16.1 points higher compared to the 2D MOCART scores based on a Bland–Altman analysis. “Defect fill” and “total points” of both MOCART scores correlated with corresponding categories of Wakitani and Sellers scores (all $P \leq 0.05$). “Subchondral bone plate” also correlated between 3D MOCART and Sellers scores ($P < 0.001$).

Conclusions: Most categories of the 2D and 3D MOCART systems correlate, while total scores were generally higher using the 3D MOCART system. Structural categories “total points” and “defect fill” can reliably be assessed by 9.4 T MRI evaluation using either system, “subchondral bone plate” using the 3D MOCART score. High-field MRI is valuable to objectively evaluate osteochondral repair in translational settings.

© 2014 Osteoarthritis Research Society International. Published by Elsevier Ltd. All rights reserved.

Introduction

Magnetic resonance imaging (MRI) is of great value for translational studies of osteochondral repair^{1–3}. MRI is the major noninvasive tool to assess the structure of normal and osteoarthritic articular cartilage and cartilaginous repair tissues^{4–10}.

Particularly the development of the 2D and 3D MOCART system has greatly influenced and advanced non-destructive investigations of cartilage repair^{11–14}. Clinical scanners with field strengths of 1.5 and 3.0 T (T) are also applied to assess cartilage repair in translational models *in vivo*^{15,16}. Using indirect arthrography at 1.5 T *in vivo*, ovine osteochondral repair was shown to correlate with histological findings¹⁶. This ability to provide information on the structure of the repair tissue is of great value because histological evaluation – the main pillar to reliably and reproducibly investigate articular cartilage repair – is more time-dependent^{16,17}. Recently, a higher degree of spatial resolution and image quality has been achieved by greatly enhancing the field strength of the applied systems¹⁵. Particularly the development of high-field MRI scanners at 9.4 T allows for a detailed assessment of experimental cartilage

* Address correspondence and reprint requests to: H. Madry, Kirrberger Strasse, Building 37-38, 66421 Homburg/Saar, Germany. Tel: 49-6841-1624515; Fax: 49-6841-1624988.

E-mail addresses: lgoebel@gmx.de (L. Goebel), david.zurakowski@childrens.harvard.edu (D. Zurakowski), andreas.mueller@uniklinikum-saarland.de (A. Müller), dietrichpape@yahoo.de (D. Pape), mmcucchiariini@hotmail.com (M. Cucchiariini), henning.madry@uks.eu (H. Madry).

repair, especially when dedicated transmit/receive coils for small samples are employed¹⁸. An increase in field strength directly correlates with a better signal-to-noise ratio (SNR) and higher resolutions, a main pillar when morphological MRI analysis are performed, while high-field MRI offers a vast range of possible applications^{15,19–21}. Moreover, it has been already shown that semiquantitative macroscopic analysis of articular cartilage repair correlates with the 2D MOCART score using high-field MRI¹⁸.

However, it remains unknown whether histological repair of articular cartilage defects in a large animal model correlates with the MOCART scores assessed by a high-field MRI at 9.4 T. Therefore, the first aim of this study was to compare the 2D and 3D MOCART systems obtained at 9.4 T for the *ex vivo* analysis of osteochondral repair in a sheep model. The rationale was based on the fact that the 3D MOCART score permits a more accurate and detailed assessment of cartilage repair compared with the 2D system^{12,13}. Second, we tested the hypothesis that the structural data from the 2D and 3D MOCART scoring systems significantly correlate with the respective categories from semiquantitative histological analysis using the elementary Wakitani²² and complex Sellers²³ score as gold standards.

Materials and methods

Study design

Adult Merino sheep received standardized full-thickness cartilage defects in the weight-bearing area of the medial femoral condyle of their stifle joints that were treated by Pridie drilling. After 6 months, the animals were sacrificed and the explanted osteochondral units containing the defects were scanned in a 9.4 T high-field MRI. The 2D and adapted 3D MOCART scores were applied independently by two different observers (A and B), and additionally a second time by observer A. By keeping a time interval of 19 months between both evaluations of observer A, a bias by recognition was ruled out. Data of both MOCART systems were compared between each other and correlated with the categories of a semiquantitative elementary and a complex histological scoring system (Fig. 1).

Animal experiments

Animal experiments were in accordance with the German legislation on protection of animals and the NIH Guidelines for the Care and Use of Laboratory Animals [NIH Publication 85-23, Rev.

1985] and were approved by the local governmental animal care committee (see Fig. 2). Osteochondral units were obtained from a previous study focusing on the development of a macroscopic scoring system for cartilage repair and its correlation with 9.4 T MRI¹⁸. The animal model has been reported before²⁴. Briefly, standardized full-thickness chondral defects (4 × 8 mm, rectangular) were created in the weight-bearing area of the medial femoral condyle in each stifle joint ($n = 44$) in healthy, skeletally mature female Merino sheep ($n = 22$; age between 2 years and 4 years; average weight 70 ± 20 kg) after entering the stifle joint through a medial parapatellar approach. The articular cartilage, including the calcified cartilage, was meticulously removed down to the cement line. Based on an *ex vivo* 9.4 T MRI analysis of two medial femoral condyles of a non-operated, age-matched, healthy, skeletally mature female Merino sheep, cartilage thickness ranged between 1.0 and 1.1 mm on either edge of the created cartilage defects. No bleeding from the subchondral bone was observed. Six subchondral drill holes (diameter: 1.0 mm) were introduced into each defect using a Kirschner wire to a depth of 10 mm in a standardized manner (2 × 3 parallel drill holes per defect). Animals were allowed fully weight-bearing *post operationem*. Preoperative, osteoarthritis has been excluded by X-ray examination. Three sheep ($n = 3/22$) were excluded due to infection. After 6 months, the sheep ($n = 19/22$) were sacrificed, the medial femoral condyles were explanted ($n = 38$), fixated in 4% formalin, transferred to 70% ethanol and prepared for further investigation.

Evaluation by 2D and 3D MOCART score with 9.4 T high-field MRI

Explanted medial condyles were examined in a 9.4 T high-field MRI scanner developed for imaging of small animals (Biospec Avance III 9.4/20, Bruker Biospin, Ettlingen, Germany) as previously described¹⁸. A circular polarized volume coil (inner diameter: 40 mm) adapted for imaging experiments of rat brain, in receive/transmit configuration was used. A three-dimensional (3D) spoiled gradient echo (GE) sequence was chosen to perform isovolumetric scans of the osteochondral samples. Optimized imaging categories were evaluated as: repetition time (TR): 10 ms, time echo (TE): 3 ms, flip angle (FA): 10°, number of excitations (NEX): 10 and bandwidth (BW): 98,684.2 kHz. To minimize acquisition time and warming of the samples and the employed coil system, readout direction was placed in alignment with the longest dimension of the scanned objects, adapting the matrix size to completely cover the samples (typically consisting of a set of $256 \times 128 \times 128$ voxels).

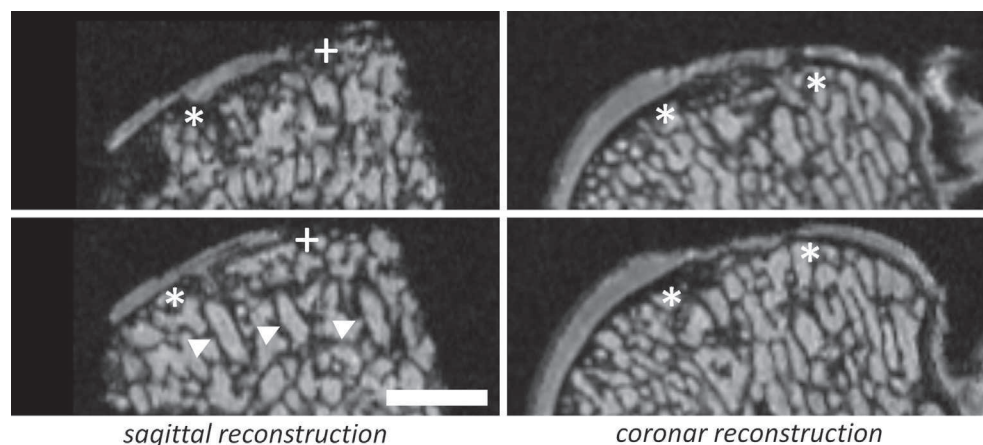


Fig. 1. Example of coronar and sagittal reconstructions of an osteochondral sample in a 9.4 T high-field MRI. Isometric voxel size (edge length = 120 μm) allows to virtually reconstruct MRI evaluations in any plane in space without losing steric information. Asterisks indicate the integration zone of the repair tissue with the adjacent normal articular cartilage, in the sagittal plane crosses demarcate artifacts caused by sample preparation, arrowheads point at drill holes. Scale bar, 4 mm.

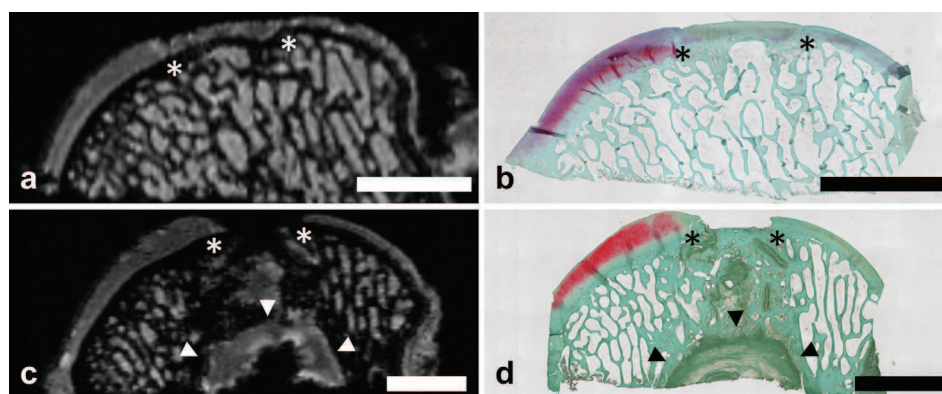


Fig. 2. Examples of osteochondral repair in corresponding high-field MRI images and histological sections. Example of good (a, b) and poor (c, d) osteochondral repair shown in representative coronar high-field MRI images (a, c) and corresponding coronar histological sections (b, d) of the same samples. The first osteochondral specimen illustrating good repair (a, b) is characterized by a complete filling of the defect, good integration at the margins, and a congruent articular surface. There is some degree of subchondral bone plate remodeling. In contrast, the second osteochondral specimen illustrating poor repair (c, d) shows no filling of the defect, lack of a congruent articular surface, and disturbance of the subchondral bone plate together with a large subchondral cyst. Asterisks indicate the integration zone of the repair tissue with the adjacent normal articular cartilage, arrowheads show the dimension of the subchondral cyst. Scale bar, 4 mm.

Standard voxel size was of $120 \times 120 \times 120 \mu\text{m}$, allowing for multiplanar reconstructions without losing spatial resolution. Consecutive to the scans, reconstructions in three orthogonal planes were performed in identical spatial resolution (Paravision 5.1, JIVE tool, Bruker Biospin) and analyzed with ImageJ version 1.45 (NIH, Bethesda, MD, USA; Fig. 1). Applying a standardized procedure, the anterior 3.5 mm of the defects were analyzed to avoid any influence caused by sample preparation.

First, the repair tissue of all defects was evaluated using a modification of the 2D MOCART score (a clinical scoring system for cartilage repair)¹¹ as previously described (Table I)¹⁸. Next, the 3D MOCART scoring system was adapted for the *ex vivo* analysis of small osteochondral samples as published by Trattnig *et al.*⁷. Point allocation was adopted from the modified 2D MOCART score while the different categories were fitted for *ex vivo* analyses^{11,18}. This

modified 3D MOCART scoring system then similarly ranged from 0 points (no repair) to 100 points (excellent cartilage defect repair; Table II).

The categories “defect fill”, “cartilage interface” (integration with adjacent cartilage), “bone interface” (integration to subchondral bone), “signal intensity” (of repair tissue) and “chondral osteophytes” (intralesional osteophytes) were used unchanged. From the category “surface”, the item “adhesions” was removed and considered as an independent category (analyzed by clinical examination). “Structure” was further subclassified, distinguishing four characteristics in the adapted 3D MOCART score (Table II). The new category “integrity of subchondral bone plate” was included, based on a scale developed by Ochs *et al.*²⁵. The different items from the category “subarticular spongiosa” were summarized into different groups to allow for a more comprehensive evaluation. The category “effusion” from the original 3D MOCART system was merged to the items “yes” or “absent” and determined by clinical inspection.

Table I

Modification of the clinical 2D MOCART score developed by Marlovits *et al.* for the evaluation of *ex vivo* osteochondral samples

2D MOCART score		
Category	Item	Points
Defect fill	Subchondral bone exposed	0
	Incomplete < 50%	5
	Incomplete > 50%	10
	Complete	20
	Hypertrophy	15
Cartilage interface	Complete	15
	Demarcating border visible	10
	Defect visible < 50%	5
	Defect visible > 50%	0
Surface	Surface intact	10
	Surface damaged < 50% of depth	5
	Surface damaged > 50% of depth	0
Adhesions	Absent	5
	Yes	0
Structure	Homogeneous	5
	Inhomogeneous or cleft formation	0
Signal intensity	Normal	30
	Nearly normal	10
	Abnormal	0
Subchondral lamina	Intact	5
	Not intact	0
Subchondral bone	Intact	5
	Granulation tissue, cyst, sclerosis	0
Effusion	Absent	5
	Yes	0
Total points		100

Intra- and interobserver reliability

The different reconstructions of the osteochondral samples gained in a 9.4 T high-field MRI were independently evaluated by two different observers (A and B), and additionally a second time by observer A. Between both evaluations of observer A, a time interval of 19 months was kept to prevent any bias by recognition. Observer A was a registrar for orthopedic surgery and observer B a consultant for orthopedic surgery.

Histological analysis

Decalcified and paraffin-embedded coronal sections of the osteochondral samples perpendicular to the articular surface (thickness $5 \mu\text{m}$) were stained with hematoxylin and eosin to detect cells and safranin O/fast green to detect proteoglycans as previously described²⁶. All cartilage defects were analyzed with the semiquantitative scoring systems developed by Wakitani *et al.* and Sellers *et al.*^{17,22,23} by observer A. A total of 418 sections were scored (11 sections per defect).

Internal and external correlation

2D and 3D MOCART scoring systems were correlated between each other (internal correlation). Therefore, reconstructions with

Table II

3D MOCART scoring system as described by Trattinig *et al.* adapted for the evaluation of *ex vivo* osteochondral samples

3D MOCART score		
Category	Item	Points
Defect fill	0%	0
	0–25%	3
	25–50%	5
	50–75%	10
	75–100%	15
	100%	20
	100–125%	15
	125–150%	7
	150–200%	3
	>200%	0
Cartilage interface	Complete	10
	Demarcating border	8
	Defect visible < 50%	3
	Defect visible > 50%	0
Bone interface	Complete	10
	Partial delamination	5
	Complete delamination/delamination of periosteal flap	0
Surface	Intact	10
	Damaged < 50% depth	5
	Damaged > 50% depth	0
Structure	Homogeneous	10
	Inhomogeneous	5
	Cleft formation	2
	Absence of repair tissue	0
Signal intensity	Normal (identical to adjacent cartilage)	10
	Nearly normal (slight areas of signal alteration)	5
	Abnormal (large areas of signal alteration)	0
Chondral osteophytes	Absent	5
	<50% of chondral thickness	3
	>50% of chondral thickness	0
Integrity of subchondral bone plate	>75%	10
	50–75%	8
	25–50%	5
	0–25%	3
	0%	0
Subarticular spongiosa	Intact	10
	Granulation tissue	8
	Sclerosis	8
	Cyst	5
	Granulation tissue and sclerosis	5
	Granulation tissue and cyst	2
	Sclerosis and cyst	2
	Granulation tissue, sclerosis and cyst	0
Adhesions	Absent	3
	Yes	0
Effusion	Absent	2
	Yes	0
Total points		100

Point allocation was based on the scale described by Trattinig *et al.* Category “remodelling of subchondral bone plate” was adopted from a scale suggested by Ochs *et al.*, “bone marrow edema” was excluded while “adhesions” and “effusion” were clinically determined.

identical orientation were compared between the 2D and 3D MOCART scores: coronal (2D coronar vs 3D coronar) and sagittal (2D sagittal vs 3D sagittal), as well as different reconstructions within identical scoring systems (2D coronar vs sagittal and 3D coronar vs sagittal). For external correlation, coronal and sagittal 2D and 3D MOCART scores were compared with Wakitani and Sellers scores from coronal sections.

Statistical evaluation

Results are expressed as mean value, 95% confidence interval (95% CI) and range or standard deviation (SD). To determine relationships between coronal and sagittal 2D and 3D MOCART total scores, the Bland–Altman method for calculating correlation

coefficients was used²⁷ to determine the average difference between the 2D and 3D systems (mean difference) and 95% CI for this difference (plus or minus two SDs). A paired *t*-test was applied to detect significant differences. For intra- and interobserver correlation, a linear correlation analysis was performed (Pearson correlation coefficient) for sagittal and coronal reconstructions of 2D and 3D MOCART scoring systems. When comparing 2D and 3D MOCART scores with Sellers and Wakitani scores, Pearson correlation coefficient was used to determine a possible relationship between histological and 9.4 T high-field MRI data. Calculations were performed with SPSS version 19.0 (SPSS Inc/IBM, Chicago, IL, USA). A *P* value <0.05 was considered to be statistically significant.

Results

Intra- and interobserver reliability

Both 2D and 3D MOCART scores were applied to grade articular cartilage repair on coronar and sagittal reconstructions based on a high-field MRI evaluation at 9.4 T (Table III).

Intraobserver reliability for total points of observer A between two different time points was always significant for the 2D MOCART (coronal reconstructions: $r = 0.804$, $P < 0.001$; sagittal reconstructions: $r = 0.496$, $P = 0.002$) and 3D MOCART systems (coronal reconstructions: $r = 0.821$, $P < 0.001$; sagittal reconstructions: $r = 0.642$, $P < 0.001$).

Interobserver reliability for total points between observer A and B was also significant for the 2D MOCART (coronal reconstructions: $r = 0.819$, $P < 0.001$; sagittal reconstructions: $r = 0.684$, $P < 0.001$) and 3D MOCART systems (coronal reconstructions: $r = 0.875$, $P < 0.001$; sagittal reconstructions: $r = 0.727$, $P < 0.001$).

Comparison of experimental articular cartilage repair between 2D and 3D MOCART scores

When total point values of the 2D and the 3D MOCART scores were correlated, strong correlations were found for both, coronal ($r = 0.940$, $P < 0.001$) and sagittal ($r = 0.931$, $P < 0.001$, Table IV), reconstructions. However, mean point values of 3D MOCART scores tended to be 15.8 ± 3.5 points (mean \pm SD) higher for coronal reconstructions and 16.1 ± 3.8 points for sagittal reconstructions than 2D MOCART scores. In this case, correlation did not necessarily imply agreement as the difference between total point values was significant for coronal (paired *t*-test = 28.15 on 37 degrees of freedom, $P < 0.001$) and sagittal (paired *t*-test = 26.15 on 37 degrees of freedom, $P < 0.001$) reconstructions yielding significantly higher total MOCART scores for the 3D MOCART system. Next, a Bland–Altman plot was done separately for coronal and sagittal reconstructions (Fig. 3), denoting the mean difference (referred to as the “bias”) and the limits of agreement as dashed lines (plus or minus two SDs). Based on this analysis, total scores tended to be generally higher using the 3D MOCART system: they are expected to be between 9 and 21 points higher for coronal and 8 to 24 points for sagittal reconstructions, than those obtained on the 2D MOCART system. A correlation analysis between the average of the 2D and 3D measurements vs the difference between the two systems was not significant for coronal ($P = 0.970$) or sagittal reconstructions ($P = 0.490$), revealing that the bias across the range of possible total scores of the 2D and 3D MOCART systems was constant.

Correlation of 2D and 3D MOCART scores with an elementary and a complex histological scoring system for cartilage repair

Overall, the internal correlation between the elementary Wakitani and complex Sellers semiquantitative histological scoring

Table III

9.4 T high-field MRI assessment of articular cartilage repair based on the semiquantitative 2D and 3D MOCART scoring systems

Category		2D MOCART										3D MOCART									
		Coronal reconstruction					Sagittal reconstruction					Coronal reconstruction					Sagittal reconstruction				
		A – I	A – II	A – mean	B – I	All – mean	A – I	A – II	A – mean	B – I	All – mean	A – I	A – II	A – mean	B – I	All – mean	A – I	A – II	A – mean	B – I	All – mean
Defect fill	mean	5.3	4.6	4.9	4.7	4.9	4.9	4.5	4.7	5.3	4.9	4.7	4.2	4.5	3.9	4.3	4.1	4	4.1	4.8	4.3
	CI	4.4–6.2	3.7–5.5	4.1–5.7	3.7–5.7	4.1–5.7	4–5.8	3.5–5.5	3.8–5.6	4.3–6.3	4.1–5.7	3.5–5.9	3–5.4	3.4–5.6	2.7–5.1	3.2–5.4	2.9–5.3	2.8–5.2	3–5.2	3.5–6.1	3.2–5.4
	range	0–10	0–10	0–10	0–10	0–10	0–10	0–10	0–10	0–10	0–10	0–15	0–15	0–15	0–15	0–15	0–15	0–15	0–15	0–15	0–15
Cartilage interface	mean	1.1	2.1	1.6	2.1	1.8	0.9	2.2	1.6	2.9	2	0.8	1.5	1.1	1.5	1.3	0.6	1.6	1.1	2.1	1.4
	CI	0.2–2	1–3.2	0.7–2.5	1–3.2	0.9–2.7	0–1.9	1.1–3.3	0.7–2.5	1.5–4.3	1.1–2.9	0.1–1.5	0.7–2.3	0.4–1.8	0.6–2.4	0.6–2	0–1.3	0.8–2.4	0.5–1.7	1.1–3.1	0.7–2.1
	range	0–10	0–10	0–10	0–10	0–10	0–15	0–10	0–12.5	0–15	0–11.7	0–8	0–8	0–8	0–8	0–8	0–10	0–8	0–9	0–10	0–8.7
Bone interface	mean	n.a.	n.a.	n.a.	n.a.	n.a.	n.a.	n.a.	n.a.	n.a.	n.a.	10	10	10	10	10	10	10	10	10	10
	CI											n.d.	n.d.	n.d.	n.d.	n.d.	n.d.	n.d.	n.d.	n.d.	n.d.
	range											n.d.	n.d.	n.d.	n.d.	n.d.	n.d.	n.d.	n.d.	n.d.	n.d.
Surface	mean	0.5	0.7	0.6	0.7	0.6	0.4	1.1	0.7	1.1	0.8	0.5	0.7	0.6	0.7	0.6	0.4	1.1	0.7	1.1	0.8
	CI	0–1	0.2–1.2	0.2–1	0–1.4	0.2–1	0–0.8	0.4–1.8	0.2–1.2	0.4–1.8	0.3–1.3	0–1	0.2–1.2	0.2–1	0–1.4	0.2–1	0–0.8	0.4–1.8	0.2–1.2	0.4–1.8	0.3–1.3
	range	0–5	0–5	0–5	0–10	0–6.7	0–5	0–5	0–5	0–5	0–5	0–5	0–5	0–5	0–10	0–6.7	0–5	0–5	0–5	0–5	0–5
Structure	mean	0.3	0.3	0.3	0.1	0.2	0.1	0.3	0.2	0	0.1	5.3	5.3	5.3	5.1	5.2	5.1	5.3	5.2	5	5.1
	CI	0–0.7	0–0.7	0–0.6	0–0.4	0–0.5	0–0.4	0–0.7	0–0.4	n.d.	0–0.2	4.9–5.7	4.9–5.7	5–5.6	4.8–5.4	4.9–5.5	4.8–5.4	4.9–5.7	5–5.4	n.d.	5–5.2
	range	0–5	0–5	0–5	0–5	0–5	0–5	0–5	0–2.5	n.d.	0–1.7	5–10	5–10	5–10	5–10	5–10	5–10	5–10	5–7.5	n.d.	5–6.7
Signal intensity	mean	10	4.5	7.2	4.2	6.2	9.5	5.3	7.4	4.6	6.4	4.7	2.1	3.4	2.1	3	4.6	2.4	3.5	2.3	3.1
	CI	8.2–11.8	2.4–6.6	5.5–8.9	2.6–5.8	4.8–7.6	8–11	2.9–7.7	5.9–8.9	3–6.2	5–7.8	4.1–5.3	1.2–3	2.8–4	1.3–2.9	2.4–3.6	4–5.2	1.4–3.4	2.9–4.1	1.5–3.1	2.5–3.7
	range	0–30	0–30	0–30	0–10	0–23.3	0–30	0–30	0–20	0–10	0–16.7	0–10	0–10	0–10	0–5	0–8.3	0–10	0–10	0–7.5	0–5	0–6.7
Chondral osteophytes	mean	n.a.	n.a.	n.a.	n.a.	n.a.	n.a.	n.a.	n.a.	n.a.	n.a.	4.8	4.5	4.6	4.4	4.6	4.7	4.3	4.5	4.3	4.4
	CI											4.5–5.1	4.2–4.8	4.4–4.8	4–4.8	4.3–4.9	4.3–5.1	3.8–4.8	4.1–4.9	3.9–4.7	4–4.8
	range											0–5	3–5	1.5–5	0–5	1–5	0–5	0–5	0–5	0–5	0–5
Subchondral bone plate	mean	0	0	0	0	0	0	0.1	0.1	0.1	0.1	0.8	2.7	1.8	3.8	2.5	0.9	3.4	2.2	4.6	3
	CI	n.d.	n.d.	n.d.	n.d.	n.d.	n.d.	0–0.4	0–0.2	0–0.4	0–0.3	0.3–1.3	1.9–3.5	1.2–2.4	2.9–4.7	1.9–3.1	0.3–1.5	2.6–4.2	1.6–2.8	3.7–5.5	2.4–3.6
	range	n.d.	n.d.	n.d.	n.d.	n.d.	n.d.	0–5	0–2.5	0–5	0–3.3	0–5	0–8	0–6.5	0–8	0–7	0–5	0–10	0–6.5	0–10	0–7.7
Subarticular spongiosa	mean	0.1	0	0.1	0	0	0.1	0	0.1	0	0	3.6	2.9	3.3	2.6	3	3.4	3.4	3.4	3	3.3
	CI	0–0.4	n.d.	0–0.2	n.d.	0–0.1	0–0.4	n.d.	0–0.2	n.d.	0–0.1	2.6–4.6	1.9–3.9	2.4–4.2	1.8–3.4	2.2–3.8	2.4–4.4	2.4–4.4	2.5–4.3	2.1–3.9	2.5–4.1
	range	0–5	n.d.	0–2.5	n.d.	0–1.7	0–5	n.d.	0–2.5	n.d.	0–1.7	0–10	0–8	0–9	0–8	0–7.7	0–10	0–8	0–9	0–8	0–8
Adhesions	mean	5	5	5	5	5	5	5	5	5	5	3	3	3	3	3	3	3	3	3	3
	CI	n.d.	n.d.	n.d.	n.d.	n.d.	n.d.	n.d.	n.d.	n.d.	n.d.	n.d.	n.d.	n.d.	n.d.	n.d.	n.d.	n.d.	n.d.	n.d.	n.d.
	range	n.d.	n.d.	n.d.	n.d.	n.d.	n.d.	n.d.	n.d.	n.d.	n.d.	n.d.	n.d.	n.d.	n.d.	n.d.	n.d.	n.d.	n.d.	n.d.	n.d.
Effusion	mean	4.9	4.9	4.9	4.9	4.9	4.9	4.9	4.9	4.9	4.9	1.9	1.9	1.9	1.9	1.9	1.9	1.9	1.9	1.9	1.9
	CI	4.6–5.2	4.6–5.2	4.6–5.2	4.6–5.2	4.6–5.2	4.6–5.2	4.6–5.2	4.6–5.2	4.6–5.2	4.6–5.2	1.8–2	1.8–2	1.8–2	1.8–2	1.8–2	1.8–2	1.8–2	1.8–2	1.8–2	1.86–2
	range	0–5	0–5	0–5	0–5	0–5	0–5	0–5	0–5	0–5	0–5	0–2	0–2	0–2	0–2	0–2	0–2	0–2	0–2	0–2	0–2
Total points	mean	27.1	22	24.5	21.7	23.6	25.8	23.3	24.5	23.7	25.1	40.2	38.8	39.5	39.2	39.4	38.9	40.3	39.6	42	41.3
	CI	23.8–30.4	18.4–25.6	21.2–27.8	18.4–25	20.4–26.8	22.7–28.9	19.6–27	21.5–27.5	20.2–27.2	21.9–28.3	37.2–43.2	35.3–42.3	36.4–42.6	35.6–42.8	36.2–42.6	35.9–41.9	36.6–44	36.6–42.6	38.3–45.7	38–44.6
	range	10–70	10–65	12.5–67.5	10–55	13.3–63.3	10–70	10–50	10–55	10–50	11.7–50	27–73	25–74	29–73.5	27–79	29.3–75.3	27–76	25–69	27.5–67.5	27–72	28.7–66.3

Results are expressed as mean value (mean), 95% CI and minimum and maximum values (range) for all ($n = 38$) tested samples. A and B indicate two different observers; I and II two time points. A – mean indicates the mean point values for all observations by observer A, respectively; all – mean indicates mean point values for all observations, and all observers together. n.d.: not determined. n.a.: not applicable.

Table IV

Internal correlation of the 2D and 3D MOCART systems at 9.4 T and external correlation with the Sellers and Wakitani histological scoring systems

Internal correlation									
Category	2D – cor. vs sag.		3D – cor. vs sag.		2D vs 3D – cor.		2D vs 3D – sag.		
	<i>r</i>	<i>P</i>	<i>r</i>	<i>P</i>	<i>r</i>	<i>P</i>	<i>r</i>	<i>P</i>	
Defect fill	0.841	<0.001	0.863	<0.001	0.927	<0.001	0.930	<0.001	
Cartilage interface	0.714	<0.001	0.695	<0.001	0.995	<0.001	0.996	<0.001	
Bone interface	n.d.	n.d.	1	<0.001	n.d.	n.d.	n.d.	n.d.	
Surface	0.833	<0.001	0.322	0.048	1	<0.001	0.553	0.001	
Structure	0.487	0.002	0.487	0.002	1	<0.001	1	<0.001	
Signal intensity	0.803	<0.001	0.853	<0.001	0.976	<0.001	0.985	<0.001	
Chondral osteophytes	n.d.	n.d.	0.944	<0.001	n.d.	n.d.	n.d.	n.d.	
Subchondral bone plate	n.d.	n.d.	0.796	<0.001	n.d.	n.d.	0.395	0.014	
Subarticular spongiosa	1	<0.001	0.903	<0.001	0.309	0.058	0.294	0.092	
Adhesions	1	<0.001	1	<0.001	1	<0.001	1	<0.001	
Effusion	1	<0.001	1	<0.001	1	<0.001	1	<0.001	
Total points	0.718	<0.001	0.723	<0.001	0.940	<0.001	0.931	<0.001	
External correlation									
Category	Wakitani score					Sellers score			
	With 2D MOCART		With 3D MOCART		With 2D MOCART		With 3D MOCART		
	Coronar	Sagittal	Coronar	Sagittal	Coronar	Sagittal	Coronar	Sagittal	
Defect fill	<i>r</i>	−0.757	−0.714	−0.774	−0.770	−0.763	−0.736	−0.800	−0.812
	<i>P</i>	<0.001	<0.001	<0.001	<0.001	<0.001	<0.001	<0.001	<0.001
Cartilage interface	<i>r</i>	−0.164	−0.242	−0.156	−0.424	−0.122	−0.214	−0.117	−0.213
	<i>P</i>	0.325	0.143	0.348	0.142	0.464	0.198	0.485	0.198
Surface	<i>r</i>	−0.105	0.034	−0.105	0.162	−0.147	−0.004	−0.147	0.150
	<i>P</i>	0.529	0.838	0.529	0.331	0.377	0.980	0.377	0.367
Structure	<i>r</i>	n.d.	n.d.	n.d.	n.d.	−0.239	−0.419	−0.239	−0.419
	<i>P</i>					0.148	0.009	0.148	0.009
Subchondral bone plate	<i>r</i>	n.d.	n.d.	n.d.	n.d.	n.d.	−0.219	−0.522	−0.600
	<i>P</i>						0.186	0.001	<0.001
Total points	<i>r</i>	−0.512	−0.458	−0.479	−0.445	−0.598	−0.442	−0.630	−0.520
	<i>P</i>	<0.001	0.004	0.002	0.005	<0.001	0.005	<0.001	0.001

For internal correlation, identical categories were directly correlated. For external correlation, coronal and sagittal reconstructions of the 2D and 3D MOCART scores were applied. Here, fitting and/or corresponding items were correlated. 2D = 2D MOCART score; 3D = 3D MOCART score; cor. = coronal planes; sag. = sagittal planes; both = both planes. Pearson *r* and *P* values were determined. Significant *r* values are in bold (n.d. = not done).

systems was reasonable good with $r = 0.777$ for total score ($P < 0.001$), $r = 0.963$ for defect fill ($P < 0.001$), $r = 0.979$ for integration ($P < 0.001$), $r = 0.919$ for matrix staining ($P < 0.001$), $r = 0.706$ for cell morphology ($P < 0.001$), and $r = 0.966$ for surface ($P < 0.001$).

Coronal and sagittal reconstructions of the 2D and 3D MOCART total scores (averaged between all observations and observers) were next compared with the Wakitani and Sellers scoring systems

(Tables IV and V). The results obtained by the 3D MOCART score were, in general, better than with the 2D system.

Based on these results, Sellers and Wakitani histological scoring systems (Fig. 4) were plotted against the 3D MOCART system with the objective of assessing this relationship for coronal vs sagittal reconstructions. The inverse relationships (for both coronal and sagittal) were in average better with respect to predicting Sellers than Wakitani histological scores (Table IV). When the Sellers score

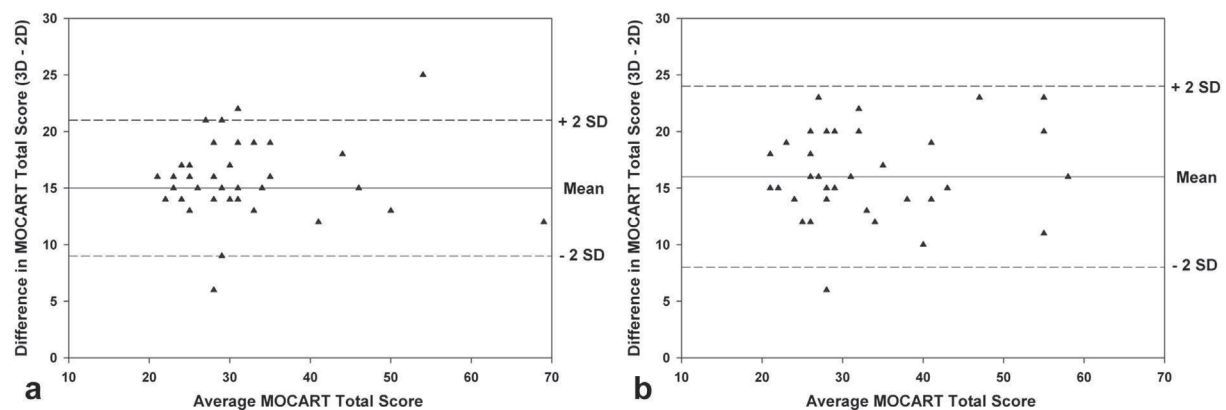


Fig. 3. Bland–Altman plot of 2D and 3D MOCART scoring systems for coronal (a) and sagittal (b) reconstructions. The average of the two scoring systems total points are plotted on the x-axis ($(2D + 3D \text{ MOCART systems total points})/2$) and the difference between the two systems on the y-axis ($3D - 2D \text{ MOCART systems total points}$). For coronal reconstructions (a), the mean difference was 15 points and the 95% CI was between 9 and 21 points higher with the modified 3D MOCART scoring system. Limits of agreement are denoted as dashed lines. Correlation analysis between the average of the 2D and 3D measurements vs the difference was not significant ($P = 0.970$). For sagittal reconstructions (b), mean difference was 16 points with 95% CI between 8 and 24 points higher for the modified 3D MOCART scoring system. Here, correlation analysis was also not significant ($P = 0.490$).

Table V

Results of an elementary (Wakitani) and a complex (Sellers) semiquantitative histological scoring system serving as examples for established articular cartilage repair grading systems

Category	Mean	95% CI	Range
Wakitani score			
Cell morphology	1.7	1.6–1.8	1.0–2.2
Matrix staining	2.9	2.7–3.0	1.2–3.0
Surface regularity	2.2	2.0–2.5	0.6–3.0
Thickness of cartilage	1.4	1.2–1.7	0–2.0
Integration	0.8	0.6–1.0	0–2.0
Total points	9.0	8.4–9.6	6.1–11.9
Sellers score			
Filling	3.1	2.7–3.5	0–4.0
Integration	1.8	1.5–2.0	0.6–3.0
Matrix staining	3.8	3.6–4.0	1.5–4.0
Cellular morphology	4.4	4.2–4.7	1.7–5.0
Architecture defect	2.7	2.3–3.1	0.5–4.0
Architecture surface	2.3	2.1–2.5	0.6–3.1
Subchondral bone	1.6	1.2–2.0	0–4.0
Tidemark	4.0	3.9–4.0	3.1–4.0
Total points	23.5	22.3–24.8	14.1–29.6

Results are expressed as mean value (mean), 95% CI and minimum and maximum values (range) for all ($n = 38$) tested samples.

was plotted against the 3D MOCART score (Fig. 4), the fitted linear equations were $y = 33 - 0.25 \cdot x$ for coronal reconstructions ($R^2 = 41\%$ (of variance explained)) and $y = 35 - 0.28 \cdot x$ ($R^2 = 49\%$) for sagittal reconstructions. For the Wakitani score (Fig. 4), fitted linear equations were described with $y = 13 - 0.09 \cdot x$ ($R^2 = 25\%$) for coronal reconstructions and $y = 13 - 0.11 \cdot x$ ($R^2 = 32\%$) for sagittal reconstructions, when plotted against the 3D MOCART system. Here, similar relationships were found for both – coronal and sagittal-reconstructions in predicting Sellers or Wakitani scores.

Discussion

The major finding of the present study is that key histological categories of both an elementary and a complex histological scoring system for experimental osteochondral repair can reliably be determined by non-destructive 9.4 T high-field MRI evaluation. Histological categories “total points” and “defect fill” of both the Wakitani and Sellers scores can reliably be assessed by 9.4 T high-field MRI using either the 2D or 3D MOCART system. Second, the adapted 3D MOCART score allows to reliably assess the category subchondral bone plate of the Sellers histological scoring system. Third, correlation analysis between 2D and 3D MOCART scores was high, while, based on a Bland–Altman analysis, 3D MOCART scores

tend to reach averagely 15 points more for coronal and 16 points for sagittal assessments compared to the 2D system.

The MOCART scoring systems were initially defined for the *in vivo* assessment of articular cartilage repair in patients, and are usually performed with scanners at 1.5, respectively 3.0 T^{7,11–13}. Previously, we found high correlations between macroscopic scoring systems and 9.4 T MRI when the 2D MOCART scoring system was adapted for the *ex vivo* analysis of osteochondral samples of cartilage repair¹⁸. The 3D MOCART system represents a significant improvement of the 2D MOCART score, allowing for a more accurate and detailed assessment of osteochondral repair^{7,12}. Further developments in MRI, such as increased field strength, allow for higher resolutions and improved image quality. The limitations in sample volume usually necessitate an *ex vivo* analysis of specimen from large translational animal models^{18,28–31}. In the present work, the 3D MOCART system was adapted to be applicable for the *ex vivo* assessment of osteochondral samples. In this system, point allocation was adjusted to the 2D MOCART system, while categories “adhesions” or “edema” were chosen to be determined by clinical examination. “Subchondral bone plate”, a category based on a pointing scale by Ochs *et al.*²⁵, was included because the integrity of the subchondral bone is a key for preserving the function of the entire osteochondral unit^{32,33}. This category is already similarly represented as histological category “subchondral bone” in the Sellers score²³. Likewise, the different items of the original 3D MOCART score category “subchondral bone” were combined to different groups in the adapted category “subarticular spongiosa” to allow for an improved description of possible alterations. Altogether, the structure and point allocation of this adapted 3D MOCART score is now similar to major histological scoring systems, emphasizing the close association between data obtained by 9.4 T high-field MRI and histological analyses. The possibility of performing MRI immediately after explantation of the samples is of great advantage as it allows for a rapid assessment of cartilage repair^{2,3,8}. Important outcome categories of experimental cartilage repair such as “defect fill” and “total points” can be directly assessed, while histological analyses are more time-consuming. More importantly, MRI allows for a straightforward non-destructive evaluation in different planes that is complicated to achieve for histological assessments based on (serial) sections of parallel planes²⁶.

When individual categories of the 2D MOCART score were correlated with the corresponding categories of the 3D MOCART score in a 9.4 T high-field MRI, all categories exhibited high internal correlation except for “subarticular spongiosa”. This may be explained by the fact that the 2D MOCART only distinguishes

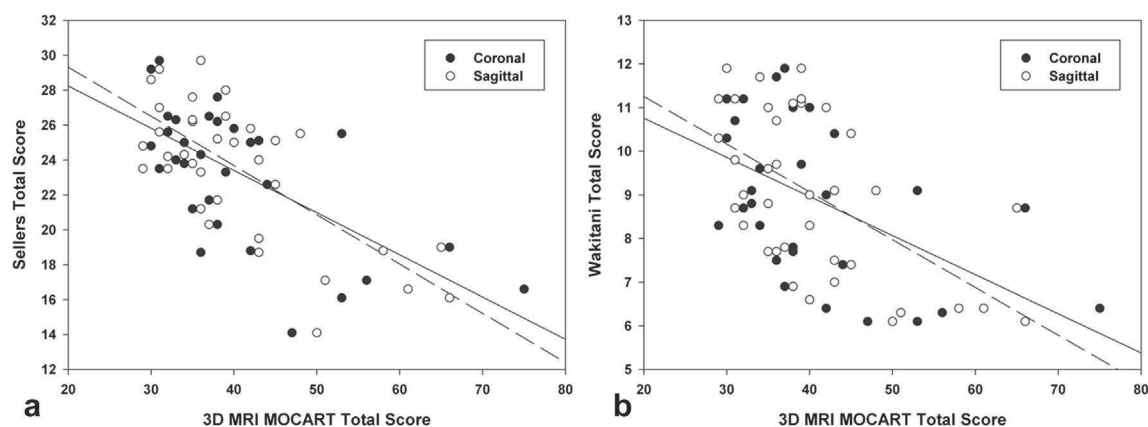


Fig. 4. Inverse relationship of the 3D MOCART scoring system with histological scoring systems. Coronal (solid line) and sagittal (dashed line) 3D MOCART total scores were plotted against the Sellers (a) and Wakitani scores (b). A similar relationship in predicting histological scores were found for both, coronal and sagittal, reconstructions.

normal from altered cancellous bone, while the 3D MOCART system distinguishes seven different groups of alterations. Correlations between coronal and sagittal planes within the same scoring system were always high, emphasizing the possibility to reliably assess cartilage repair in different planes with both MOCART scores. When 2D or 3D MOCART systems are applied, investigators need to be aware of a bias when comparing both systems. The Bland–Altman analysis clearly suggests that the MOCART total score depends on whether the 2D or 3D systems are used. While the correlation is very high, analysis based on Bland–Altman agreement confirms considerably higher scores using the modified 3D system. Thus, highly correlated but evidence suggests a lack of agreement judging from the average difference of 15 points for coronal and 16 points for sagittal assessments, and the use of the 3D MOCART score is recommended, provided that the bias in terms of average difference is kept in mind when comparing the 2D with the 3D system.

Of note, the categories “defect fill” and “total points” of the 2D and 3D MOCART scores reflected well the corresponding categories of the Sellers and Wakitani histological scores. Also, the category “subchondral bone plate” of the 3D MOCART system correlated with the respective category of the Sellers system. This shows that histological “defect fill” and “total points” – important structural categories of cartilage repair – can reliably be estimated at a very early time point by 9.4 T high-field MRI evaluation, as well as “subchondral bone plate” when using the 3D system. The linear relationship for 2D and 3D MOCART total scores (averaged between the two independent observers and time points) were compared between different reconstructions and each histological score. The results obtained by 3D were, in general, better than 2D and therefore 3D MOCART total scores were plotted with each histological score with the objective of assessing this relationship for coronal vs sagittal planes. The inverse relationships for both, coronal and sagittal, were better with respect to predicting Sellers than Wakitani, mostly because the range of scores is narrower for Wakitani and consequently this restriction of range attenuates the correlation (and thus, a lower R^2). Only structural categories as e.g., “defect fill”, and “total points” correlated, as all tested systems describe structural categories. *Vice versa*, other histological categories as “cell structure” or “matrix staining” were lacking a congruent MRI counterpart. Previous studies have already proven that macroscopic “defect fill” as well as “total points” correlated with articular cartilage repair assessed by 9.4 T high-field MRI¹⁸.

Although the present findings strongly link experimental 9.4 T high-field MRI to macroscopic and histological assessment of cartilage repair based on the high correlations for key categories between both, MRI and macroscopy¹⁸, and MRI and histology, a limitation remains the inability of MRI to depict single cells and their arrangement. Moreover, a direct *in vivo* assessment of cartilage repair in large animals has not been performed yet due to the inherent small coil size of current experimental 9.4 T high-field MRI scanners. While *in vivo* high-field MRI at 9.4 T, to the best of our knowledge, has only been performed for small animal models (e.g., rat³⁴ or guinea pig³⁵), future studies are warranted to expand these findings: High-field MRI with 7.0 T or above allow for new applications. One advantage is that the SNR and possible spatial resolution directly correlate with the field-strength. The increased sensitivity to susceptibility effects may be used for susceptibility weighted-imaging (SWI) which may allow to gain completely new contrast possibilities at higher field-strength^{15,36}. While clinical MRI scanners at 1.5 or 3.0 T usually rely on protons, other nuclei as ²³Na, ³¹P or ¹⁷O may allow a more specific diagnosis because of a closer relationship to the pathology^{15,21}. Nuclei other than protons are less sensitive and provide lower signals, resulting either in larger voxel size or increased measure time, or both. Here, MRI with a higher field strength of 7.0 or 9.4 T may play a key role to foster

clinical applications of non-proton MRIs^{15,20}. When the field strength is enlarged, proton relaxation times of the tissues change, as e.g., observed for T1, increases³⁷. On the other hand high-field MRI is more challenging to perform, as an increased severity to artifacts, higher motion sensitivity, increased sensitivity to physiological noise, increased radiofrequency inhomogeneities and specific absorption rate effects (SAR), as caused by tissue heating in the MRI, are observed. SAR increases with the square of the magnetic field strength, and therefore heating issues may become a problem at higher field-strengths³⁸.

New generation of experimental high-field MRI with larger gentry size or clinical MRI scanners with increased field-strength will allow to perform *in vivo* analyses in large animal models. Recently, some studies have already reported imaging of knee or ankle cartilage at 7.0 T in clinical ultra-high-field MRI in patients^{39,40}. For example, cartilage and trabecular bone can be imaged in ultra-high-field MRI as described by Krug *et al.*¹⁹ where quantitative MRI for the assessment of trabecular bone structure at the tibia, wrist, and knee were employed. Welsch *et al.*⁴¹ reported results of *in vivo* biochemical MRI at 7.0 T for dGEMRIC, T2, and T2* mapping of articular cartilage and found promising results for the differentiation of healthy and affected articular cartilage for a zonal assessment of deep and superficial cartilage layers.

A strength of this study is the combined assessment of cartilage repair by histological and high-field MRI at 9.4 T, showing that the 2D and 3D MRI scoring systems correlate with each other, while being aware of a bias of 15–16 points when the 3D system is applied, and with histological assessments. Also, the original and now adapted 2D and 3D MOCART scores share several similar categories with the applied histological scoring systems. This enables to reliably compare key categories of cartilage repair for either system. In principle, high-field MRI provides an improved non-invasive method to visualize articular cartilage repair in any desired plane. Moreover, high-field MRI with a voxel size of 120 μ m edge length may link macroscopy to histology.

Altogether, these findings emphasize the value of 9.4 T high-field MRI as it offers novel avenues to objectively evaluate osteochondral repair in translational settings.

Contributions

Conception and design of the study: Henning Madry. Acquisition of the data: Lars Goebel, David Zurakowski, Andreas Müller, Dietrich Pape, Magali Cucchiari, Henning Madry. Analysis and interpretation: Lars Goebel, David Zurakowski, Andreas Müller, Magali Cucchiari, Dietrich Pape, Henning Madry. All authors participated in drafting and critically revising of the article, and final approval.

Role of funding source

Supported in part by the Gesellschaft für Arthroskopie und Gelenkchirurgie (AGA; Forschungsförderung Nr. 29). This study sponsor was not involved in the study design, data collection or analysis or in the writing of the manuscript. Furthermore, it did not affect the decision to submit the manuscript for publication.

Competing interests

All authors declare no competing interests.

References

1. Buck RJ, Wyman BT, Le Graverand MP, Wirth W, Eckstein F. An efficient subset of morphological measures for articular cartilage in the healthy and diseased human knee. *Magn Reson Med* 2010;63:680–90.

2. Ding C, Zhang Y, Hunter D. Use of imaging techniques to predict progression in osteoarthritis. *Curr Opin Rheumatol* 2013;25:127–35.
3. Eckstein F, Guermazi A, Roemer FW. Quantitative MR imaging of cartilage and trabecular bone in osteoarthritis. *Radiol Clin North Am* 2009;47:655–73.
4. Roemer FW, Eckstein F, Guermazi A. Magnetic resonance imaging-based semiquantitative and quantitative assessment in osteoarthritis. *Rheum Dis Clin North Am* 2009;35:521–55.
5. Roemer FW, Kwok CK, Hannon MJ, Crema MD, Moore CE, Jakicic JM, et al. Semiquantitative assessment of focal cartilage damage at 3T MRI: a comparative study of dual echo at steady state (DESS) and intermediate-weighted (IW) fat suppressed fast spin echo sequences. *Eur J Radiol* 2011;80:e126–131.
6. Roemer FW, Crema MD, Trattnig S, Guermazi A. Advances in imaging of osteoarthritis and cartilage. *Radiology* 2011;260:332–54.
7. Trattnig S, Domayer S, Welsch GW, Mosher T, Eckstein F. MR imaging of cartilage and its repair in the knee – a review. *Eur Radiol* 2009;19:1582–94.
8. Crema MD, Roemer FW, Marra MD, Burstein D, Gold GE, Eckstein F, et al. Articular cartilage in the knee: current MR imaging techniques and applications in clinical practice and research. *Radiographics* 2011;31:37–61.
9. Gallo RA, Mosher TJ. Imaging of cartilage and osteochondral injuries: a case-based review. *Clin Sports Med* 2013;32:477–505.
10. Guermazi A, Hayashi D, Eckstein F, Hunter DJ, Duryea J, Roemer FW. Imaging of osteoarthritis. *Rheum Dis Clin North Am* 2013;39:67–105.
11. Marlovits S, Singer P, Zeller P, Mandl I, Haller J, Trattnig S. Magnetic resonance observation of cartilage repair tissue (MOCART) for the evaluation of autologous chondrocyte transplantation: determination of interobserver variability and correlation to clinical outcome after 2 years. *Eur J Radiol* 2006;57:16–23.
12. Welsch GH, Zak L, Mamisch TC, Resinger C, Marlovits S, Trattnig S. Three-dimensional magnetic resonance observation of cartilage repair tissue (MOCART) score assessed with an isotropic three-dimensional true fast imaging with steady-state precession sequence at 3.0 Tesla. *Invest Radiol* 2009;44:603–12.
13. Welsch GH, Zak L, Mamisch TC, Paul D, Lauer L, Mauerer A, et al. Advanced morphological 3D magnetic resonance observation of cartilage repair tissue (MOCART) scoring using a new isotropic 3D proton-density, turbo spin echo sequence with variable flip angle distribution (PD-SPACE) compared to an isotropic 3D steady-state free precession sequence (True-FISP) and standard 2D sequences. *J Magn Reson Imaging* 2011;33:180–8.
14. Lee KT, Choi YS, Lee YK, Cha SD, Koo HM. Comparison of MRI and arthroscopy in modified MOCART scoring system after autologous chondrocyte implantation for osteochondral lesion of the talus. *Orthopedics* 2011;34:e356–362.
15. Moser E, Stahlberg F, Ladd ME, Trattnig S. 7-T MR – from research to clinical applications? *NMR Biomed* 2012;25:695–716.
16. Streitparth F, Schottle P, Schlichting K, Schell H, Fischbach F, Denecke T, et al. Osteochondral defect repair after implantation of biodegradable scaffolds: indirect magnetic resonance arthrography and histopathologic correlation. *Acta Radiol* 2009;50:765–74.
17. Orth P, Zurakowski D, Wincheringer D, Madry H. Reliability, reproducibility and validation of five major histological scoring systems for experimental articular cartilage repair in the rabbit model. *Tissue Eng Part C Methods* 2012;18:329–39.
18. Goebel L, Orth P, Muller A, Zurakowski D, Buckner A, Cucchiari M, et al. Experimental scoring systems for macroscopic articular cartilage repair correlate with the MOCART score assessed by a high-field MRI at 9.4 T – comparative evaluation of five macroscopic scoring systems in a large animal cartilage defect model. *Osteoarthritis Cartilage* 2012;20:1046–55.
19. Krug R, Stehling C, Kelley DA, Majumdar S, Link TM. Imaging of the musculoskeletal system in vivo using ultra-high field magnetic resonance at 7 T. *Invest Radiol* 2009;44:613–8.
20. Moser E. Ultra-high-field magnetic resonance: why and when? *World J Radiol* 2010;2:37–40.
21. Trattnig S, Welsch GH, Juras V, Szomolanyi P, Mayerhoefer ME, Stelzeneder D, et al. ²³Na MR imaging at 7 T after knee matrix-associated autologous chondrocyte transplantation preliminary results. *Radiology* 2010;257:175–84.
22. Wakitani S, Goto T, Pineda SJ, Young RG, Mansour JM, Caplan AI, et al. Mesenchymal cell-based repair of large, full-thickness defects of articular cartilage. *J Bone Joint Surg Am* 1994;76:579–92.
23. Sellers RS, Peluso D, Morris EA. The effect of recombinant human bone morphogenetic protein-2 (rhBMP-2) on the healing of full-thickness defects of articular cartilage. *J Bone Joint Surg Am* 1997;79:1452–63.
24. Orth P, Goebel L, Wolfram U, Ong MF, Graber S, Kohn D, et al. Effect of subchondral drilling on the microarchitecture of subchondral bone: analysis in a large animal model at 6 months. *Am J Sports Med* 2012;40:828–36.
25. Ochs BG, Muller-Horvat C, Albrecht D, Schewe B, Weise K, Aicher WK, et al. Remodeling of articular cartilage and subchondral bone after bone grafting and matrix-associated autologous chondrocyte implantation for osteochondritis dissecans of the knee. *Am J Sports Med* 2011;39:764–73.
26. Schmitz N, Laverty S, Kraus VB, Aigner T. Basic methods in histopathology of joint tissues. *Osteoarthritis and Cartilage* 2010;18:S113–6.
27. Bland JM, Altman DG. Statistical methods for assessing agreement between two methods of clinical measurement. *Lancet* 1986;1:307–10.
28. Ramaswamy S, Gurkan I, Sharma B, Cascio B, Fishbein KW, Spencer RG. Assessment of tissue repair in full thickness chondral defects in the rabbit using magnetic resonance imaging transverse relaxation measurements. *J Biomed Mater Res B Appl Biomater* 2008;86B:375–80.
29. Kangarlou A, Gahunia HK. Magnetic resonance imaging characterization of osteochondral defect repair in a goat model at 8 T. *Osteoarthritis Cartilage* 2006;14:52–62.
30. Batiste DL, Kirkley A, Laverty S, Thain LM, Spouge AR, Holdsworth DW. Ex vivo characterization of articular cartilage and bone lesions in a rabbit ACL transection model of osteoarthritis using MRI and micro-CT. *Osteoarthritis Cartilage* 2004;12:986–96.
31. Wang M, Radjenovic A, Stapleton TW, Venkatesh R, Williams S, Ingham E, et al. A novel and non-destructive method to examine meniscus architecture using 9.4 Tesla MRI. *Osteoarthritis Cartilage* 2010;18:1417–20.
32. Goldring MB, Goldring SR. Articular cartilage and subchondral bone in the pathogenesis of osteoarthritis. *Ann N Y Acad Sci* 2010;1192:230–7.
33. Gomoll AH, Madry H, Knutsen G, van Dijk N, Seil R, Brittberg M, et al. The subchondral bone in articular cartilage repair: current problems in the surgical management. *Knee Surg Sports Traumatol Arthrosc* 2010;18:434–47.
34. McErlain DD, Ulici V, Darling M, Gati JS, Pitelka V, Beier F, et al. An in vivo investigation of the initiation and progression of

- subchondral cysts in a rodent model of secondary osteoarthritis. *Arthritis Res Ther* 2012;14:R26.
35. Fenty MC, Dodge GR, Kassey VB, Witschey WR, Borthakur A, Reddy R. Quantitative cartilage degeneration associated with spontaneous osteoarthritis in a guinea pig model. *J Magn Reson Imaging* 2012;35:891–8.
 36. Deistung A, Rauscher A, Sedlacik J, Stadler J, Witoszynskyj S, Reichenbach JR. Susceptibility weighted imaging at ultra high magnetic field strengths: theoretical considerations and experimental results. *Magn Reson Med* 2008;60:1155–68.
 37. Rooney WD, Johnson G, Li X, Cohen ER, Kim SG, Ugurbil K, et al. Magnetic field and tissue dependencies of human brain longitudinal $^1\text{H}_2\text{O}$ relaxation in vivo. *Magn Reson Med* 2007;57:308–18.
 38. Van den Bergen B, van den Berg CA, Klomp DW, Lagendijk JJ. SAR and power implications of different RF shimming strategies in the pelvis for 7T MRI. *J Magn Reson Imaging* 2009;30:194–202.
 39. Garnov N, Grunder W, Thormer G, Trampel R, Turner R, Kahn T, et al. In vivo MRI analysis of depth-dependent ultrastructure in human knee cartilage at 7 T. *NMR Biomed* 2013;26:1412–9.
 40. Theysohn JM, Kraff O, Maderwald S, Kokulinsky PC, Ladd ME, Barkhausen J, et al. MRI of the ankle joint in healthy non-athletes and in marathon runners: image quality issues at 7.0 T compared to 1.5 T. *Skeletal Radiol* 2013;42:261–7.
 41. Welsch GH, Mamisch TC, Hughes T, Zilkens C, Quirbach S, Scheffler K, et al. In vivo biochemical 7.0 Tesla magnetic resonance: preliminary results of dGEMRIC, zonal T2, and T2* mapping of articular cartilage. *Invest Radiol* 2008;43:619–26.

6 Danksagung

Nach intensiven Jahren der Arbeit liegt nun endlich meine Dissertation vor. Dies ist nun der Zeitpunkt, den Menschen D A N K E zu sagen, die mich in dieser so spannenden Phase meines Lebens begleitet und, vor allem, unterstützt haben.

An erster Stelle gilt hier mein besonderer Dank dem Betreuer meiner Doktorarbeit, Prof. Dr. med. Henning Madry, der von Anfang an mein wissenschaftliches Interesse gefördert hat und mir in den letzten Jahren als wissenschaftlicher Mentor stets freundschaftlich und fördernd zur Seite gestanden hat. Ohne seine unermüdliche Unterstützung wäre diese Arbeit sicherlich nicht möglich gewesen. Ihm gilt dafür meine höchste Anerkennung.

Meinen Eltern Isolde und Rüdiger, meinem Großvater Heinrich und Marga gilt hier auch mein allerliebster Dank für die herzliche und aufopfernde Unterstützung während meines Studiums und die Schaffung eines familiären Umfeldes, dessen Rückhalt ich mir auch in schweren Zeiten immer sicher sein konnte. Ihr Lebensweg war mir stets ein Vorbild. Meiner Freundin Salina danke ich für ihre liebevolle und motivierende Art, ihr Verständnis und ihre Durchhalteparolen, wenn der Weg mal wieder endlos schien und ich wieder ein Wochenende voll mit Arbeit anstatt mit ihr verbrachte.

Herzlich danken möchte ich auch Frau Prof. Dr. rer. nat. Magali Cucchiarini für ihre wertvollen und motivierenden Ratschläge und ihr technisches Know-how, was mir so manchen Fehlversuch vermeiden half. Auch möchte ich mich bei allen weiteren studentischen und festangestellten Mitarbeitern des Zentrums für Experimentelle Orthopädie in Homburg bedanken, die mir in den letzten Jahren wertvolle Arbeitskollegen geworden sind, insbesondere bei Gertud Schmitt, Raphaela Ziegler und PD Dr. med. Patrick Orth.

Ferner möchte ich mich bei Dr. Andreas Müller für etliche Abende und Wochenenden bedanken, die wir gemeinsam am μ MRT verbracht haben, um dann am Ende doch feststellen zu müssen, dass der Steuerungscomputer abgestürzt war.

An dieser Stelle möchte ich mich auch bei allen Kooperationspartnern sowie ihren Mitarbeitern bedanken, die in irgendeiner Form an dieser Arbeit beteiligt waren: Prof. Dr. Dieter Kohn stellvertretend für die Klinik für Orthopädie und Orthopädische Chirurgie (Homburg), PD Dr. Stefan Gräber und Frau Dr. Mei Fang Ong stellvertretend für das Institut für Medizinische Biometrie, Epidemiologie und Medizinische Informatik (Homburg), Prof. Dr. Arno Bücken stellvertretend für die Klinik für Diagnostische und Interventionelle Radiologie (Homburg), Frau Prof. Dr. Anita Ignatius und Dr. Uwe Wolfram stellvertretend für das Institut für Unfallchirurgische Forschung und Biomechanik (Ulm) sowie Prof. Dr. David Zurakowski (Harvard Medical School, Boston, MA, USA) für seine statistische Expertise und Prof. Dr. Dietrich Pape (Centre Hospitalier, Luxembourg, Luxembourg) für die Durchführung der Tierversuche gemeinsam mit Prof. Dr. Henning Madry. Des Weiteren gilt mein Dank dem Forschungszentrum für Medizintechnik und Biotechnologie (Bad Langensalza) und dessen Mitarbeitern, an dem die Tierversuche durchgeführt wurden.

Dem Zentrum für Experimentelle Orthopädie (Homburg), der Klinik für Orthopädie und Orthopädische Chirurgie (Homburg), der AGA - Gesellschaft für Arthroskopie und Gelenkchirurgie sowie den Firmen Arthrex GmbH (Garching) und Synthes GmbH (Umkirch) gilt mein besonderer Dank für die Bereitstellung finanzieller Mittel für die Umsetzung dieser Projekte.

7 Publikationen

Publikationen in *peer reviewed* Journalen:

Goebel L, Zurakowski D, Müller A; Pape D, Cucchiarini M, Madry H. 2D and 3D MOCART scoring systems assessed by 9.4 Tesla high-field MRI correlate with elementary and complex histological scoring systems in a translational model of osteochondral repair. *Osteoarthritis Cartilage*, 2014, 22(10):1386-95.

Ziegler R, **Goebel L**, Seidel R, Cucchiarini M, Pape D, Madry H. Effect of open wedge high tibial osteotomy on the lateral tibiofemoral compartment in sheep. Part III: analysis of the microstructure of the subchondral bone and correlations with the articular cartilage and meniscus. *Knee Surg Sports Traumatol Arthrosc*, Epub 2014 Jun 14, doi: 10.1007/s00167-014-3134-y.

Orth P, Meyer HL, **Goebel L**, Eldracher M, Ong MF, Cucchiarini M, Madry H. Improved repair of chondral and osteochondral defects in the ovine trochlea compared with the medial condyle. *J Orthop Res*, 2013, 31(11):1772-9.

Ziegler R, **Goebel L**, Cucchiarini M, Pape D, Madry H. Effect of opening wedge high tibial osteotomy on the lateral compartment in sheep. Part II: standard and overcorrection do not cause articular cartilage degeneration. *Knee Surg Sports Traumatol Arthrosc*, 2014, 22(7):1666-1677.

Madry H, Ziegler R, Orth P, **Goebel L**, Ong MF, Kohn D, Cucchiarini M, Pape D. Effect of opening wedge high tibial osteotomy on the lateral compartment in sheep. Part I: analysis of the lateral meniscus. *Knee Surg Sports Traumatol Arthrosc*, 2013, 21(1):39-48.

Goebel L, Orth P, Müller A, Zurakowski D, Bückner A, Cucchiarini M, Pape D, Madry H. Experimental scoring systems for macroscopic articular cartilage repair correlate with the MOCART score assessed by a high-field MRI at 9.4 Tesla - comparative evaluation of five macroscopic scoring systems in a large animal cartilage defect model. *Osteoarthritis Cartilage*, 2012, 20(9):1046-55.

Orth P, **Goebel L**, Wolfram U, Ong MF, Gräber S, Kohn D, Cucchiari M, Ignatius A, Pape D, Madry H. Effect of subchondral drilling on the microarchitecture of subchondral bone: analysis in a large animal model at 6 months. *Am J Sports Med*, 2012, 40(4):828-36.

Kongressvorträge und Abstracts:

Morscheid Y, **Goebel L**, Madry H. - Aufbau und Funktion des hyalinen Gelenkknorpels und des subchondralen Knochens. *NOVOCART Anwendertreffen (Bochum), 2014 (Vortrag)*.

Goebel L, Orth P, Müller A, Zurakowski D, Pape D, Kohn D, Cucchiari M, Madry H. - Die valgusierende Standardkorrektur verbessert die Reparatur fokaler Knorpeldefekte - eine translationale Studie im Schafmodell. *Deutsche Gesellschaft für Orthopädie und Orthopädische Chirurgie (Berlin), 100. Tagung, 2014 (Vortrag)*.

Goebel L, Friesenhahn-Ochs B, Bachelier F, Kohn D, Lorbach O. - 23jähriger Mann mit Epiphysiolysis capitis femoris bei hypogonadotropen Hypogonadismus. Ein Fallbericht. *Deutsche Gesellschaft für Orthopädie und Orthopädische Chirurgie (Berlin), 100. Tagung, 2014 (Posterpräsentation)*.

Orth P, Meyer HL, **Goebel L**, Eldracher M, Ong MF, Kohn D, Cucchiari M, Madry H. Topographische Unterschiede in der Knorpelreparatur in vivo zwischen Femurkondyle und Trochlea im Schafmodell. *Deutsche Gesellschaft für Orthopädie und Orthopädische Chirurgie (Berlin), 99. Tagung, 2013*.

Orth P, **Goebel L**, Ong MF, Kohn D, Cucchiari M, Madry H. Topographic defect location dictates articular cartilage repair in the sheep model. *Gesellschaft für Arthroskopie und Gelenkchirurgie (Wiesbaden), 30. Jahreskongress, 2013*.

Goebel L, Pape D, Ziegler R, Kohn D, Cucchiarini M, Madry H. Influence of High Tibial Osteotomy on the medial meniscus with a concomitant cartilage defect in the medial femoral condyle in a sheep model. *University of the Greater Region - 2nd Cartilage Net Congress (Luxemburg, Luxemburg), 2012 (Vortrag)*.

Goebel L, Pape D, Sicks R, Kohn D, Cucchiarini M, Madry H. - Einfluss der Tibiakopfosteotomie bei bestehendem medialen femoralen Knorpeldefekt auf den Innenmeniskus im Schafmodell. *Deutsche Gesellschaft für Orthopädie und Orthopädische Chirurgie (Berlin), 98. Tagung, 2012 (Posterpräsentation)*.

Madry H, Orth P, **Goebel L**, Wolfram U, Kohn D, Pape D. - Subchondral drilling affects the microarchitecture of the subchondral bone: analysis at 6 months postoperatively in a preclinical large animal model. *European Society of Sports Traumatology, Knee Surgery and Arthroscopy (Genf, Schweiz), 15th ESSKA Congress, 2012*.

Orth P, **Goebel L**, Wolfram U, Ong MF, Gräber S, Kohn D, Ignatius A, Pape D, Madry H. Effect of marrow stimulation on the microarchitecture of the subchondral bone - long-term analysis in a preclinical large animal model. *Orthopaedic Research Society Annual Meeting (San Francisco, USA), 58th Annual Meeting, 2012*.

Richardson JB, **Goebel L**, Bhattacharjee A, Qureshi A, Kuiper JH, Dugard N, Madry H. Combination of Osteotomy with Autologous Chondrocyte Implantation for treatment of early Osteoarthritis of Knee. *Orthopaedic Research Society Annual Meeting (San Francisco, USA), 58th Annual Meeting, 2012*.

Orth P, **Goebel L**, Wolfram U, Gräber S, Kohn D, Madry H. Der subchondrale Knochen nach markraumeröffnenden Verfahren: Eine Mikro-CT Untersuchung im Schafmodell. *Deutsche Gesellschaft für Orthopädie und Orthopädische Chirurgie (Berlin), 97. Tagung, 2011*.